



Winding Current Reconstruction of Brushless Permanent Magnet Motor

Wisaruda Wiriyakitja

Submitted to the Faculty of Engineering for the degree of
Master of Engineering Science

Department of Electrical and Electronic Engineering
Adelaide University
Australia



2 April 2001

Table of Contents

| | |
|--------------------------------|------------|
| Table of Contents | i |
| Abstract | iv |
| Declaration | v |
| Acknowledgments | vi |
| Abbreviations | vii |
| List of Figures | ix |
| List of Tables | xiv |

Chapter 1:

| | |
|--------------------------------|----------|
| Introduction | 1 |
| 1.1 Overview and Problem | 1 |
| 1.2 Outline of the Thesis..... | 2 |

Chapter 2:

| | |
|--|----------|
| Brushless Permanent Magnet Drive | 4 |
| 2.1 Introduction | 4 |
| 2.2 Comparison of Brushless Permanent Magnet Motor and Other Types of Motors.. | 5 |
| 2.3 Mathematical Model of the Motor and Drive System | 8 |
| 2.4 Inverter and Current Commutation States | 13 |
| 2.4.1 Commutation Interval..... | 13 |
| 2.4.2 Conduction Interval | 15 |
| 2.5 Current Control mode..... | 15 |
| 2.5.1 Hysteresis Control | 15 |
| 2.5.2 PWM Current Control | 16 |
| 2.6 Conclusion | 17 |

Chapter 3:

Current Measurement Techniques and Switching States in Three-phase

| | |
|----------------------------------|-----------|
| Inverter | 18 |
| 3.1 Introduction | 18 |
| 3.2 Current Sensing Device | 19 |

| | |
|---|----|
| 3.3 The Number of the Sensor and their Locations in the Inverter | 19 |
| 3.4 Literature Survey on the Use of DC Link Current | 24 |
| 3.4.1 Voltage Space Vector | 26 |
| 3.4.2 Switching State Analysis | 27 |
| 3.5 The Relationship between the Phase Currents and the DC Link Current | 27 |
| 3.5.1 Switching Pattern..... | 29 |
| 3.5.2 Current Direction Pattern | 30 |
| 3.5.3 Conducting Devices and the DC Link Current..... | 31 |
| 3.6 Conclusion | 37 |

Chapter 4:

Computer Simulation of the Motor Drive and Reconstruction of Phase

| | |
|---|-----------|
| Currents..... | 38 |
| 4.1 Introduction | 38 |
| 4.2 Basic Layout of the Simulation Model..... | 38 |
| 4.3 Motor Simulation Program..... | 40 |
| 4.3.1 Motor SubVI..... | 44 |
| 4.3.2 Drive SubVI..... | 44 |
| 4.4 Simulation Results of the Motor Drive..... | 46 |
| 4.5 Analysis of the Inverter Currents..... | 58 |
| 4.6 Implementation of the DC Link Current | 60 |
| 4.7 The Current Reconstruction Module | 70 |
| 4.8 The Simulation Results of the Phase Current Reconstruction..... | 72 |
| 4.9 Conclusion | 79 |

Chapter 5:

| | |
|--|-----------|
| Experiment Results..... | 81 |
| 5.1 Introduction | 81 |
| 5.2 Hardware of the experimental setup..... | 82 |
| 5.3 Current Reconstruction Algorithm used in the real tests..... | 85 |
| 5.4 Experiment results | 88 |
| 5.5 Conclusion | 95 |

Chapter 6:

| | |
|--|------------|
| Conclusions and Suggestions | 96 |
| 6.1 Conclusions | 96 |
| 6.2 Suggestions | 99 |
| | |
| Reference | 101 |

Appendices

| | |
|---|-----|
| A-1 The detailed analysis of the switching state | 103 |
| A-2 The details in the block diagram of the motor simulation program | 114 |
| A-3 The details in the main block diagram of the program to reconstruct the phase current using the experimental data..... | 122 |

Abstract

Brushless Permanent Magnet (BLPM) motors have many benefits, such as high efficiency and high power density, which make them a popular choice in advance motor drive systems. However, the values of the three-phase currents of the motor are required to control the torque of the motor, which has to be measured using multiple current sensors. The current sensors are expensive and reduce the reliability of the system. In addition to this, current sensors may degrade the signal and introduce errors, which may results in torque ripple in a practical motor drive.

Several researchers have proposed various methods to reduce the number of current sensors. One of those methods suggested using a single current sensor to measure the DC link current and using the switching signals to reconstruct the three-phase currents of the motor. Although this was possible, it should be emphasised that in some instances of the switching state, the motor current does not flow through the DC link, but it circulates inside the inverter circuit. In several articles, the method to find the three-phase currents using a similar method was explained. However, none of these studies considered the circulating inverter current in the reconstruction of the phase currents.

This thesis provides a comprehensive motor simulation program that can be used to study a number of operating modes of the motor drive, and can introduce artificial faults and noises that may appear in the real drive. The thesis also provides a detailed analysis of the DC link current and inverter switching states. The current reconstruction algorithm and a compensation routine are given in the thesis. The practical data from the real motor drive are obtained, the simulation studies are verified, and the limitations of the method are highlighted. It is demonstrated that a single current sensor on the DC link and the switching signals can be used to reconstruct the three-phase currents of the BLPM motor. However, a real-time implementation of such a method requires a noise-free measurement and further improvements on the current compensation technique, which can be investigated in the future.

Declaration

This work contains no material which has been accepted for the award of any other degree or diploma in any university or other tertiary institution and, to the best of my knowledge and belief, contains no material previously published or written by another person, except where due reference has been made in the text.

I give consent to this copy of my thesis, when deposited in the University Libraries, being available for photocopying and loan.

Signature:...

Date: 2/4/01.....

Acknowledgment

This research was conducted under the supervision of Dr. Nesimi Ertugrul. I wish to thank him for his patience and guidance to bring this thesis completion. I am also grateful to Mr. Li Ying for providing the experimental data and many suggestions. Finally, special thanks to Karen, my family and friends for encouragement and understanding for all times.

Abbreviations

| Abbreviation | Variable Name | Units |
|-----------------------|---|-------------------|
| θ_e | Electrical position | rad |
| Δ_{error} | DC link current error = real DC link current - simulated DC link current | A |
| Δh | Hysteresis bandwidth for current | A |
| ω_e | Electrical velocity of the motor | rad/s |
| ω_r | Angular speed of the rotor | rad/s |
| Δt | Sampling interval | sec |
| AC | Alternating current | |
| B | Damping coefficient | Nm·s |
| BLDC | Brushless DC | |
| BLPM | Brushless Permanent Magnet | |
| CSI | Current Source Inverter | |
| DC | Direct current | |
| $e_{1,2,3}$ | Instantaneous back emf voltages of phase1, 2 and 3 respectively | V |
| $i_{1,2,3}$ | Instantaneous phase currents of phase1, 2 and 3 respectively | A |
| $I_{compensate1,2,3}$ | The phase currents of the simulator after compensating | A |
| I_{dc} or i_{dc} | DC link current, average or instantaneous values respectively | A |
| $I_{dcphase}$ | The current of a phase of which the absolute amplitude of the current is equal to the absolute amplitude of the DC link current | A |
| $I_{model1,2,3}$ | The phase currents of the simulator | A |
| $I_{motor1,2,3}$ | The phase currents of the real motor | A |
| J | Moment of inertia | kg·m ² |
| k_e | Maximum back emf constant | V·sec/rad |
| L | Inductance of the motor winding | H |

| Abbreviation | Variable Name | Units |
|--------------|---|----------|
| n | The number of step of the integration | |
| PID | Proportional Integral Differential | |
| PWM | Pulse Width Modulation | |
| R | Resistance of the motor winding | Ω |
| rpm | Revolutions per minute | |
| T_e | Electromagnetic torque | N·m |
| T_L | Load torque | Nm |
| $v_{1,2,3}$ | Instantaneous phase voltage | V |
| $v_{a,b,c}$ | Instantaneous terminal voltage | V |
| V_{dc} | Voltage between the positive and the negative DC rail | V |
| v_s | Voltage at the star point in the motor circuit | V |
| VSI | Voltage Source Inverter | |

List of Figures

| | |
|---|----|
| Figure 2.1 Equivalent circuit model of the BLPM motor circuit | 9 |
| Figure 2.2 Back emf voltage waveforms | 10 |
| Figure 2.3 Common three-phase inverter circuit topology..... | 13 |
| Figure 2.4 Three-phase inverter connected to the motor windings | 14 |
| Figure 2.5 Hysteresis current control..... | 16 |
| Figure 2.6 PWM waveform generation method | 17 |
| Figure 3.1 Position of 4 current sensors in the conventional three-phase inverter..... | 20 |
| Figure 3.2 Potential fault current paths in the inverter | 21 |
| Figure 3.3 2-sensor method | 22 |
| Figure 3.4 Circuit indicating the method of connection utilising a single sensor | 23 |
| Figure 3.5 Equivalent circuit diagram to measure all possible current faults | 23 |
| Figure 3.6 Diagram of electronically commutated motor drive with integrated current sensor | 24 |
| Figure 3.7 DC link current in three-phase PWM inverter | 25 |
| Figure 3.8 Equivalent circuits for "one switch active (T6) state" (a), "two switch active (T1 and T6) state" (b)..... | 27 |
| Figure 3.9 Current flow path in the inverter when T2 and T3 are turned on..... | 28 |
| Figure 3.10 Directions of the currents in phase2 and 3; when T3 and T2 or D5 and D6 are conducting current | 28 |
| Figure 3.11 Diagram of the direction of phase currents when the switching pattern is U, O, O..... | 32 |
| Figure 3.12 Diagram of the direction of phase currents when switching pattern is U, O, O..... | 33 |
| Figure 3.13 Diagram of the direction of phase currents when switching pattern is U, O, O..... | 33 |
| Figure 3.14 Diagram of the direction of phase currents when the switching pattern is U, U, O..... | 34 |
| Figure 3.15 Diagram of the direction of phase currents when the switching pattern is U, U, O..... | 35 |
| Figure 3.16 Diagram of the direction of phase currents when the switching pattern is U, L, U | 36 |

| | |
|--|----|
| Figure 3.17 Diagram of the direction of phase currents when the switching pattern is changed to the U, U, L and the current direction is still +, -, + | 36 |
| Figure 4.1 Block diagram of the simulation of the motor drive and current reconstruction | 39 |
| Figure 4.2 Main loop program of the simulate motor | 41 |
| Figure 4.3 PID SubVI (See Appendix A-2)..... | 41 |
| Figure 4.4 Chg Point SubVI (See Appendix A-2)..... | 41 |
| Figure 4.5 Current control SubVI (See Appendix A-2) | 42 |
| Figure 4.6 Drive SubVI (See Appendix A-2)..... | 42 |
| Figure 4.7 Motor SubVI (See Appendix A-2)..... | 42 |
| Figure 4.8 ω and rpm SubVI (See Appendix A-2)..... | 42 |
| Figure 4.9 TPS SubVI (See Appendix A-2)..... | 42 |
| Figure 4.10 Block diagram of Motor SubVI..... | 43 |
| Figure 4.11 The block diagram of Drive SubVI..... | 43 |
| Figure 4.12 Emf SubVI (See Appendix A-2)..... | 44 |
| Figure 4.13 Torque SubVI (See Appendix A-2) | 45 |
| Figure 4.14 Speed SubVI (See Appendix A-2) | 45 |
| Figure 4.15 Position SubVI (See Appendix A-2)..... | 46 |
| Figure 4.16 Terminal Voltage SubVI (See Appendix A-2)..... | 46 |
| Figure 4.17 DC link SubVI (See Appendix A-2) | 46 |
| Figure 4.18 Simulation results of the motor drive operating from standstill, with rectangular current excitation, hysteresis current control and trapezoidal back emf waveforms..... | 49 |
| Figure 4.19 Simulation results of the motor drive while it is accelerating from standstill, the sinusoidal current excitation, PWM current control and sinusoidal back emf waveforms | 50 |
| Figure 4.20 Simulation results of the motor drive under the transient operation, the rectangular current excitation, PWM current control and sinusoidal back emf waveforms | 51 |
| Figure 4.21 Simulation results of the motor drive under the transient operation starting from standstill, sinusoidal current excitation, hysteresis current control and trapezoidal back emf waveforms..... | 52 |

| | |
|--|----|
| Figure 4.22 Simulation results of the motor drive with a rectangular current excitation, hysteresis current control and trapezoidal back emf waveforms | 54 |
| Figure 4.23 Simulation results of the motor drive under the transient operation, the sinusoidal current excitation with no current control, PWM current control and sinusoidal back emf waveforms | 55 |
| Figure 4.24 Simulation results of the motor drive under step loading (increasing load torque), the trapezoidal current excitation, PWM current control and sinusoidal back emf waveforms | 56 |
| Figure 4.25 Simulation results of the motor drive under a step load change (reducing load torque), the trapezoidal current excitation, PWM current control and sinusoidal back emf waveforms | 57 |
| Figure 4.26 Bridge inverter diagram when T1, T6, T2 are conducting..... | 62 |
| Figure 4.27 Bridge inverter diagram when T4, T3, T5 are conducting..... | 63 |
| Figure 4.28 Bridge inverter diagram when D3, D4 and D5 are conducting..... | 64 |
| Figure 4.29 Bridge inverter diagram when D1, D2 and D6 are conducting..... | 65 |
| Figure 4.30 Bridge inverter diagram when T1 and T6 are conducting current..... | 66 |
| Figure 4.31 Bridge inverter diagram when D1 and D6 are conducting currents..... | 67 |
| Figure 4.32 Bridge inverter diagram when T1, T6 and D2 are conducting..... | 68 |
| Figure 4.33 Bridge inverter diagram when T4, T3 and D5 are conducting currents.. | 68 |
| Figure 4.34 Bridge inverter diagram when D4, D3 and T5 are conducting currents . | 69 |
| Figure 4.35 Bridge inverter diagram when D1, D4 and T2 are conducting current... | 70 |
| Figure 4.36 Main block diagram of the LabVIEW current reconstruction module ... | 71 |
| Figure 4.37 Drive1 or Drive2 SubVI..... | 71 |
| Figure 4.38 Comp SubVI (see Appendix A-2)..... | 72 |
| Figure 4.39 Error SubVI (see Appendix A-2) | 72 |
| Figure 4.40 Simulation results under hysteresis current control, rectangular current excitation, trapezoidal back emf, 2% constant +5% random error on the DC link current | 74 |
| Figure 4.41 Simulation results under hysteresis current control, rectangular current excitation, trapezoidal back emf, 5% constant +5% random error on the DC link current | 75 |

| | |
|---|-----|
| Figure 4.42 Simulation results under PWM current control, rectangular excitation current, sinusoidal back emf, 2% constant +5% random error on the DC link current | 76 |
| Figure 4.43 Simulation results under PWM current control, rectangular excitation current, sinusoidal back emf, 5% constant +5% random error on the DC link current | 77 |
| Figure 4.44 Simulation results under PWM current control, sinusoidal excitation current, sinusoidal back emf, 2% constant +5% random error on the DC link current | 78 |
| Figure 4.45 Simulation results under PWM current control, sinusoidal excitation current, sinusoidal back emf, 5% constant +5% random error on the DC link current | 79 |
| Figure 5.1 Steps followed to capture real time data | 82 |
| Figure 5.2 Schematic diagram of the hardware used in the tests..... | 83 |
| Figure 5.3 Diagram of the program to reconstruct the phase current using the experimental data..... | 87 |
| Figure 5.4 Test results at a speed of 50 Hz with the rectangular current excitation of the motor drive..... | 90 |
| Figure 5.5 Test results at a speed of 25 Hz with the rectangular current excitation of the motor drive..... | 91 |
| Figure 5.6 Test results at a speed of 50 Hz with the sinusoidal current excitation of the motor drive..... | 93 |
| Figure 5.7 Test results at a speed of 25 Hz with the sinusoidal current excitation of the motor drive..... | 94 |
| Figure A.1 Block diagram of PID SubVI | 114 |
| Figure A.2 Block diagram of Chg point SubVI..... | 114 |
| Figure A.3 Block diagram of Current control SubVI | 115 |
| Figure A.4 Block diagram of ω and rpm SubVI..... | 116 |
| Figure A.5 Block diagram of TPS SubVI..... | 116 |
| Figure A.6 Block diagram of Emf SubVI..... | 116 |
| Figure A.7 Block diagram of Torque SubVI..... | 117 |
| Figure A.8 Block diagram of Speed SubVI..... | 117 |
| Figure A.9 Block diagram of Position SubVI | 118 |

| | | |
|--------------------|--|-----|
| Figure A.10 | The block diagram of Terminal Voltage SubVI..... | 119 |
| Figure A.11 | Block diagram of DC link SubVI..... | 120 |
| Figure A.12 | Detail in the block diagram of Comp SubVI..... | 121 |
| Figure A.13 | Detail in the block diagram of Error SubVI..... | 121 |
| Figure A.14 | Input and output of Sep Sigs SubVI..... | 122 |
| Figure A.15 | Detail the block diagram of Sep Sigs SubVI..... | 123 |
| Figure A.16 | Input and output of Vdc SubVI..... | 123 |
| Figure A.17 | Detail in the block diagram of Vdc SubVI..... | 124 |

List of Tables

| | |
|--|-----|
| Table 2.1 Advantages and Disadvantages of BLPM motors | 5 |
| Table 2.2 Summary of the motor features | 7 |
| Table 2.3 Possible waveforms of the back emf voltage, the phase current, and the electromagnetic torque..... | 12 |
| Table 3.1 Vector states and corresponding phase currents | 26 |
| Table 3.2 Summary of switching patterns in the inverter | 30 |
| Table 3.3 Possible state of the directions of the current in the motor phases | 31 |
| Table 4.1 The specification of the motor system in the simulation results..... | 47 |
| Table 5.1 Specification of the motor in the experimental setup | 83 |
| Table 5.2 Specifications of the IRMDAC3..... | 84 |
| Table 5.3 Specifications of ADMC300 | 84 |
| Table 5.4 Specifications of PCI6110 DAQ card..... | 85 |
| Table 5.5 Motor parameters and initial values used in the algorithm..... | 86 |
| Table A-1 Switching state, conducting device, DC link number and circulate number | 105 |

Chapter I

Introduction

1.1 Overview and Problem

Brushless Permanent Magnet (BLPM) motors are widely used in applications where a high performance motor drive is needed. Such motors have higher power density and higher efficiency than their counterparts. Moreover, BLPM motors have higher reliability, lower maintenance and longer life.

However, such motors are used only in small and medium ranges, and the high cost of the motor drives is the major disadvantage of these motors. Although the costs of permanent magnets and the power electronic devices are decreasing, average cost of the BLPM motor drive still remains high due to the cost of accurate position sensors and the current sensors, which are required in the drive.

A commonly used BLPM motor drive contains a three-phase motor and a conventional inverter with a suitable control circuit. The inverter provides the current commutation based on the real motor currents that generate the torque of the motor. Therefore, to control such motor drive, it is necessary to know the values of the three-phase currents. In a three-phase brushless PM motor drive, usually three current sensors are needed to measure the three-phase winding currents. Normally, three Hall-Effect current sensors are used, but the prices of such sensors are high. Instead of using Hall-Effect current sensors, low-value resistors can also be used to measure the phase currents. However, there are some disadvantages of this method such as no electrical isolation and additional power losses in the resistors.

The number of Hall-Effect current sensors can be reduced to two sensors in the star connected winding because the summation of the three-phase currents is equal to zero. However, the reduction of the number of sensors cannot be achieved further unless some other methods are implemented. One of the alternative methods is to use the DC link current measurement only. Such a method requires only one current sensor, and may eliminate the problem of the torque ripple that is primarily due to the

DC offset in 2 Hall-Effect current sensor method. However, the major disadvantage of such a method is that, in some instances of the inverter states, there is no information on the DC link current. In these instances, the currents of the motor circulate in the inverter circuit, and hence the DC link current cannot be observed.

A number of researchers have been identified who investigated the characteristic of the DC link current and studied the reconstruction of the three-phase currents of the AC motor. However, no researcher has analysed every possible state of the switching state in the inverter and has suggested no solution in the case of a circulating inverter current. In addition, these earlier studies have reported the switching states only in the case of PWM control strategy, which is not sufficient to cover all possible states. Moreover, the earlier studies used the "Space Vector" to analyse the switching state of the PWM strategy. However, the method was found to be inefficient to convert 3D array to 2D array and then back to 3D array again.

The main objective of this thesis is to reconstruct the winding currents accurately by using the information of DC link current and the switching signals. This thesis highlights the above problem by analysing every possible current conduction state in a practical inverter and motor.

1.2 Outline of the Thesis

Chapter 2 describes the advantages and disadvantages of the BLPM motor and presents a comparative study. The characteristics of the BLPM motor are investigated, and mathematical model of the motor is given. The chapter also provides the operation principles of the motor drive, and highlights the principal control methods.

Chapter 3 reports the current measurement techniques and related devices and then discusses the requirement of current sensors and their locations in detail. The minimum number of sensors used in the practical system is summarised. The chapter also analyses the DC link current in a conventional inverter and extends the discussion further to include the Voltage Space Vector, which is used to investigate

the switching state of the inverter. The chapter concludes with the discussions about the relationships between the three-phase currents and the DC link current.

Chapter 4 explains the simulation program of the BLPM motor drive. The complete simulation system is described, and details of the subprograms are explained. A number of simulation results, which contains phase current waveforms, back emf voltage waveforms, torque, and speed of the BLPM motor, are provided in the chapter to demonstrate the flexibility of the motor simulator. The characteristic features of the current in the inverter are also analysed, and the phase current reconstruction method and current compensation modules are explained and supported by simulation studies.

Chapter 5 describes the experimental setup that is used to validate the simulation results presented in Chapter 4. Due to the hardware limitations only a limited number of test results are given in this section. The switching signals that are used in the current reconstruction algorithm are determined from the measured current and voltage waveforms of the motor drive. As demonstrated in this chapter, the results of the current reconstruction from the practical system diverts significantly from those of the pure computer simulation due to the presence of the electrical noises.

Appendix provides the details of all possible switching states of the inverter that is obtained by analysing the switching patterns and the directions of the currents. The details of the LabVIEW-based simulation block diagrams are also given in this section.

Chapter II

Brushless Permanent Magnet Drive System

2.1 Introduction

Brushless permanent Magnet (BLPM) motors are widely used in applications where higher efficiency and higher power density are prime concerns. Since the rotor has no winding, the volume is reduced, which makes the BLPM motor smaller in size and also lighter in weight [1]. In addition, due to the absence of brushes, no maintenance is required and the speed limit is increased. However, an inverter circuit is needed to perform the functions of the commutator that is available in conventional brush DC machines. The inverter is controlled by digital signals, which establish the current commutations in the windings.

BLPM motors can be classified into two types: Brushless DC motor (BLDC motor) and BLPM synchronous motors [2]. Both types have permanent magnets on the rotor and have no brushes. However, the shapes of the back emf voltages of these motors are different. The back emf voltage of the BLDC motor is trapezoidal, whereas the back emf voltage of the BLPM synchronous motor is sinusoidal because the windings and the rotor construction of the both motors are different. However, they have similar control strategies. One of the desired outputs in the control of such motors is a smooth torque. Therefore, accurate torque control is needed to obtain a ripple free torque. As will be explained in this chapter, the electromagnetic torque of the BLPM motor is directly related to the shape of the currents and the back emfs. Hence, the line currents should be controlled in order to achieve a ripple free torque.

In the following sections of this chapter, distinguishing features of the BLPM motors are described, and some comparisons are made. The electrical equivalent circuit of the motor is also provided. Next, the characteristics of the motor are described via the voltage equations, the back emf equations and the torque equation. Finally, the inverter topology is explained together with the operating states, and current control modes.

2.2 Comparison of Brushless Permanent Magnet Motors and Other Types of Motors

As mentioned earlier, BLPM motors have no brushes and commutators. Therefore, they are usually maintenance-free motors. In addition, acoustic noise and sparking, which frequently occur in conventional brush DC motors, do not occur in BLPM motors. In maintenance free, high efficiency, and high performance motor drive applications, BLPM motors are the ideal choice.

In brush DC motors, a field winding is required to generate the magnetic flux. Therefore, some room in the motor housing should be reserved for the accommodation of the field windings. In permanent magnet motors, however, the magnet, which generates the magnetic field, requires much less room than the field winding.

BLPM motors are usually built in a low and medium power range [3]. The principal reason for this is that the high power and high volume permanent magnets are very expensive. Moreover, one of the largest disadvantages of PM motor is the absence of the field control. Therefore the only way to achieve a control in these motors is to control the voltage and current of the windings. The following table summarises the advantages and disadvantages of BLPM motors, which can be used in the selection of such motors in industrial applications.

Table 2.1 Advantages and Disadvantages of BLPM motors

| Advantages of BLPM motor | Disadvantages of BLPM motor |
|--|--|
| 1. Lightweight 2. Higher efficiency 3. No maintenance 4. Operation under various environmental conditions 5. Smooth torque with correct control 6. Smaller size | 1. Small and medium power range 2. Limitation in high temperature operations 3. High cost 4. Absence of the field control |

Although the BLPM motor itself has many benefits as shown above, it is important to look at its counterparts. The following sections, from (a) to (e), summarise the basic features of the motors; including traditional brush DC motor, PM brush DC motor, induction motor, conventional synchronous motor, brushless PM DC motor, brushless PM synchronous motor and switched reluctance motor [3].

a) Traditional brush DC motor

The structure of the traditional DC motor is simple. It is easy to control, especially if the motor is driven from an adjustable voltage source. Moreover, its torque is smooth. However, the presence of brushes and commutators has some limitations, such as the speed limitation, the acoustic noise, potential sparking, the need of regular maintenance, and the additional space for brushes, commutators and cooling system.

b) PM brush DC motor

This motor has the benefits of permanent magnets, which eliminate the field winding on the stator but keep the brushes and the commutators. This arrangement reduces the size of the motor. Such a motor is low in cost and high in reliability. They are usually used in fixed-speed applications and built in small and very small power ratings.

c) Squirrel cage induction motor

The AC current in the stator windings induces the current in the rotor of the squirrel cage induction motor. It is the most popular brushless motor type used in the majority of industrial applications because of the endurance and various sizes. Moreover, the large power-rating machines are available. Two of the largest disadvantages of these motors are lagging power factor and low efficiency due to the slip.

d) Synchronous motor

The structure of the synchronous motor is similar to that of the induction motor, but there is a current feeding the field rotor through slip rings. Due to the field winding, in medium and large power range, the cooling system required the increment of the total cost. However, these motors can operate at unity power factor. The motors are usually operated at constant speed.

e) Switched reluctance motor

The stator and the rotor of a switched reluctance motor have salient poles, but only the salient poles of the stator have windings. The number of salient poles for stator and rotor is not equal. The number of the poles at the stator is more than the number of the poles at the rotor. The structure of the switched reluctance motor is simple. Therefore the manufacturing process is much easier and the overall cost is lower than other machines. Since there is no magnet in the motor, it can operate in a high temperature environment. In addition, there is no speed limit in these machines. However, the torque ripple and acoustic noise are the major problems in the switched reluctance motor.

Table 2.2 Summary of the motor features

| The motor type | Advantages | Disadvantages |
|----------------------------|--|--|
| Traditional brush DC motor | <ol style="list-style-type: none"> 1. Flexible control (by controlling both armature and field circuit) 2. Smooth and predictable torque and speed | <ol style="list-style-type: none"> 1. Require regular maintenance 2. High cost 3. Speed and current limitation 4. Acoustic noise |
| Brush PM DC motor | <ol style="list-style-type: none"> 1. Smooth torque 2. Smaller size 3. Low cost | <ol style="list-style-type: none"> 1. Speed limitation 2. Acoustic noise 3. Limitation in power rating |
| Induction motor | <ol style="list-style-type: none"> 1. Robust structure 2. Cheaper and easier to manufacture 3. Large power rating machines possible | <ol style="list-style-type: none"> 1. Lagging power factor 2. Low efficiency |
| Synchronous motor | <ol style="list-style-type: none"> 1. Unity and leading power factor 2. High efficiency | <ol style="list-style-type: none"> 1. No over loading 2. Constant speed 3. Acoustic noise |

Table 2.2 Summary of the motor features (continued)

| The motor type | Advantages | Disadvantages |
|-----------------------------|---|--|
| Brushless DC motor | <ol style="list-style-type: none"> 1. High efficiency and high torque per ampere 2. Higher power density 3. Easier control 4. Requires cheaper position sensor 5. Maintenance free | <ol style="list-style-type: none"> 1. High cost 2. Small and medium power range 3. Limited maximum speed 4. Temperature limitation |
| Brushless Synchronous motor | <ol style="list-style-type: none"> 1. High efficiency and high torque per ampere 2. Higher power density 3. Easier control 4. Maintenance free 5. Usage in high performance positioning system | <ol style="list-style-type: none"> 1. High cost 2. Small and medium power range 3. Limited maximum speed 4. Temperature limitation 5. Requirement for complex and expensive control circuit 6. Expensive position sensor |
| Switched Reluctance motor | <ol style="list-style-type: none"> 1. Simple structure and low cost 2. Operation in high temperature environment 3. Maintenance free 4. Operation at high speed | <ol style="list-style-type: none"> 1. Torque ripple 2. Higher acoustic noise 3. Low efficiency 4. Complex and expensive control circuit |

2.3 Mathematical Model of the Motor and Drive System

As discussed above, brushless PM motors are preferred in many applications. Therefore, operation and performance of these types of motors are the primary concern in this thesis. In the following paragraphs, the mathematical model of the motors will be given and the drive system used in these motors will be explained.

Generally, the composition of the BLPM motor is similar to the traditional synchronous motors, except the field winding. In a synchronous motor, there are two sides of the equivalent circuit: field winding and armature winding. Since the rotor of the BLPM motor has permanent magnets only, there is only one electrical equivalent circuit. **Fig.2.1** shows the equivalent circuit of the three-phase BLPM motor [4]. In the figure, v_a , v_b and v_c are the terminal voltages of phase1, phase2 and phase3 of the motor respectively. L is the equivalent inductance of each phase winding. R is the equivalent resistance of each phase winding. i_1 , i_2 and i_3 are the line currents of the motor and e_1 , e_2 and e_3 are the back emf voltages of phase1, phase2 and phase3 of the motor respectively.

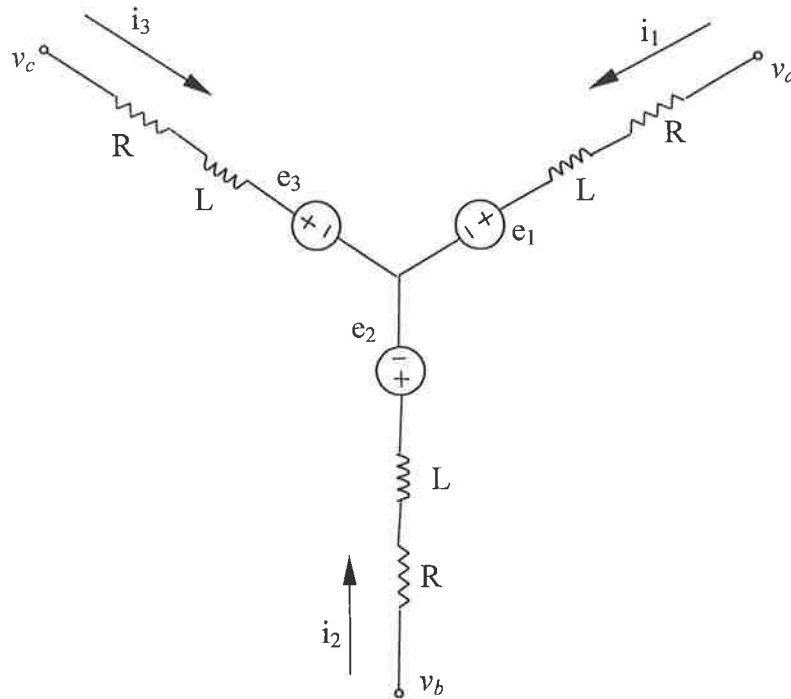


Figure 2.1 Equivalent circuit model of the BLPM motor circuit

The voltage equations of three-phase BLPM motor can be given as

$$\begin{aligned}
 v_1 &= L \frac{di_1}{dt} + R i_1 + e_1 \\
 v_2 &= L \frac{di_2}{dt} + R i_2 + e_2 \\
 v_3 &= L \frac{di_3}{dt} + R i_3 + e_3
 \end{aligned} \tag{2.1}$$

Here, v_1 , v_2 and v_3 are the phase voltages of phase1, phase2 and phase3 of the motor respectively. As mentioned previously, there are two types of BLPM motors: the BLDC motor, which has trapezoidal back emf waveform, and the PM synchronous motor, which has sinusoidal back emf waveform.

In general, the three-phase back emf voltage equations of the BLPM motor are given by

$$\begin{aligned} e_1 &= \omega_r k_e e_1(\theta_e) \\ e_2 &= \omega_r k_e e_2(\theta_e) \\ e_3 &= \omega_r k_e e_3(\theta_e) \end{aligned} \quad (2.2)$$

Where e_1 , e_2 , and e_3 are the back emf voltages of phase1, 2 and 3 respectively; ω_r is the angular velocity of the motor; k_e is the back emf voltage constant; θ_e is the electrical position of the rotor; $e_1(\theta_e)$, $e_2(\theta_e)$ and $e_3(\theta_e)$ are the per-unit back emf voltages of phase1, 2 and 3 respectively. **Fig.2.2** shows typical back emf waveforms of the BLDC motor and the PM synchronous motor [4].

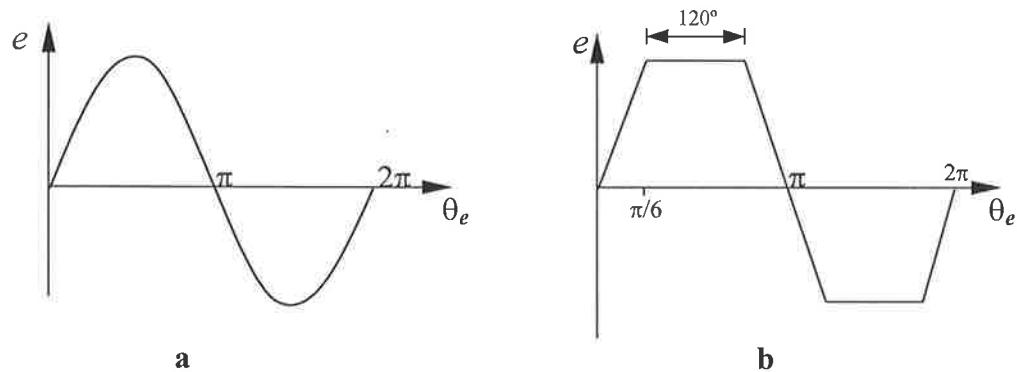


Figure 2.2 Back emf voltage waveforms per phase

- a) Sinusoidal waveform of the PM synchronous motor
- b) Trapezoidal waveform of the BLDC motor

In the case of sinusoidal back emf waveforms, the equations in per-unit form can be given as,

$$\begin{aligned}
 e_1(\theta_e) &= \sin\theta_e \\
 e_2(\theta_e) &= \sin\left(\theta_e - \frac{2\pi}{3}\right) \\
 e_3(\theta_e) &= \sin\left(\theta_e - \frac{4\pi}{3}\right)
 \end{aligned} \tag{2.3}$$

where

$$\theta_e = \omega_e t \tag{2.4}$$

Here, ω_e is the electrical velocity of the motor. However, in the case of trapezoidal back emf waveforms, the modelling can be possibly shown in discrete form. For a single phase it is,

$$\begin{aligned}
 e_1(\theta_e) &= \frac{1}{\pi/6} \times \theta_e, \quad 0 \leq \theta_e \leq \frac{5\pi}{6} \\
 e_1(\theta_e) &= 1, \quad \frac{\pi}{6} \leq \theta_e \leq \frac{5\pi}{6} \\
 e_1(\theta_e) &= \frac{-1}{\pi/6} \times (\theta_e - \pi), \quad \frac{5\pi}{6} \leq \theta_e \leq \frac{7\pi}{6} \\
 e_1(\theta_e) &= -1, \quad \frac{7\pi}{6} \leq \theta_e \leq \frac{11\pi}{6} \\
 e_1(\theta_e) &= \frac{1}{\pi/6} \times (\theta_e - 2\pi), \quad \frac{11\pi}{6} \leq \theta_e \leq 2\pi
 \end{aligned} \tag{2.5}$$

The per-unit of the back emf voltages for the other two phases can be achieved by shifting θ_e by $2\pi/3$ and $4\pi/3$.

The interaction between the magnetic flux and the phase current produces electromagnetic torque. Therefore, the electromagnetic torque can be derived as,

$$T_e = \frac{1}{\omega_r} \times (e_1 \cdot i_1 + e_2 \cdot i_2 + e_3 \cdot i_3) \tag{2.6}$$

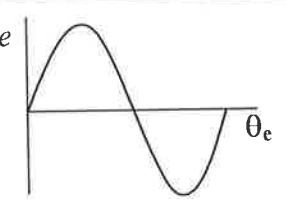
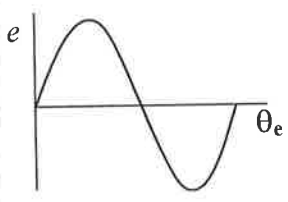
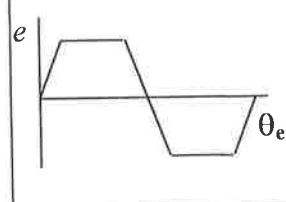
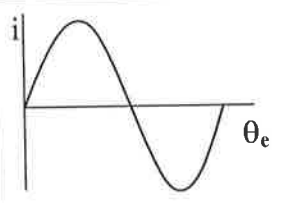
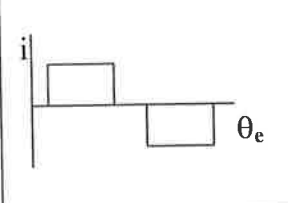
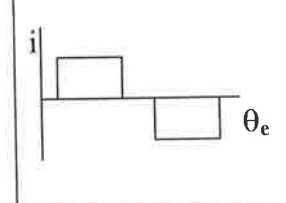
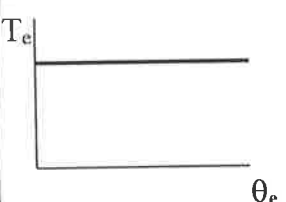
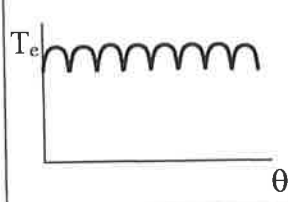
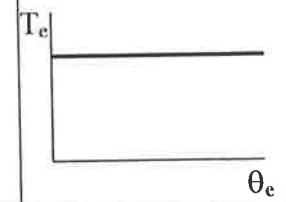
where, $e_1, i_1, e_2, i_2, e_3,$ and i_3 are all position dependent parameters. From the equation of motion, the dynamic equation can also be given by

$$T_e = J \frac{d\omega_r}{dt} + B \cdot \omega_r + T_L \tag{2.7}$$

Here, J is the moment of inertia, B is the damping coefficient, T_L is the load torque or mechanical torque. This equation can be used to find the angular speed of the motor.

Table 2.3 shows the summary of the relationships of the back emf voltage, the phase current and the total electromagnetic torque of the BLPM motor [4]. As shown in **Table 2.3**, if the back emf voltage has a sine wave shape, there are two possible current waveforms that can be applied to the corresponding motor phases. If the current is sine wave, the torque is smooth; if the current is not sine wave, the torque has ripples. Furthermore, if the back emf voltage is trapezoidal in shape and the input current is a rectangular wave, the torque has no ripple either.

Table 2.3 Possible waveforms of the back emf voltage, the phase current, and the electromagnetic torque. Note that only one-phase voltage and current waveforms are shown.

| Descriptions | Sinusoidal Excitation | Rectangular Excitation | |
|--------------------|---|--|---|
| | BLPM synchronous motor | BLPM synchronous motor | BLDC motor |
| Back emf form |  |  |  |
| Ideal current form |  |  |  |
| Ideal Torque form |  |  |  |

As can be seen from the above discussion, the developed torque of the motor depends upon the amplitudes of the phase currents and the back emfs. Since the back emf of the motor is proportional to the speed, the control of the torque depends upon the phase current that can be externally controlled.

2.4 Inverter and Current Commutation States

The inverter, used in the BLPM motor drives, is a three-phase bridge inverter which is shown in **Fig.2.3**. The bridge inverter consists of 6 power switches, T1 to T6, and 6 diodes, D1 to D6. One power switch and one diode are matched together and there are 2 pairs of the power switch and diode in each phase of the inverter. While the upper pair is connected to the positive voltage, the lower pair is connected to the negative voltage. The three-phase voltage outputs are the terminals v_a , v_b , and v_c , which can be connected to a three-phase load (star or delta connected). It should be remembered that the switches on the same leg must not be turned on to prevent a supply short circuit. When the inverter operates, there are 2 types of the conducting state happening in the inverter: Commutation Interval and Conduction Interval.

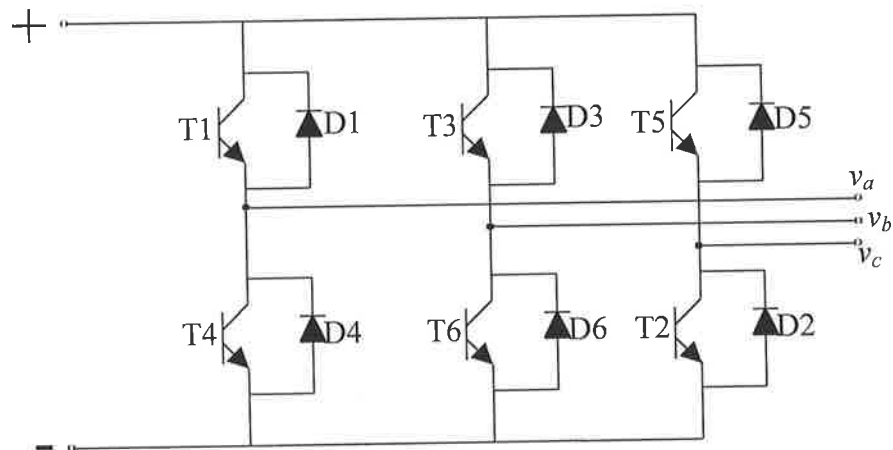


Figure 2.3 Common three-phase inverter circuit topology.

2.4.1 Commutation Interval

Even when two phases are conducting current via two of the power switches as in the rectangular current control mode, three-phase current conduction occurs during the current commutation period. When one of the transistors is turned off, the current commutation occurs via the diode that is connected parallel to the other transistor on the same leg.

Fig.2.4 illustrates the three-phase inverter and motor circuit that are used in the computer simulation. The terminal voltages, v_a , v_b , and v_c , in the circuit can be given as a reference to the mid-point of the DC supply.

$$\begin{aligned}
 v_a &= \frac{V_{dc}}{2} = L \frac{di_1}{dt} + Ri_1 + e_1 + v_s \\
 v_b &= \frac{V_{dc}}{2} = L \frac{di_2}{dt} + Ri_2 + e_2 + v_s \\
 v_c &= -\frac{V_{dc}}{2} = L \frac{di_3}{dt} + Ri_3 + e_3 + v_s
 \end{aligned} \tag{2.8}$$

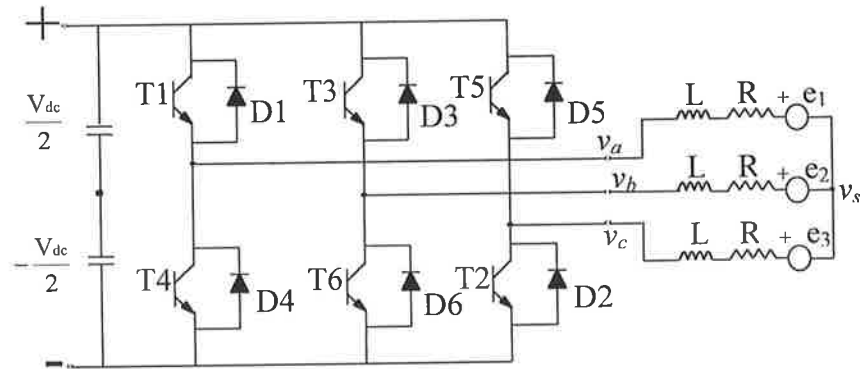


Figure 2.4 Three-phase inverter connected to the motor windings.

Where the star point voltage of the motor, and $\frac{V_{dc}}{2}$ is half of the value of the DC link voltage. During the commutation interval, if all three phases are conducting current and if the relations of $i_1+i_2+i_3 = 0$ and $e_1+e_2+e_3 = 0$ are assumed the star point voltage can be given by

$$v_s = \frac{V_{dc}}{6} \tag{2.9}$$

Hence, the voltages across the motor winding as a function of the DC link voltage become

$$\begin{aligned}
 v_1 &= \frac{V_{dc}}{2} - v_s = \frac{1}{3} V_{dc} \\
 v_2 &= \frac{V_{dc}}{2} - v_s = \frac{1}{3} V_{dc} \\
 v_3 &= \frac{V_{dc}}{2} - v_s = -\frac{2}{3} V_{dc}
 \end{aligned} \tag{2.10}$$

It should be noted here that this is always true in the case of a sinusoidal current excited machine.

2.4.2 Conduction Interval

However, in the rectangular (120° conduction) current excited motors, during the conduction interval, there are two phases connected to DC rail [4]. As shown in Fig.2.4, when T5 and T6 are turned on, and there is no current in phase1, the terminal voltage at phase1 is equal to 0 but the phase voltage of phase1 is not equal to 0 because there is the back emf voltage of that phase. So the phase voltage of phase1 is equal to e_1 . Hence, the terminal voltages become

$$\begin{aligned} v_a = 0 &= L \frac{di_1}{dt} + Ri_1 + e_1 + v_s \\ v_b = -\frac{V_{dc}}{2} &= L \frac{di_2}{dt} + Ri_2 + e_2 + v_s \\ v_c = \frac{V_{dc}}{2} &= L \frac{di_3}{dt} + Ri_3 + e_3 + v_s \end{aligned} \quad (2.11)$$

And since $i_2=i_3$, the equations can be rearranged, and the star point voltage is obtained,

$$v_s = -\frac{(e_2 + e_3)}{2}$$

Hence, the winding voltages are given as

$$\begin{aligned} v_1 &= e_1 \\ v_2 &= -\frac{V_{dc}}{2} - v_s = -\frac{V_{dc}}{2} + \frac{(e_2 + e_3)}{2} \\ v_3 &= \frac{V_{dc}}{2} - v_s = \frac{V_{dc}}{2} + \frac{(e_2 + e_3)}{2} \end{aligned} \quad (2.13)$$

2.5 Current Control Mode

There are two methods to control the current of the motor: hysteresis control and pulse width modulation (PWM) control.

2.5.1 Hysteresis Control

As can be seen from the voltage equations of Brushless PM motor, the motor current cannot be constant because of the inductance and the back emf voltage of the windings. The principal idea of the current control is to make the current as close as possible to the reference current, in order to obtain a smooth torque. The principle of the hysteresis current control is to keep the actual current varying in a specified region

by turning on and off the electronic switches of the inverter. The hysteresis current control varies the current as shown in **Fig.2.5**. Here Δh is the specified region in which the actual current fluctuates.

The reference current in **Fig.2.5** is assumed to be the positive half cycle current of phase one, which uses the switches T1 and T4 to control the current. As seen in the figure, when T1 is turned on the reference current rises from zero. Since the actual current reaches the upper limit of the reference current, then the actual current declines through the diode D4 until it reaches the lower limit. This process is repeated until the end of the first half cycle of the reference current. As can be seen in **Fig.2.5**, if Δh is narrower, the actual current will reach the boundaries quickly. So turning on and off frequency of the semiconductor switch is higher, which means the accuracy of the actual current is better. However, if the switching frequency is high, the switching losses become significantly high. In addition, the switching frequency cannot be increased above the value for which the device is designed to operate.

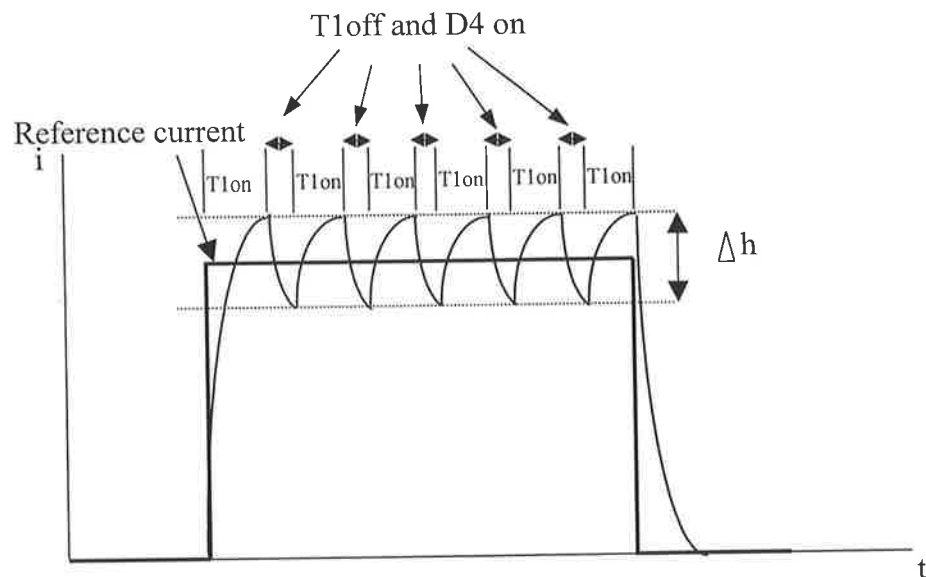


Figure 2.5 Hysteresis current control

2.5.2 PWM Current Control

In this method, the current error is used to adjust the actual current. The current error is the difference between the reference current and the actual current. **Fig.2.6** shows the current error and sawtooth waveform for phase1 of the motor. The basic control

principle is that the current error is compared with the sawtooth signal and PWM signals are generated. The current controller should make sure that the actual current follows the desired reference. The greatest advantage of this technique is that the switching frequency is limited by the frequency of the sawtooth waveform, and hence the switching losses can be limited.

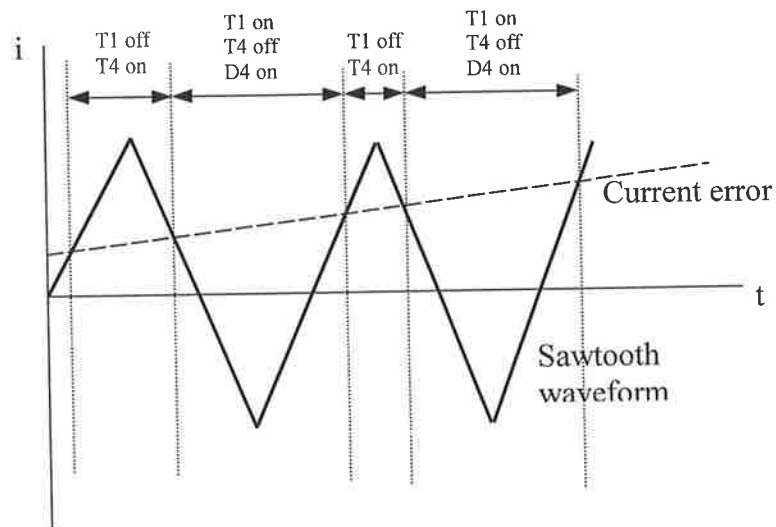


Figure 2.6 PWM waveform generation method

2.6 Conclusion

This chapter has introduced the fundamentals of the BLPM motor drive. Firstly, some basic features of BLPM motors were given and compared with the other motor types. Secondly, the equations of the BLPM motor were derived and given in a general form, which can be used in sinusoidal back emf and trapezoidal back emf PM motor.

The chapter has also shown how the motor works and why the shapes of the phase currents are important in the control. The inverter circuit, used to control BLPM motor, was explained. Finally, the concepts of the current control strategies were explained briefly. The next chapter will explain the current measurement techniques and the relationships between the switching signals and the current waveforms in a close loop motor control.

Chapter III

Current Measurement Techniques and Switching States in Three-phase Inverters

3.1 Introduction

As explained in Chapter 2, in order to control the torque of BLPM motors, the phase current must be controlled. Since the instantaneous torque is proportional to the instantaneous three-phase currents, to obtain a ripple free operation, an accurate knowledge of the currents is necessary. The most common method of measurement of current is to use low-value resistors or Hall-Effect current sensors. Since the BLPM motor usually has three phases, three current sensors are used. However, the Hall-Effect current sensors are expensive; using three of them might add a huge price to the motor drive. Although the low-value resistor is cheaper, the power loss in the resistors can be high and an additional electrical isolation circuits are required to interface with the controller.

There are many researches investigating to reduce the number of using current sensors. Evans and Hill-Cottingham, [5], investigated the relationship between the DC link current and the three-phase currents, and then revealed that it was possible to calculate the values of the three-phase currents from the values of the DC link current.

This thesis aims to study a method to reconstruct the three-phase current using a single current sensor. In this chapter, the current measurement techniques and the relationships between the DC link current and the three-phase currents are investigated in detail. Firstly, the chapter discusses the two current-measuring devices, and then extends the discussions to cover the most suitable locations for the sensors. Next, the literature relating to the analysis of the DC link current and the three-phase currents are explained. Finally, the chapter highlights and analyses the current paths of the possible switching states in the inverter circuitry.

3.2 Current Sensing Device

As stated earlier, a low value resistor or a Hall-Effect current sensor may be used in series with the motor line to obtain the instantaneous line current of the motor. The low-value resistor is cheaper and easier to install than Hall-Effect current sensor. When the low value resistance is connected in series with the motor line, the voltage across the resistor that is proportional to the current flows through it. This method offers low cost and accuracy, but no electrical isolation is provided. Moreover, depending upon the value of the resistor and the level of the current, the voltage drop across the resistor and the power loss in the resistor can be significant.

Hall-Effect devices provide electrical isolation and operate on the magnetic field that is generated by the current in the device. However, such sensors are expensive, especially when high bandwidth measurement is required.

Presently the development of power electronic device can produce intelligent device which has several functions in the same device. For example, in GS601 chip of half-bridge gate drive is the current sensor embeded [9]. However, the motor current does sometimes not circulate through the switching devices, the motor current is not known at the moment and most intelligent devices are expensive.

3.3 The Number of the Sensor and their Locations in the Inverter

Ideally, 4 current sensors are needed in a three-phase motor application: three on the lines and one on the DC link. **Fig.3.1** illustrates the possible locations of 4 current sensors. The three current sensors are placed on the motor lines because it is necessary to know the information of the three-phase currents for controlling the motor. However, another sensor on the DC link is added to detect the potential faults in the inverter circuit.

As shown in **Fig.3.1**, the DC link current sensor, sensor1, is required to detect the potential inverter of over current faults in the inverter. There are 3 types of the over current faults [6], as shown in **Fig.3.2**.

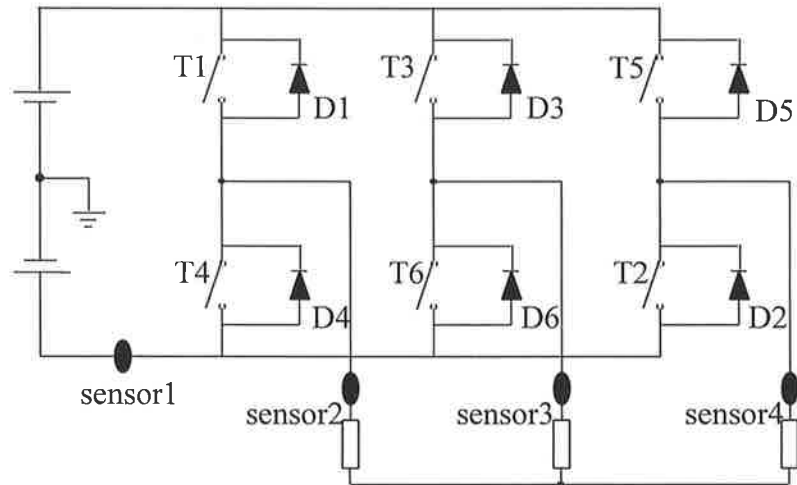
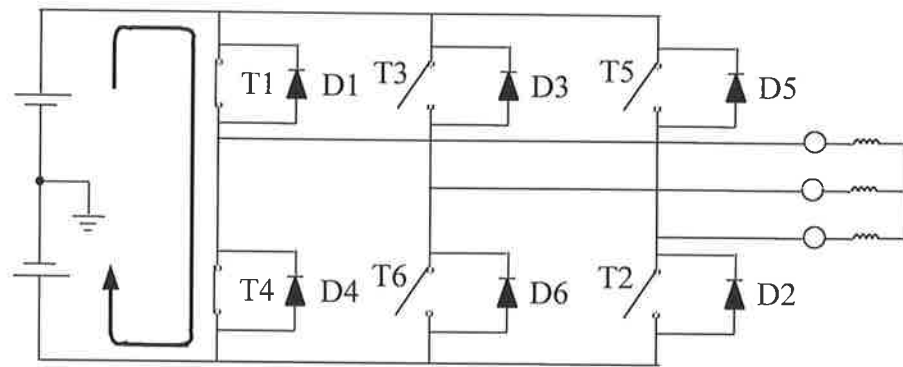
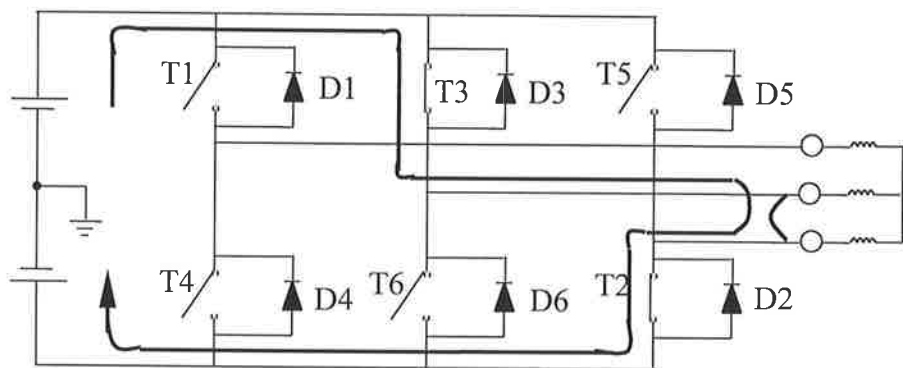


Figure 3.1 The position of 4 current sensors in the conventional three-phase inverter

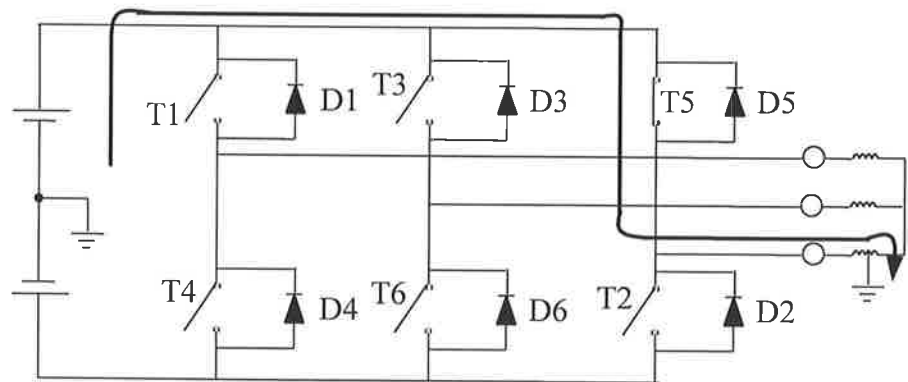
In **Fig.3.2(a)**, the Shoot-through fault may occur when the power switches, which control current in the same phase, are closed. Therefore, it should be remembered that the upper and the lower power switches on the same leg of the inverter must not be turned on at the same time, since a supply short-circuit occur. If the short circuit happens after the inverter circuit and before the motor circuit, the current flows and returns to the inverter without going through the motor circuit, as shown in **Fig.3.2(b)**. If the current flows from the inverter to the motor and returns to the ground as shown in **Fig.3.2(c)**, the DC link sensor located on the negative rail, as shown in **Fig.3.1**, cannot detect it. This is because the fault current does not flow through the DC link.



(a) The Shoot-through fault



(b) The line-to-line fault



(c) The ground fault

Figure 3.2 Potential fault current paths in the inverter

To detect all of the potential over-current faults and to determine the three-phase currents, various current measurement techniques are developed in the literature, which can be classified under 5 groups that are based on the number of current sensors in the power circuit.

1. **4-sensor method:** Three sensors are used for measuring each phase current in the motor and the fourth one is used to measure the DC link current for protective purposes, as shown in **Fig.3.1**.
2. **3-sensor method:** Two sensors are used to measure 2-phase of the three-phase currents of a star-connected motor. The third phase current is calculated from these measured currents since the summation of the three-phase currents of the motor is equal to zero. The third sensor is used to measure the DC link current.
3. **2-sensor method:** This technique employs two current sensors to measure the currents in the power switches and the currents in the diodes of the inverter separately, as shown in **Fig.3.3** [7]. However, this technique cannot measure the current if it circulates in the inverter and motor circuit only.

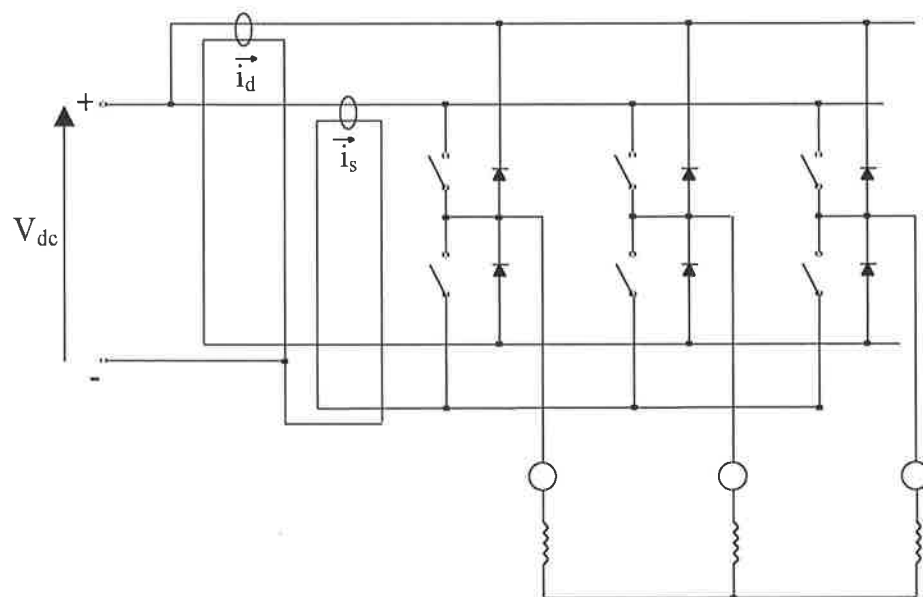


Figure 3.3 2-sensor method

4. **1-sensor method:** In this technique, the single current sensor is placed on the DC rail to measure the DC link current. Normally, it is on the negative DC rail. However, as shown in **Fig.3.2c**, when the ground fault occurs, the current sensor at the negative DC rail cannot detect the fault [8]. Therefore, an alternative connection is proposed in [9], which can overcome the limitations of the earlier connection, as illustrated in **Fig.3.4**. However, the drawback in [9] is that the current sensor measures the double amplitude of the DC link current. To solve

this problem, another circuit is proposed in [10]. Another winding is added in the current sensor to balance the effect of the current of the Hall-Effect current sensor at DC link point, as shown in Fig.3.5. Therefore, when the current is measured, the true amplitude of the DC link current is detected.

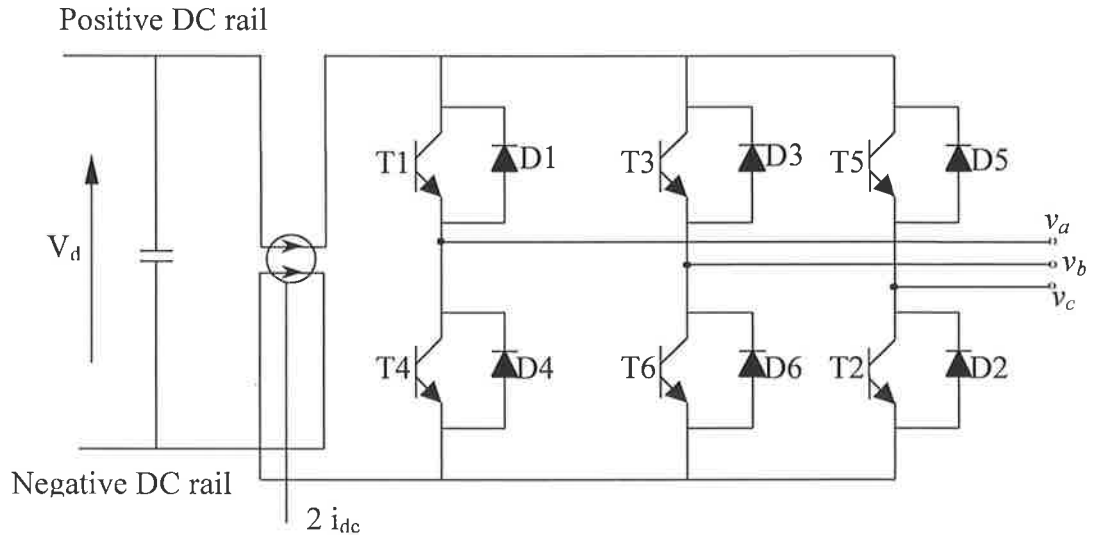


Figure 3.4 Circuit indicating the method of connection utilising a single sensor

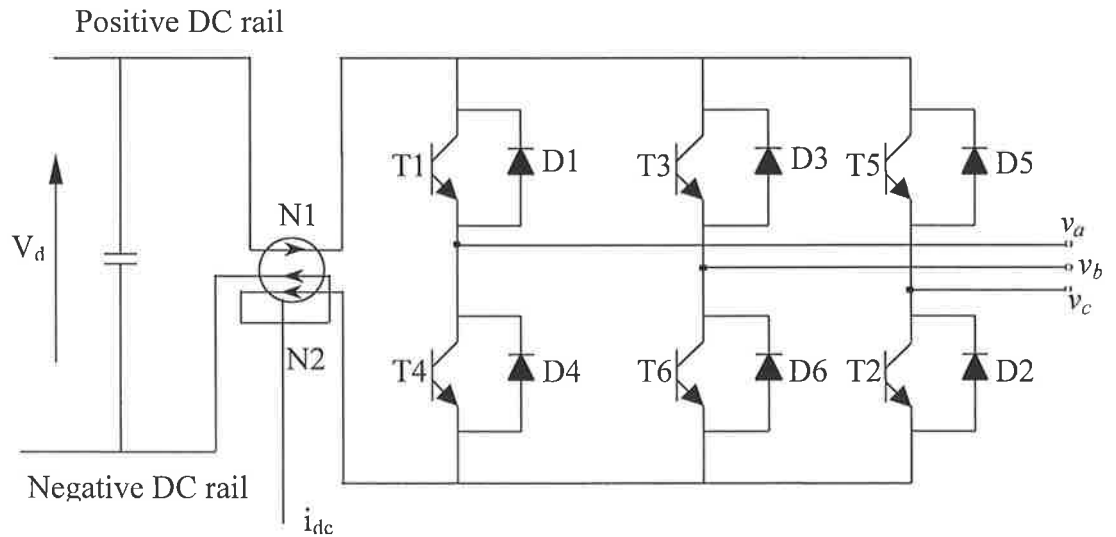


Figure 3.5 Equivalent circuit diagram to measure all possible current faults

5. **No separate current sensor:** Nowadays, it is possible to measure the currents in the power switches by using Intelligent Power Device, where the current sensors are integrated. Fig.3.6 illustrates the use of such devices in the inverter [11].

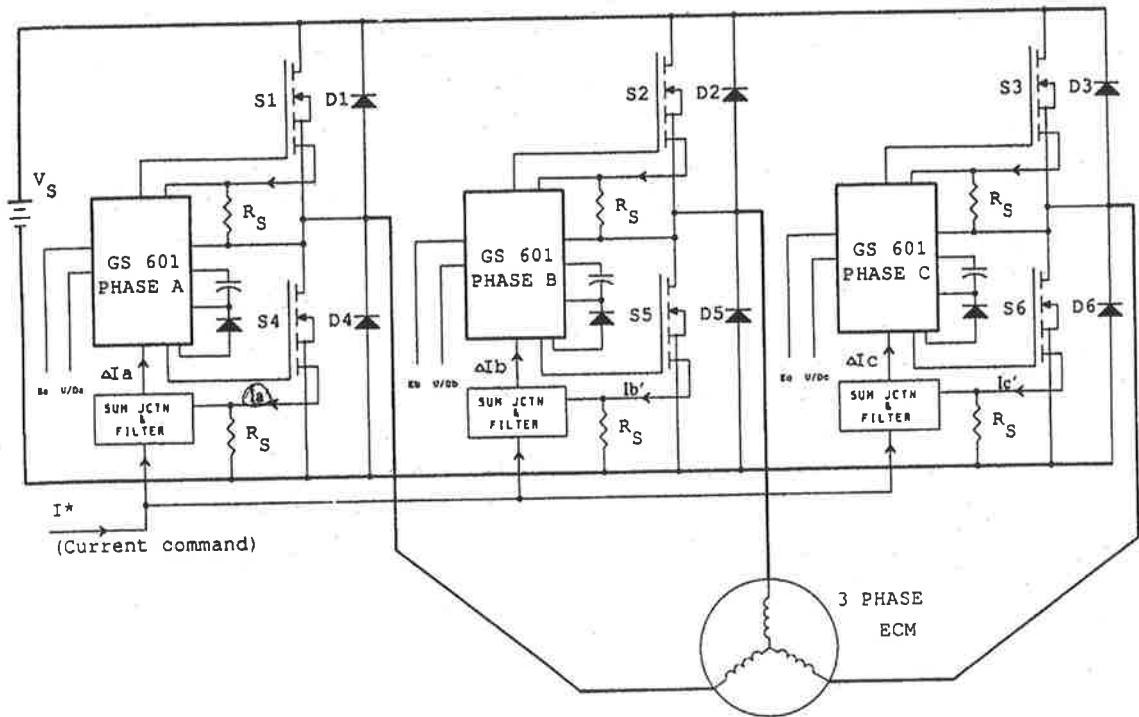


Figure 3.6 Diagram of the electronically commutated motor drive with the integrated current sensor

3.4 Literature Survey on the Use of DC Link Current

The relationship between the DC link current and three-phase currents is important for the method that uses single current sensor to find the three-phase currents since the single current sensor is placed at the DC rail to measure the DC link current. Several researchers have investigated the relationship between the DC link current and the three-phase currents.

Evan and Hill-Cottingham [5] first investigated the analysis of DC link current in 1986. This study also investigated and highlighted the relationships among the three phase currents, the switching signals and the DC link currents in the PWM inverter as shown in **Fig. 3.7**. It was thought that since the DC link current is used to detect the short circuit current in the inverter, there had to be some information to find the winding currents.

After the method proposed, Boys [12] also attempted to find the winding currents from the average value of the DC link current. However, no detailed analysis was

done to find the relationships between the switching patterns and the winding currents. This study did not recognise that there was no DC link current in some switching states of the inverter.

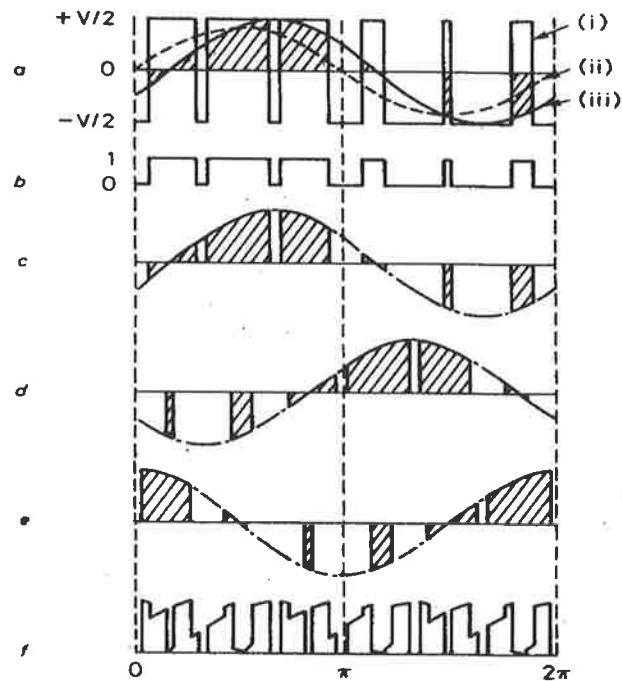


Figure 3.7 DC link current in three-phase PWM inverter

- (a) The voltage of an inverter leg
- (b) The fundamental component of the leg voltages
- (c) DC link current in phase one
- (d) DC link current in phase two
- (e) DC link current in phase three
- (f) Total DC link current

Following this study, Kavanagh et al [13] proposed an alternative method to determine the winding currents by the analysis of the conducting states of the bridge inverter. Although it was reported that there was no DC link current in some states of the inverter, no solution was proposed to overcome this limitation. Green and William [14] also analysed the relationship of the DC link current and the switching pattern in detail and recognised that there was no DC link current in some of the switching states of the inverter. However, no solution was suggested in this study either.

In the following subsections, the methods to find the winding currents from the DC link current information are classified.

3.4.1 Voltage Space Vector

This is the most popular method, mainly used in PWM current control. It has been shown that there are 8 switching patterns of the PWM current control, as stated earlier in the switching pattern section. If the switching patterns are converted into the vector forms [15], the following list can be obtained:

| | |
|-------------------|--------------------------------------|
| $V_1 = [1, 0, 0]$ | means T_1, T_6, T_2 are turned on. |
| $V_2 = [1, 1, 0]$ | means T_1, T_3, T_2 are turned on. |
| $V_3 = [0, 1, 0]$ | means T_4, T_3, T_2 are turned on. |
| $V_4 = [0, 1, 1]$ | means T_4, T_3, T_5 are turned on. |
| $V_5 = [0, 0, 1]$ | means T_4, T_6, T_5 are turned on. |
| $V_6 = [1, 0, 1]$ | means T_1, T_6, T_5 are turned on. |
| $V_7 = [0, 0, 0]$ | means T_4, T_6, T_2 are turned on. |
| $V_8 = [1, 1, 1]$ | means T_1, T_3, T_5 are turned on. |

The relationship between the Vector State and the DC link current is shown in **Table 3.1**.

Table 3.1 Vector states and corresponding phase currents.

| State | i_{dc} |
|-------|----------|
| 1 | $+i_a$ |
| 2 | $-i_c$ |
| 3 | $+i_b$ |
| 4 | $-i_a$ |
| 5 | $+i_c$ |
| 6 | $-i_b$ |
| 7,8 | 0 |

Although this method is effective when it is used in PWM switching strategy, it is not effective in other switching methods, since only 8 switching states are recognised. In addition, the Voltage Space Vector analyses only the switching patterns, not the current conduction states.

3.4.2 Switching State Analysis

In the work reported by Becerra et al [16], only two-phase currents in any instant have been considered. The switching states have been categorised into two groups: one-switch active state and two-switch active state. One-switch active means that only one-power switch is turned on and there are currents flowing through that power switch and another diode, as shown in **Fig.3.8a**. Two-switch active means two power switches are turned on and there are currents flowing through both of the switches, as shown in **Fig. 3.8b**. However, this analysis also has limitations since not all the inverter states have been considered, such as three-switch active state.

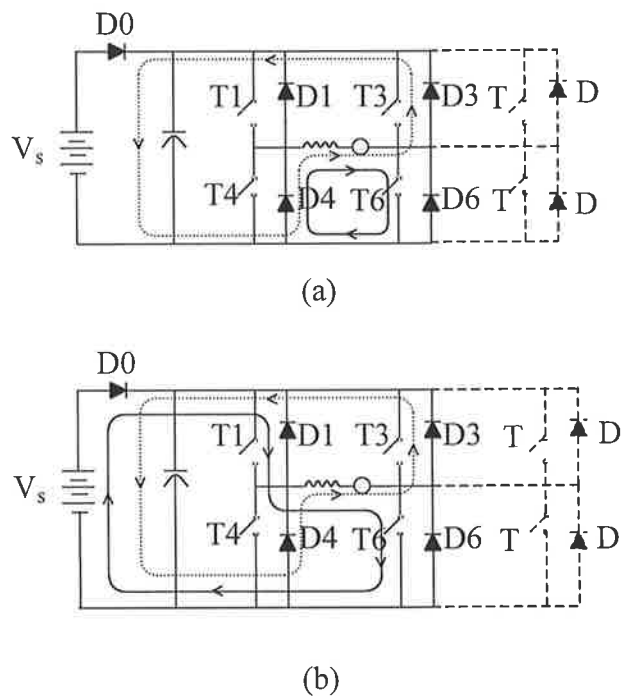


Figure 3.8 Equivalent circuits for “one switch active (T6) state” (a),
“two switch active (T1 and T6) state” (b)

3.5 The Relationship between the Phase Currents and the DC Link Current

As shown in the previous section, it is possible to use a single current sensor to detect the possible faults in the inverter. However, the determination of the phase current using a single sensor requires further analysis. In this subsection, the relationship

between the DC link current and the output currents of the inverter will be studied with the aim of determining the phase currents.

When the power switches in the inverter are turned on, the currents flow to the motor circuit. However, the currents do not always flow through the power switches that are turned on. Due to the stored energy in the inductances of the windings, the currents try to keep the same direction as the previous state. For example, in **Fig.3.9**, T3 and T2 are turned on and the currents flow through them. Then, T5 and T6 are suddenly turned on, the currents still flows in the same direction due to the finite inductance of the windings. Therefore, the currents flow through D5 and D6, as shown in **Fig.3.10**.

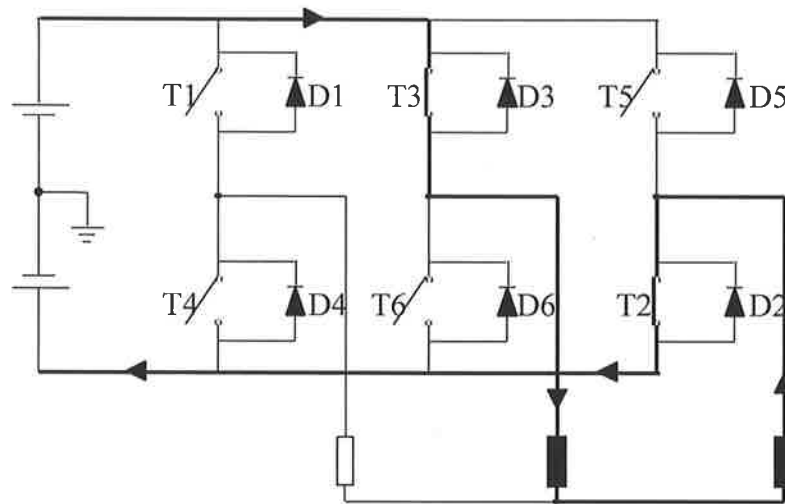


Figure 3.9 Current flow path in the inverter when T2 and T3 are turned on

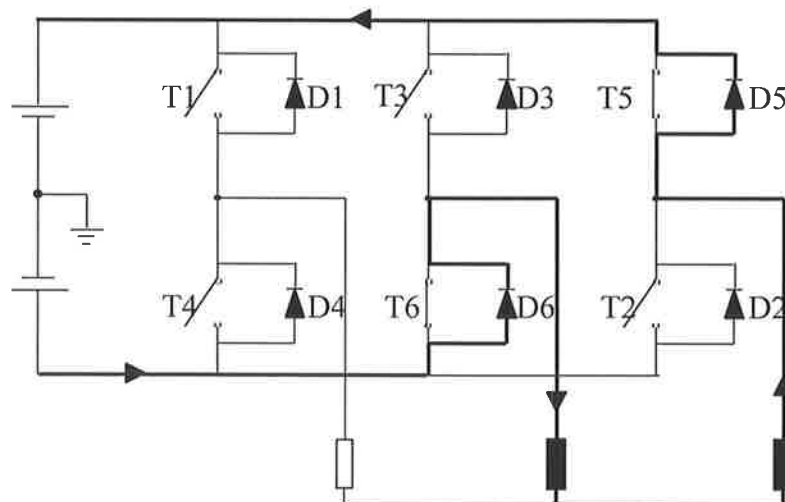


Figure 3.10 Directions of the currents in phase2 and 3 when D5 and D6 are conducting current.

Moreover, in some states of the inverter, the currents may circulate inside the inverter circuitry, not flowing through the DC link. Furthermore, in some states both DC link current and circulating current may flow. This means that the status of the DC link current can be linked to the status of the power switches and the direction of the three-phase currents of the motor. In the following subsection, all the possible patterns of the switching devices, the directions of the winding currents and the DC link current are described.

3.5.1 Switching Pattern

The flowing paths of the currents are mainly determined by the previous state of the switches, which influences the paths due to the inductances of the windings. However, switching pattern, which is the status of the power switches in the inverter circuit, still plays an important role to indicate the status of the switching.

Table 3.2 indicates all possible switching patterns in the inverter. Three fundamental states can be defined: state O, state U and state L. In these definitions: state O means no switching device is on; state U means one of the switching devices on the upper rail is on; state L means one of the switching devices on the lower rail is on. It should be highlighted here that state U or L does not tell us whether the direction of the current in the phase is positive or negative. Therefore, the DC link current cannot be predicted from only the information of the switching pattern.

From **Table 3.2**, Row number 1 means there is no power switch turned on. In this pattern, it cannot tell that whether there are currents in the motor. If there are currents flowing through in the inverter, the currents can flow through only diodes. Row number 2 to 7 are the one-switch active state. This means that only one power switch of 6 switches of the inverter is turned on. The one-switch active does not appear in motor control topology, the hysteresis or PWM motor control. Row number 8 to 19 are two-switch active states. This means that two switches in the inverter are turned on. These switching patterns occur in the hysteresis motor control. Row number 20 to 27 are three-switch active states. This means three switches of the three-phase inverter are turned on. These switching patterns can occur in the hysteresis or PWM control method.

3.5.2 Current Direction Pattern

Generally, the direction of the phase currents in the motor winding can be estimated from the switching state of the transistors. However, as explained before, due to the inductance in the motor circuit, the current may not flow through the turned-on power switches. Currents may flow through only diodes or diodes and transistors.

Table 3.2 Summary of the switching patterns in the inverter

| No. | Phase 1 | Phase 2 | Phase 3 |
|-----|---------|---------|---------|
| 1 | O | O | O |
| 2 | U | O | O |
| 3 | O | U | O |
| 4 | O | O | U |
| 5 | L | O | O |
| 6 | O | L | O |
| 7 | O | O | L |
| 8 | U | U | O |
| 9 | U | O | U |
| 10 | O | U | U |
| 11 | L | L | O |
| 12 | L | O | L |
| 13 | O | L | L |
| 14 | U | L | O |
| 15 | L | U | O |
| 16 | L | O | U |
| 17 | U | O | L |
| 18 | O | U | L |
| 19 | O | L | U |
| 20 | U | L | L |
| 21 | L | U | L |
| 22 | L | L | U |
| 23 | L | U | U |
| 24 | U | L | U |
| 25 | U | U | L |
| 26 | U | U | U |
| 27 | L | L | L |

Table 3.3 Possible states of the directions of the current in the motor phases

| No. | Phase 1 | Phase 2 | Phase 3 |
|-----|---------|---------|---------|
| 1 | 0 | 0 | 0 |
| 2 | + | + | - |
| 3 | + | 0 | - |
| 4 | + | - | + |
| 5 | + | - | 0 |
| 6 | + | - | - |
| 7 | 0 | + | - |
| 8 | 0 | - | + |
| 9 | - | + | + |
| 10 | - | + | 0 |
| 11 | - | + | - |
| 12 | - | - | + |
| 13 | - | 0 | + |

A number of current direction patterns can be identified in the inverter, which are listed in **Table 3.3**. In the table, “0” means there is no current in that phase, “+” means the phase current is flowing from the inverter to the motor circuit, and “-” means that the phase current is flowing from the motor to the inverter circuit. Each of the current direction patterns in **Table 3.3** may occur with any switching pattern in **Table 3.2**. Therefore, there are 351 possible switching states in total.

3.5.3 Conducting Devices and the DC Link Current

The conducting device and the DC link current are the most important parts in the analysis of switching states. After the analysis of the switching patterns and the current direction pattern are done, the current conduction states of transistors and diodes can be determined. Moreover, it can be seen whether there is the DC link current and circulating current within the inverter in the considered state, and in which phase the amplitude is equal to the DC link current amplitude. The relationship between the conducting devices and the DC link current by the complete switching state analysis is shown below.

1) Zero-switch active

From the first row of the switching pattern in **Table 3.2** (zero-switch active), if there are currents in the windings, they flow through only diodes, and every current direction pattern has DC link current.

2) One-switch active

In one-switch active pattern, some of the switching states have only the DC link current, some have the DC link current and circulating current, and some have only the circulating current. This depends on the current directions. For example, if the switching pattern is U, O, O and the current direction is +, +, -, the upper power switch of phase1, the lower diode of phase2 and the upper diode of phase3 are conducted. That makes the amplitude of the DC link current equal to the amplitude of the current of phase2 and there is a circulating current flowing within the inverter, where the amplitude is equal to the amplitude of the current of phase1. **Fig.3.11** shows the diagram when the switching pattern is U, O, O and the current direction pattern is +, +, -.

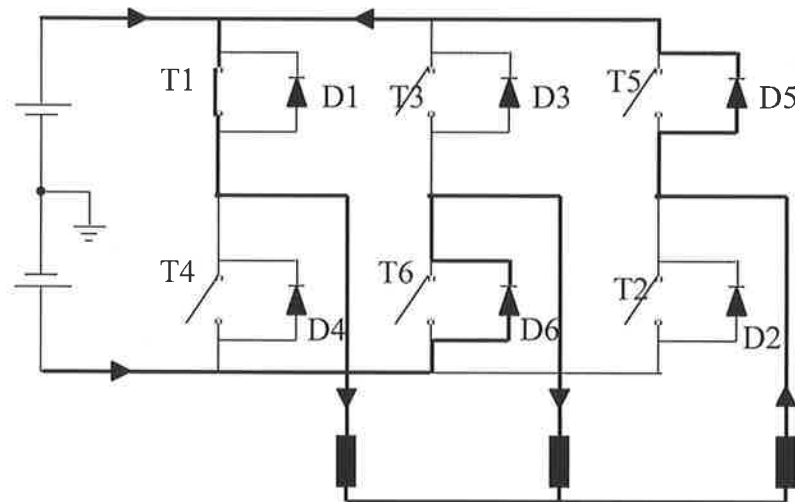


Figure 3.11 Diagram when the switching pattern is U, O, O and the current direction pattern is +, +, -.

In the case where the switching pattern is U, O, O and the current direction is -, -, +, the winding currents flow through only diodes and only the DC link current occurs. There is no circulating current. The amplitude of the DC link current is equal to the amplitude of phase3 current. **Fig.3.12** shows the diagram when the switching pattern is U, O, O and the current direction is -, -, +.

In the case where the switching pattern is U, O, O and the current direction is +, -, -, the currents flow through the upper power switch in phase1, the upper diode in phase2 and the upper diode in phase3. The currents flow only in the upper side of the inverter. In such case, there is no DC link current and only circulating current within the inverter. **Fig.3.13** shows the diagram when the switching pattern is U, O, O and the current direction is +, -, -.

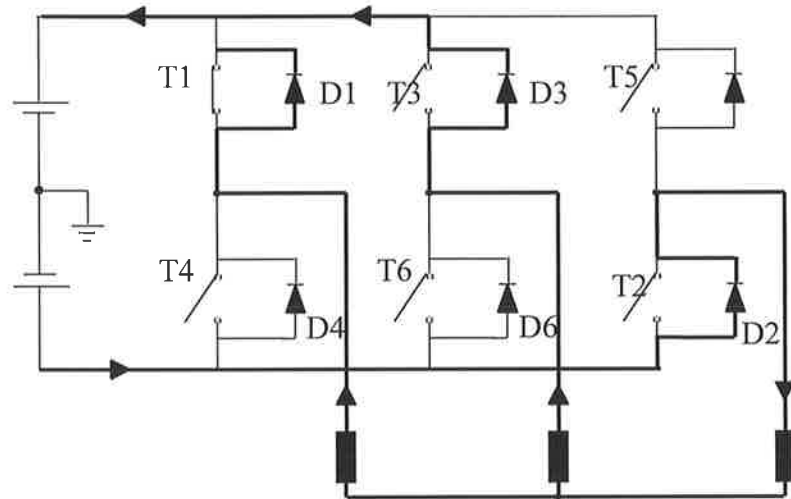


Figure 3.12 Diagram when the switching pattern is U, O, O and the current direction is -, -, +.

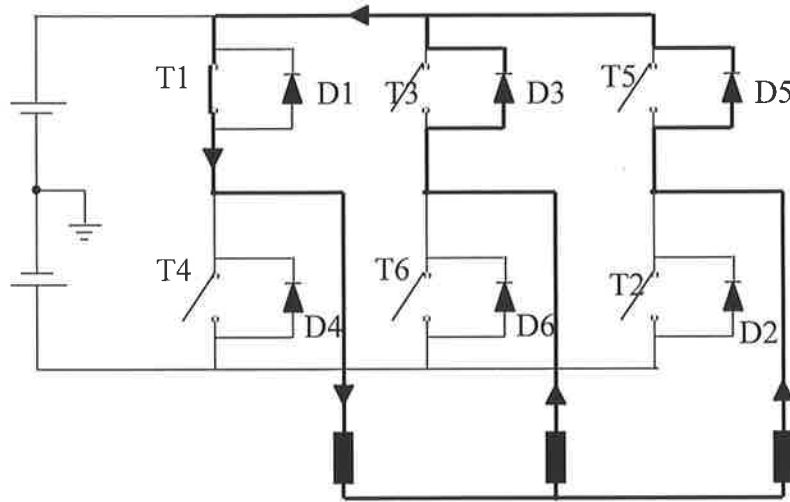


Figure 3.13 Diagram when the switching pattern is U, O, O and the current direction is +, -, -.

3) Two-switch active

In the case of a two-switch active, if the power switches are turned on at the both sides of the inverter, there is a DC link current in every switching state. For example, when the switching pattern is O, U, L and the current direction is 0, +, -, the winding currents flow through the upper switch in phase2 and the lower switch in phase3, as in **Fig.3.9**. In this case, the positive DC link current happens without the circulating current. In another case, as in **Fig.3.10**, the switching pattern is O, L, U and the current is 0, +, -. The winding currents flow through only diodes and the negative DC link current occurs without the circulating current.

On the other hand, if the power switches connected to the same DC rail are turned on at the same time, most of the switching states have the circulating current and some states have the DC link current. For example, when the switching pattern is U, U, O and the current direction is +, +, -, as in **Fig.3.14**, the winding currents flow through the power switches and the diode at the upper side of the inverter and the currents circulate only in the inverter and the motor circuit.

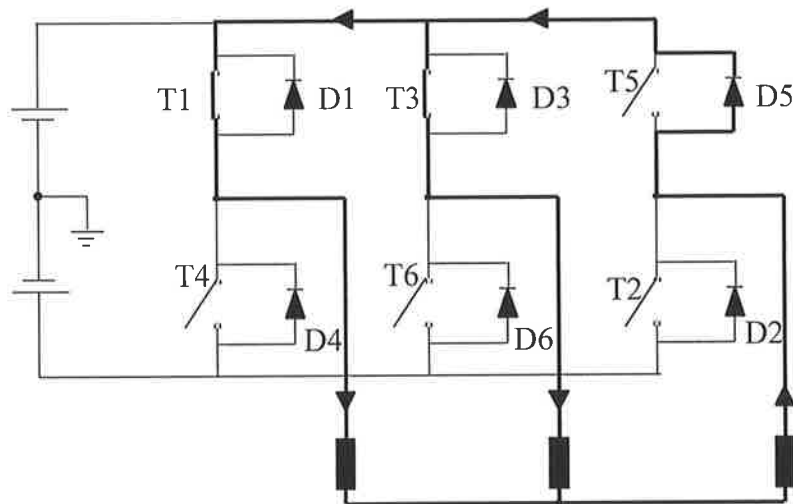


Figure 3.14 Diagram when the switching pattern is U, U, O and the current direction is +, +, -.

In the case where the switching pattern is U, U, O and the current direction is +, -, +, (as shown in **Fig3.15**), the winding currents flow through the upper power switch in phase1, the upper diode in phase2 and the lower diode in phase3. Since the conducting devices are on the opposite side of the inverter, the winding current can flow from the negative DC rail passing the diodes to the positive DC rail and the DC

link current can occur. However, when the conducting devices are diode and power switch and they are on the same side of the inverter, the circulating current can flow through them.

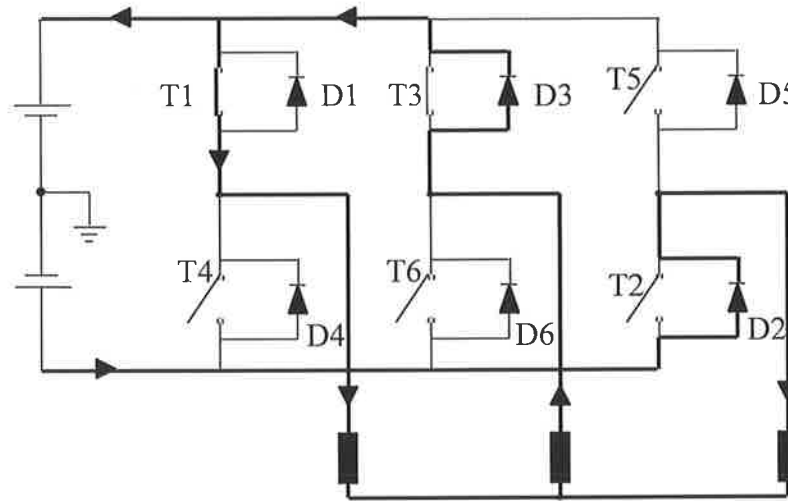


Figure 3.15 Diagram when the switching pattern is U, U, O and the current direction is +, -, +

4) Three-switch active

In the case of a three-switch active, if three switches connected to the same DC rail of the inverter are turned on, there is no DC link current. However, most of the switching states in this case have the DC link current. For example, when the switching pattern is U, L, U and the current direction is +, -, +, as shown in **Fig.3.16**, the winding currents flow through the upper power switch in phase1, the lower power switch in phase2 and the upper power switch in phase3. The amplitude of the DC link current is equal to the amplitude of the phase2 current.

However, when the switching pattern is changed to the U, U, L and the current direction is still +, -, +, as shown in **Fig.3.17**, the conducting devices are the upper power switch in phase1, the upper diode in phase2 and the lower diode in phase3. Therefore, the amplitude of the DC link current is equal to the amplitude of phase3 current and there is the circulating current in the inverter.

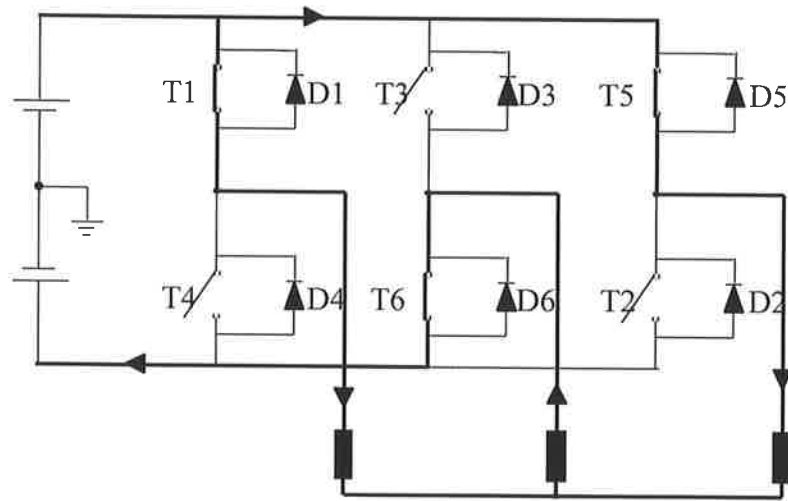


Figure 3.16 Diagram when the switching pattern is U, L, U and the current direction is +, -, +

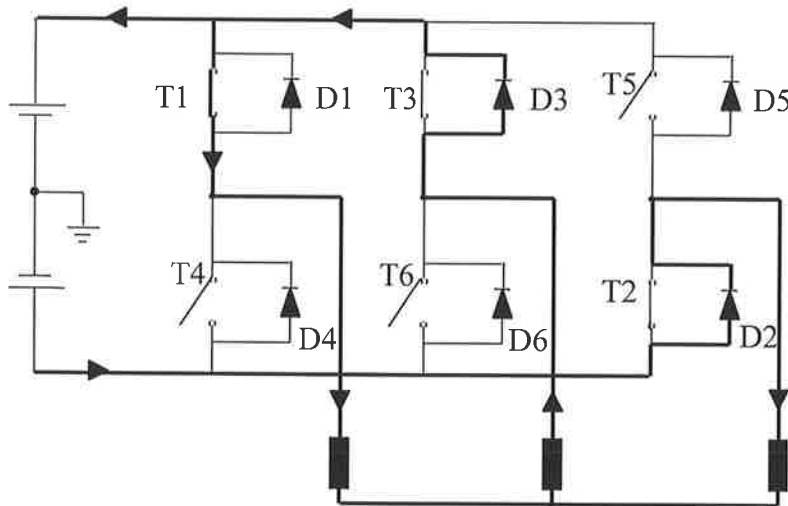


Figure 3.17 Diagram when the switching pattern is changed to the U, U, L and the current direction is still +, -, +

This is a partial analysis of the switching state in the inverter circuit. Whole of the analysis is demonstrated in **Table A-1**, Appendix A. The table shows the switching pattern, the current direction, the conducting device, the phase number, of which the current amplitude is equal to the amplitude of the DC link current, and the phase number, of which the current amplitude is equal to the amplitude of the circulating current.

3.6 Conclusion

The chapter has presented a basic introduction to current measurement techniques and current sensor used in motor control applications. As indicated, although using the low-value resistor is cheaper than other methods, the power loss and the voltage drop on the resistors should be considered in the design. In addition, if electrical isolation is required, the resistor method is not preferred. The Hall-Effect device, however, provides isolation but its cost can be significant, specifically at the high bandwidth current measurement applications.

Various methods are suggested in the literature, which aim to reduce the number of current sensors. However, most of the methods have limitations, such as not considering all possible inverter faults. The chapter has also provided comprehensive information about the inverter, switching patterns, the directions of the currents in the motor circuit and the relationship between the DC link current and the phase currents. It was also indicated that it is possible to reconstruct the phase current considering the current conduction states of the components in the inverter circuit by measuring the DC link current only.

Chapter IV

Computer Simulation of the Motor Drive and Reconstruction of Phase Currents

4.1 Introduction

In Chapter 2, the mathematical model of the Brushless Permanent Magnet (BLPM) motor was described, including the relationship between the electromagnetic torque and phase currents. In addition, the principal control methods of BLPM motor were explained. As can be seen, the information can be utilised to develop a computer model of the motor drive to study the current reconstruction techniques without implementing the hardware. The simulation can also allow the operator to introduce artificial faults.

The LabVIEW program is selected as a tool to simulate the entire motor drive. As will be demonstrated later, LabVIEW allows us to construct software modules to achieve various tasks easily. The software modules are named "SubVI", which can be called from other modules to process the data in the input and output data to the other modules or to the user interface.

Firstly, this chapter explains the general structure of the simulation system and the block diagram. Secondly, the details of the "SubVIs" implemented in this study are given. The input and output data and the objectives of each SubVI are also explained in this section. Finally, some comprehensive simulation results are provided. These results demonstrate that the simulation of the motor drive and the current reconstruction method proposed here are valid under various operating conditions.

4.2 Basic Layout of the Simulation Model

The principal purpose of this thesis is to reconstruct the three-phase current of the motor from the DC link current. To test and investigate various operating conditions, a complete computer simulation of the motor drive was implemented.

As discussed previously, there was a requirement to obtain accurate phase currents after reconstruction, but the earlier current reconstruction methods in the literature had some limitations. When three-phase currents circulate only in the inverter and motor circuit, there is no the information of the DC link current to use to reconstruct the three-phase currents.

Fig.4.1 illustrates the general block diagram of the computer simulation system. The simulation study models 2 motors: Master Motor and Motor Model that is also used to simulate the currents in the real system. The three-phase currents of Master Motor is reconstructed; Motor Model is a motor simulator of Master Motor. Thus, the values of the three-phase currents of Motor Model are near those of Master Motor. However, in the practical system, noises and non-ideal factors can cause the currents of Master Motor be distorted. Therefore, the three-phase currents of Motor Model are not equal to those of Master Motor.

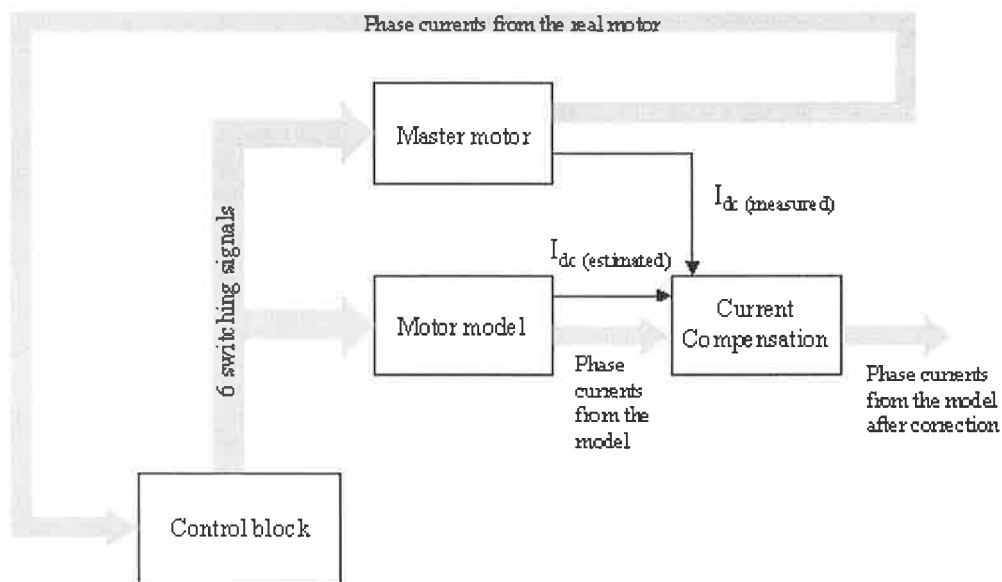


Figure 4.1 Block diagram of the simulation of the motor drive and current reconstruction

The simulated DC link current can determine whether the currents of Motor Model are now different from the currents of Master Motor. If the DC link current indicate that the three-phase currents of Motor Model are not equal to those of Master Motor, the three-phase currents of Motor Model are modified to make the currents equal to the currents of Master Motor. Therefore, the three-phase currents of Motor Model are

link to the current compensation block to be compensated by using the information of the DC link current, $I_{dc(\text{measure})}$, from Master Motor.

As seen in the figure, the DC link current from Master Motor and Motor Model and the simulated three-phase currents from Motor Model links to the current compensation block. This block outputs the reconstructed three-phase currents. It should be noted here that the estimated and the measured DC link currents are identical under ideal conditions, which are calculated from mathematics equations in chapter2.

The objective of this exercise is to know whether the reconstructed currents from the above concept are similar to the three-phase currents of Master Motor. Thus, the feedback currents to the control block are the three-phase currents from Master Motor. After the control block receives the feedback currents, it generates 6 switching signals to control the motors.

4.3 Motor Simulation Program

There are 2 motor drives, Master motor drive and Motor Model drive, in the computer simulation of the current reconstruction algorithm. This section explains the details of the simulation program of the motor drive. **Fig.4.2** shows the block diagram of the main loop of the simulated motor drive. As can be seen in the figure, the main Virtual Instrument (VI), there are 5 major subroutines (SubVIs) operating the motor drive: PID SubVI, Chg point SubVI, Drive SubVI, Current control SubVI and Motor SubVI. Moreover, there are 2 minor subroutines to show or change the unit of the motor parameters: ω and rpm SubVI, and TPS SubVI. These SubVIs will be explained briefly below.

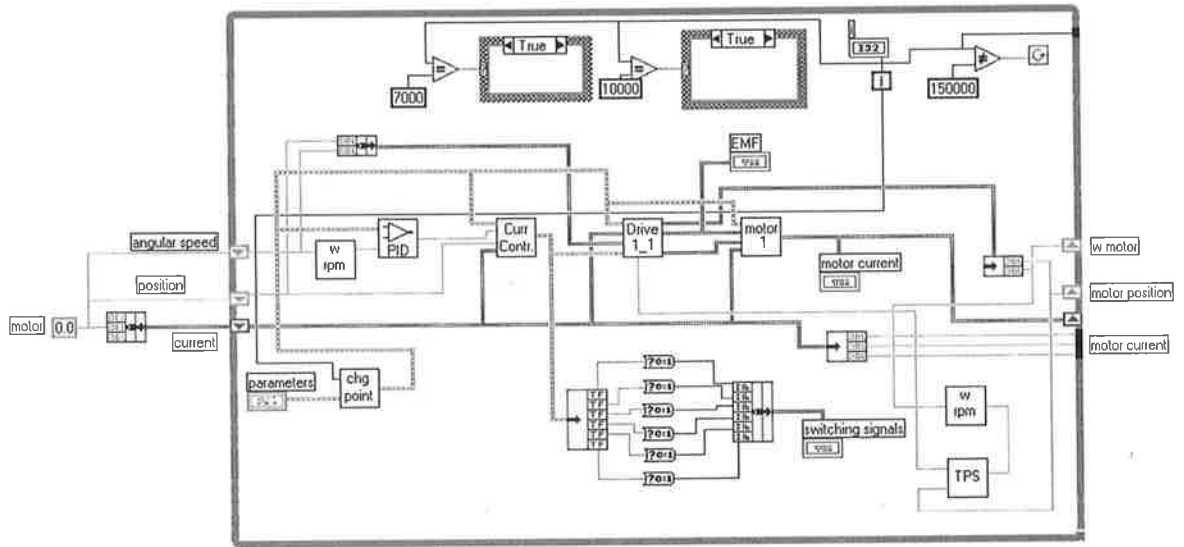


Figure 4.2 Main loop program of the simulated motor

1. **PID SubVI:** The function of this SubVI is to calculate the maximum values of the winding currents. The inputs to the SubVI are the reference speed and the actual speed of the motor.

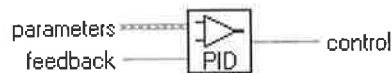


Figure 4.3 PID SubVI (See Appendix A-2)

2. **Chg point SubVI:** The function of this SubVI is to introduce the dynamic state to the simulation program by changing some parameters of the motor while the motor is operating. It can be set the point which the dynamic state introduces.



Figure 4.4 Chg point SubVI (See Appendix A-2)

3. **Current control SubVI:** This module produces the switching signals for the inverter switches. The SubVI receives and then compares the value of the reference currents and actual currents. As explained earlier in the thesis, the error, the difference between reference current and the actual current, is used to generate hysteresis and PWM current control signals.

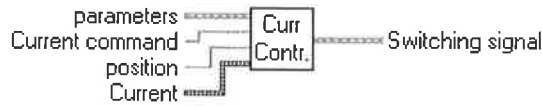


Figure 4.5 Current control SubVI (See Appendix A-2)

4. **Drive SubVI:** This module calculates the speed, the rotor position, the electromagnetic torque, the emf voltages, and the DC link current. Then it outputs the data to the Motor SubVI.

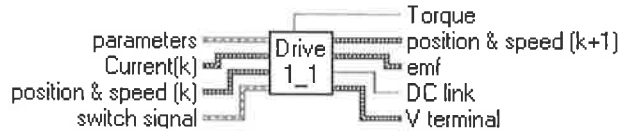


Figure 4.6 Drive SubVI (See Appendix A-2)

5. **Motor SubVI:** This SubVI calculates the three-phase currents, based on the equations given earlier in Chapter2, Eq2.1.

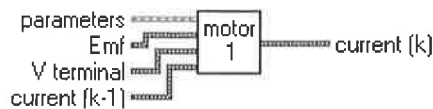


Figure 4.7 Motor SubVI (See Appendix A-2)

6. **ω and rpm SubVI:** This SubVI converts the angular speed (ω) of the motor drive from radian per second to round per minute (rpm). As shown, the output of this SubVI is linked to the PID SubVI as an input.



Figure 4.8 ω and rpm SubVI (See Appendix A-2)

7. **TPS SubVI:** This SubVI shows the value of the electromagnetic torque, position and speed of the motor in the graphs.

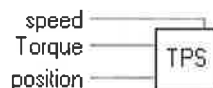


Figure 4.9 TPS SubVI (See Appendix A-2)

Two of the SubVIs, Motor SubVI and Drive SubVI, are the principal components of the simulation. Therefore, they will be explained in detail. Fig.4.10 and Fig.4.11 show the block diagram of these SubVIs. As seen in these figures, the SubVIs have also made of a number of other SubVIs and functions.

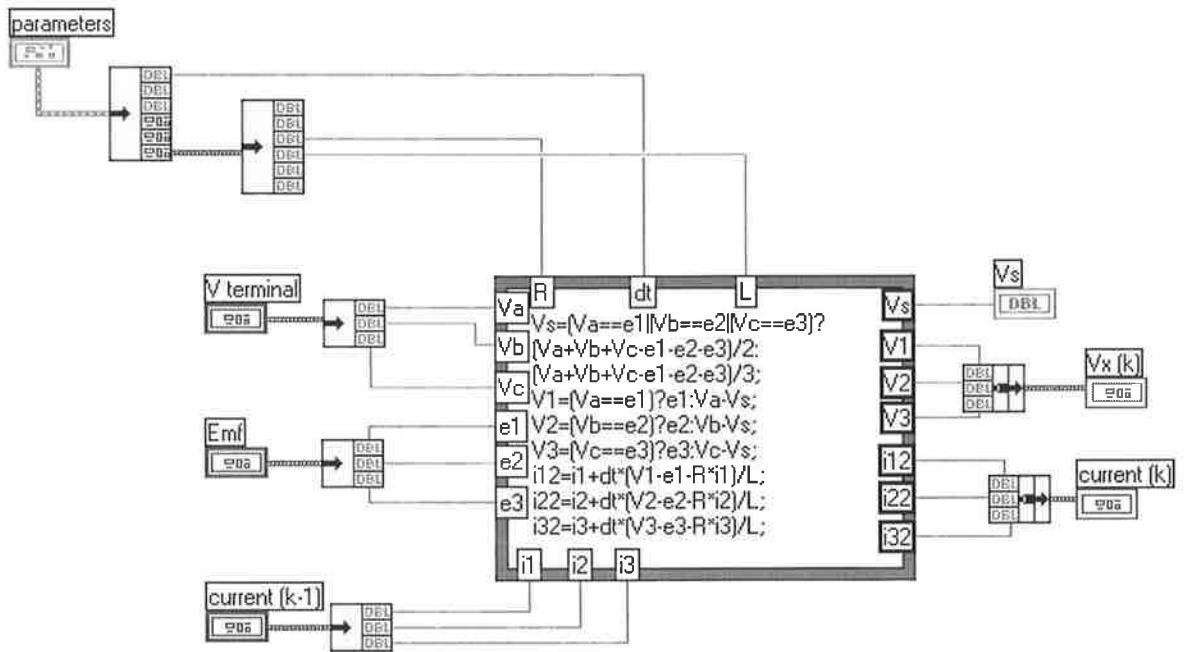


Figure 4.10 Block diagram of Motor SubVI

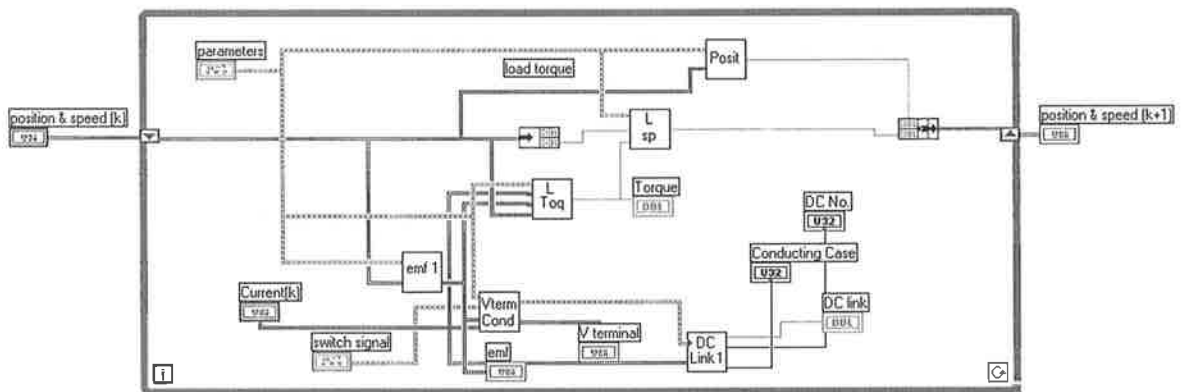


Figure 4.11 Block diagram of Drive SubVI

4.3.1 Motor SubVI

The objective of the motor simulator is to simulate the three phase currents of Master Motor. As seen in **Fig.4.10**, **Eq.2.1** is used to calculate the motor currents in the simulation. As is well known, the motor's differential equations can be solved numerically to determine the current values. A simple discrete integration method was used in this study, which requires knowledge of the current value at the previous time step. Therefore, a shift register was implemented in LabVIEW programming to determine the current. The equations used to calculate the three-phase currents are given below.

$$\begin{aligned}\frac{di_1}{dt} &= i_{1(n)} - i_{1(n-1)} \\ \frac{di_2}{dt} &= i_{2(n)} - i_{2(n-1)} \\ \frac{di_3}{dt} &= i_{3(n)} - i_{3(n-1)}\end{aligned}\quad (4.1)$$

Here, i_1 , i_2 and i_3 are the currents of phase 1, 2 and 3 respectively, n is the number of integration samples ($n = 0, 1, 2, \dots$), and $n-1$ represents the previous value of the currents.

However, to calculate the phase currents, the terminal voltages, the back emf voltages, R , L , Δt and the initial values of the currents must be known. The values of R , L and the time step (Δt), are constant. The terminal voltages and the back emf voltages are calculated by using the values of the switching states and the motor position from Drive SubVI.

4.3.2 Drive SubVI

As stated above, this SubVI produces the data of rotor position, rotor speed, electromagnetic torque, DC link current and three-phase terminal voltages for the correct operation of the motor. As shown in **Fig.4.11**, there are 6 SubVIs in this SubVI.

1. **Emf SubVI:** This module produces the emf voltage within Drive SubVI.

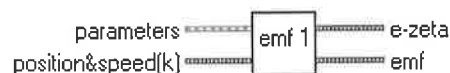


Figure 4.12 Emf SubVI (See Appendix A-2)

2. **Torque SubVI:** This SubVI calculates the electromagnetic value from the torque equation, given in Eq.2.6. It receives $e_1(\theta_e)$, $e_2(\theta_e)$ and $e_3(\theta_e)$ from Emf SubVI, and the values of the phase currents from the previous time step. In addition, the back emf constant, k_e , is a parameter provided as an input to this SubVI. Then, this module processes the input data and generates the torque value at a given time step.

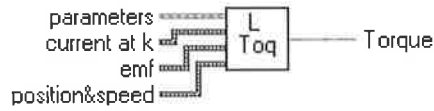


Figure 4.13 Torque SubVI (See Appendix A-2)

3. **Speed SubVI:** This module calculates the speed by using the motion equation, given in Eq.2.7. In this SubVI, the damping coefficient is assumed to be zero because it is small and generally to be neglect. The electromagnetic torque value, T_e , from Torque SubVI, and the load torque, T_L , and the moment of inertia, J , are the inputs to this SubVI. $\Delta\omega$ is the change in the speed and equal to $\omega_n - \omega_{n-1}$. The speed at the time step n is estimated by

$$\omega_n = \left[\frac{(T_e - T_L)}{J} \right] \cdot \omega_{n-1}$$

$$\frac{d\omega}{dt} = \frac{T_e - T_L}{J} \quad (4.2)$$

$$d\omega = dt \left(\frac{T_e - T_L}{J} \right)$$

$$\omega_n = \omega_{n-1} + dt \left(\frac{T_e - T_L}{J} \right)$$

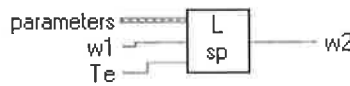


Figure 4.14 Speed SubVI (See Appendix A-2)

4. **Position SubVI:** This SubVI calculates the mechanical rotor position, θ_m , which is used to estimate the speed data estimated above. Since $\theta_e = p \cdot \theta_m$ (p = pole pairs), the electrical position, θ_e , can easily be calculated. The position equation in this SubVI is given by

$$\theta_n = \theta_{n-1} + p \cdot \omega \cdot \Delta t \quad (4.3)$$

$$\frac{(\theta_n - \theta_{n-1})}{dt} = p \cdot \omega$$

$$\theta_n - \theta_{n-1} = dt \cdot p \cdot \omega$$

$$\theta_n = \theta_{n-1} + dt \cdot p \cdot \omega$$



Figure 4.15 Position SubVI (See Appendix A-2)

5. **Terminal Voltage SubVI:** This SubVI calculates the terminal voltages of the three-phase motor and also identifies the conducting device for DC link SubVI. Since the terminal voltages depend on the switching signals, the phase currents, and the conducting devices, the values of the terminal voltages are not always equal to the voltage at the DC rail. So, to calculate the terminal voltages, the three-phase currents, the switching signals, the three-phase back emf voltages, and the voltage at DC rail must be known. They are used as the inputs in this SubVI. The output data of the VI are the three-phase terminal voltages and the conducting devices in the inverter circuit. The details of the calculation algorithm were given in the previous chapter.

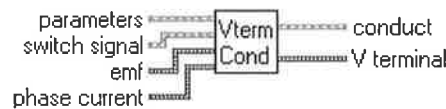


Figure 4.16 Terminal Voltage SubVI (See Appendix A-2)

6. **DC link SubVI:** This module calculates the values of the DC link current to be processed by the current reconstruction SubVI. The input data is the conducting devices in the inverter circuit and the three-phase currents of the motor.

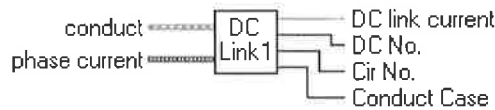


Figure 4.17 DC link SubVI (See Appendix A-2)

4.4 Simulation Results of the Motor Drive

To demonstrate the effectiveness of the motor simulator, a number of typical operating conditions are identified, and the results are obtained. The archetype of the simulated motor is a typical axial-fled industrial motor of which brand is Mavilor. The specification of the motor-drive system, which is used in the simulation results, is shown in **Table 4.1**. The operating conditions, in which the results are given, are listed below

1. Current control mode: Hysteresis and PWM
2. The status of the operation: Steady state and dynamic
3. Control status: Current control mode and no-current control mode
4. Type of the back emf voltage waveforms: Sinusoidal and trapezoidal
5. Type of the current command waveforms: Sinusoidal and rectangular

Table 4.1 Specifications of the motor system in the simulation results

| Parameters | The value of parameters | Unit |
|---|-------------------------|------------------------|
| Integration Time Step | 0.00002 | Second |
| Load torque | 4 | Nm (Newton-meter) |
| Command speed | 300 | Rpm (round per minute) |
| Hysteresis bandwidth | 0.5 | Ampere |
| Half of the Dc link Voltage | 25 | Volts |
| The back emf constant | 0.417 | V·sec/rad |
| Equivalent resistance of each phase winding | 0.8 | Ohm |
| Equivalent inductance of each phase winding | 0.00312 | Henry |
| Pole pair | 4 | |
| Inertia | 0.0080 | kg·m ² |
| Proportional constant | 10 | |
| Integral constant | 0.2 | |

In the following figures (**Fig.4.18-Fig.4.25**), the above listed operating conditions are operated and the corresponding waveforms are given.

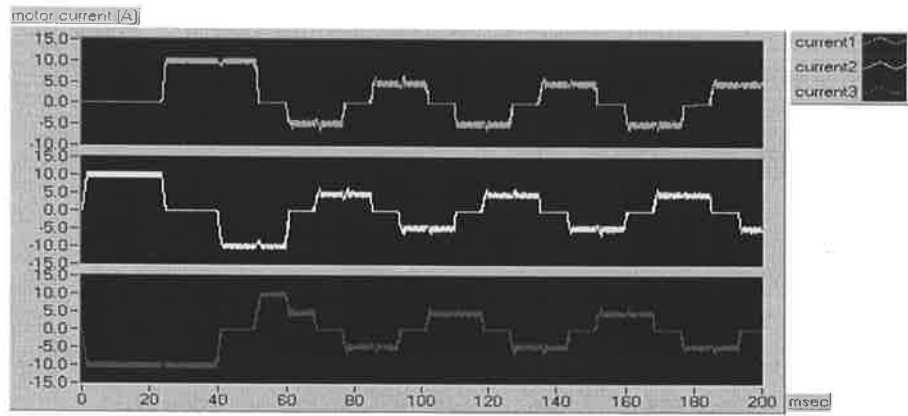
As seen in **Fig.4.18(a)**, the rectangular current waveforms had a limited hysteresis bandwidth and the currents' magnitude reduces while the motor accelerates. The trapezoidal back emf waveforms are given in **Fig.4.18(b)**, where the magnitude of the back emf varied with increased speed and reached to the steady-state around 60 ms. In addition, when the speed of the motor increased, the frequency of the back emf waveforms also increased. Total electromagnetic torque and the speed of the drive

are given in **Fig.4.18(c)** and **Fig.4.18(d)** respectively. As seen in **Fig.4.18(c)**, the torque developed by the motor was around 8 N·m until the motor reached to the steady state.

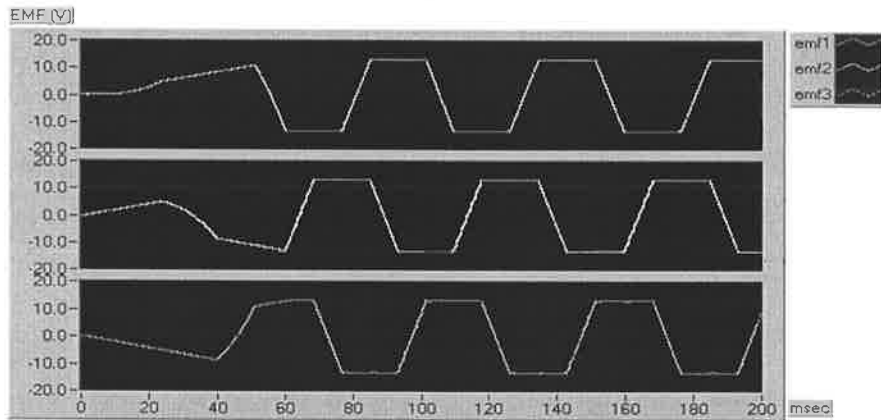
As seen in **Fig.4.19(d)**, the motor started from standstill, accelerated and reached to the steady state around 120 ms. Both the motor currents (**Fig.4.19(a)**) and the back emf waveforms (**Fig.4.19(b)**) were sinusoidal waveforms and were in phase. The developed electromagnetic torque of the motor is given in **Fig.4.19(c)**, which dropped to an average value of 4 N·m, which is the load torque, when the motor reached to the steady-state operation. Although some torque ripples were observable in the figure, which could be reduced if the modulation frequency of the PWM signals was increased.

Similar to the earlier results, the period of transient and steady state could be easily noticed both in the electromagnetic torque (**Fig.4.20(c)**) and the speed waveforms (**Fig.4.20(d)**). As expected, this operating mode of the motor drive generated more torque ripple than the ideal operating mode presented in **Fig.4.18** and **Fig.4.19**. This was because of the non-ideal current excitation that was rectangular for the sinusoidal back emf voltages. As seen in the current waveforms (**Fig.4.20(a)**), the actual current contained fluctuations after the motor reached the steady-state operation. This was due to the less effective voltage across the winding, since the back emf voltage increased at higher speeds.

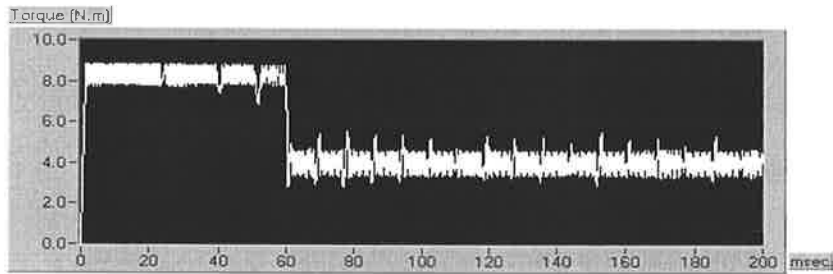
The electromagnetic torque waveform in the operating mode in **Fig 4.21(c)** was somehow similar to the waveform given in **Fig.4.20(c)**. Although the current and the back emf waveforms were in phase in this test, due to the non-ideal combinations of the waveforms, electromagnetic torque ripple became significant as seen in **Fig.4.21 (c)**. Unlike the earlier test given in **Fig.4.19**, however, the motor in this operating mode reached the steady state speed in a much shorter time (around 75 ms), which was due to the much higher electromagnetic torque developed in this test.



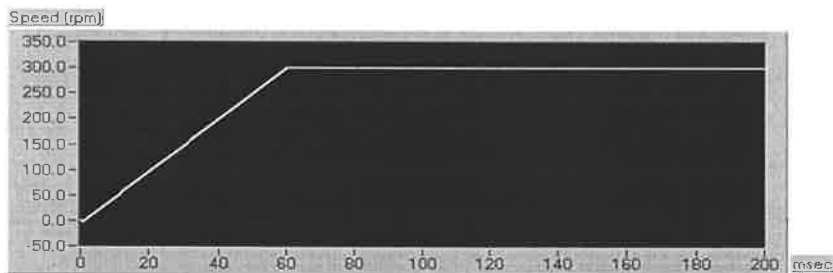
(a)



(b)

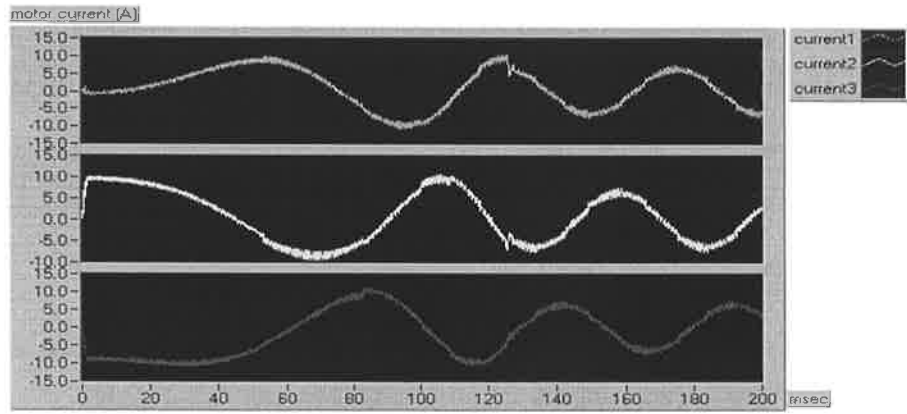


(c)

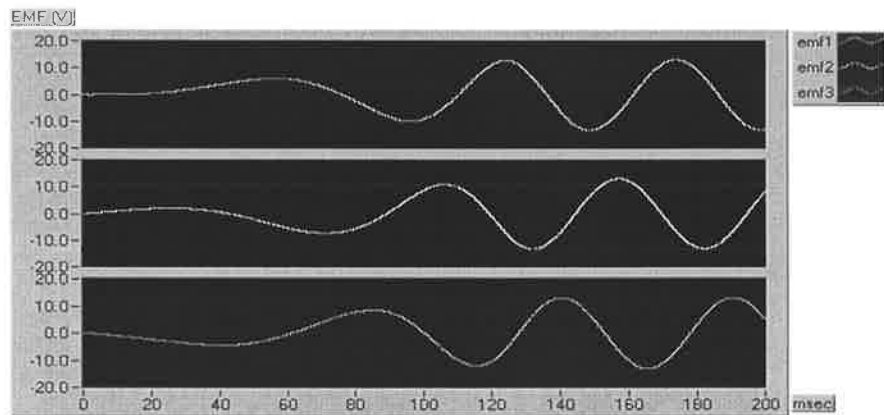


(d)

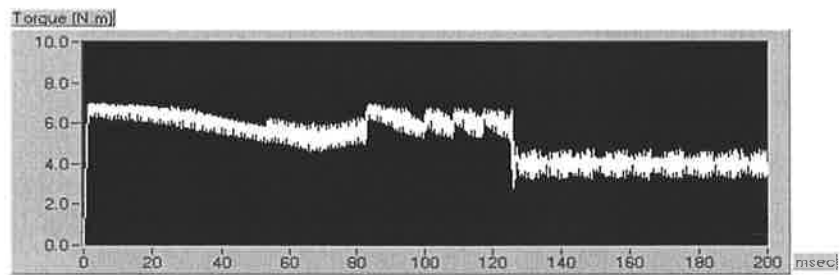
Figure 4.18 Simulation results of the motor drive operating from standstill, with rectangular current excitation, hysteresis current control and trapezoidal back emf waveforms: (a) Estimated three-phase currents, (b) Back emf waveforms, (c) Electromagnetic torque, (d) Rotor speed



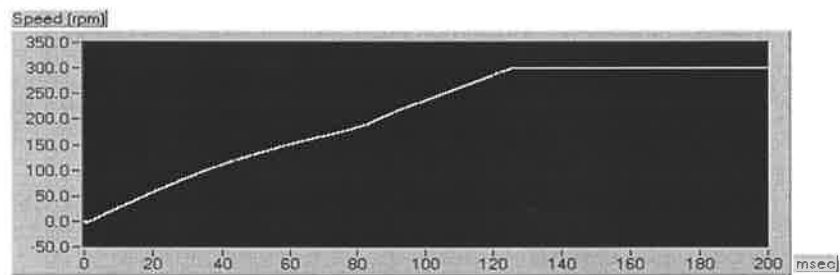
(a)



(b)

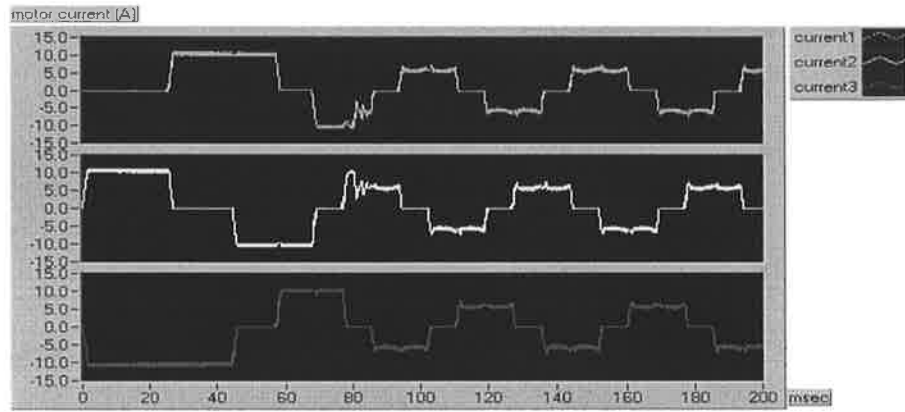


(c)

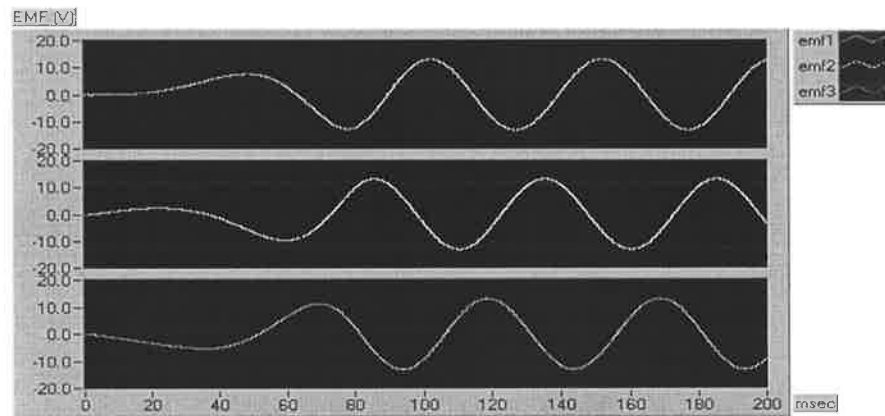


(d)

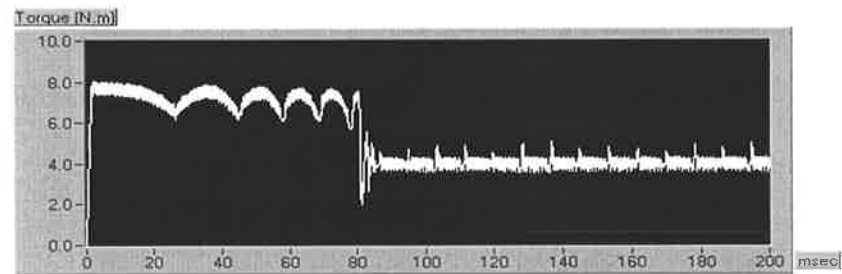
Figure 4.19 Simulation results of the motor drive while it is accelerating from standstill, the sinusoidal current excitation, PWM current control and sinusoidal back emf waveforms: (a) Estimated three-phase currents, (b) Back emf waveforms, (c) Electromagnetic torque, (d) Rotor speed



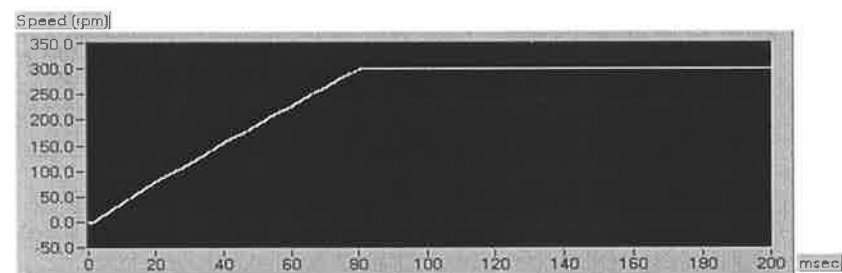
(a)



(b)

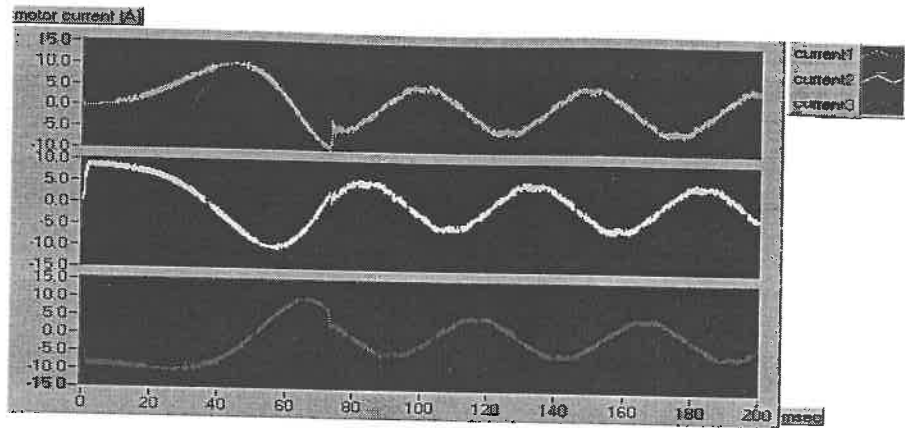


(c)

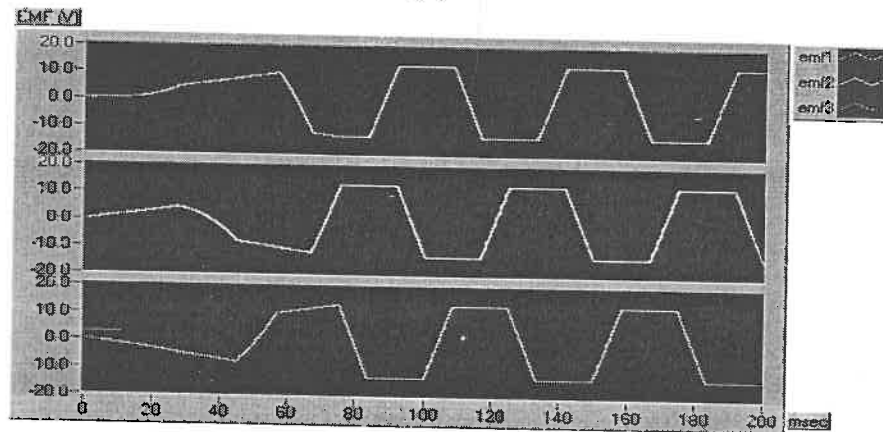


(d)

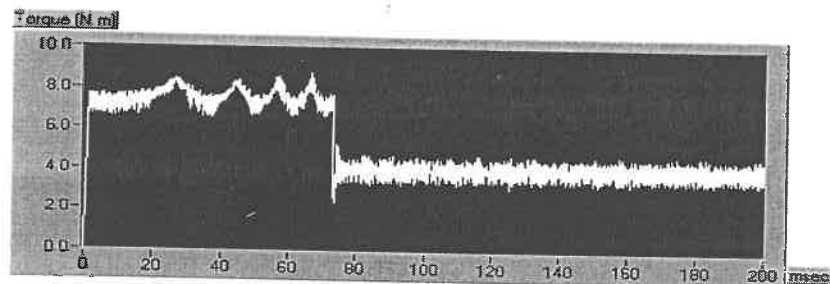
Figure 4.20 Simulation results of the motor drive under the transient operation, the rectangular current excitation, PWM current control and sinusoidal back emf waveforms: (a) Estimated three-phase currents, (b) Back emf waveforms, (c) Electromagnetic torque, (d) Rotor speed



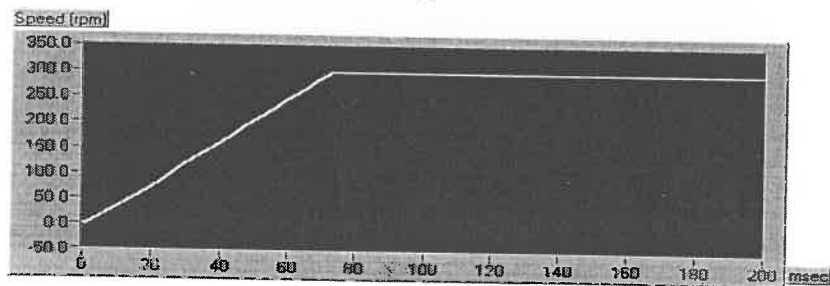
(a)



(b)



(c)



(d)

Figure 4.21 Simulation results of the motor drive under the transient operation starting from standstill, sinusoidal current excitation, hysteresis current control and trapezoidal back emf waveforms: (a) Estimated three-phase currents, (b) Back emf waveforms, (c) Electromagnetic torque, (d) Rotor speed

The results given in **Fig.4.22** and **Fig.4.23** demonstrate the operation of the motor drive under transient but at the no-current control mode.

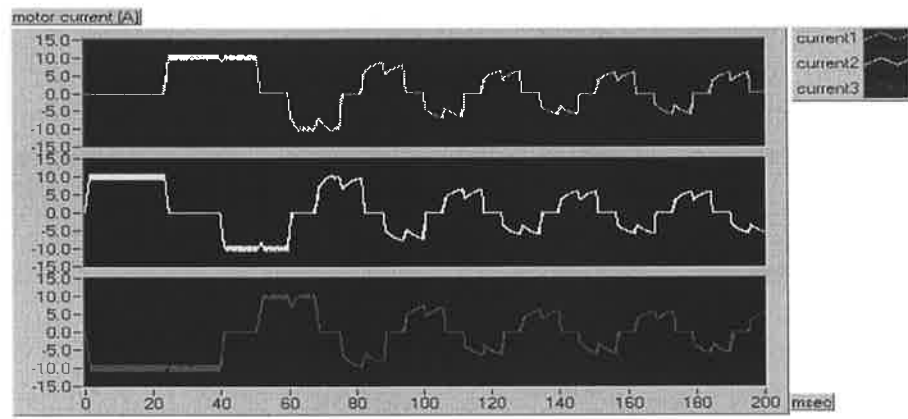
As seen in the graphs of **Fig.4.22**, after the motor reached the steady state, the current waveforms could not follow the reference waveforms. The shape of the currents is mainly determined by the level and shape of the back emf waveforms. In this operating mode, the load torque was 4 N·m. As seen in **Fig.4.22(c)** and **Fig.4.22(d)**, the motor reaches the steady-state operation after an acceleration period of 100 ms. However, at higher speeds, the currents were limited by only the back emf waveforms only.

The motor drive in the operating mode in **Fig.4.23(d)** reaches the steady-state speed of 600 rpm much slower than the previous test. This is due to a higher reference speed and a lower electromagnetic torque.

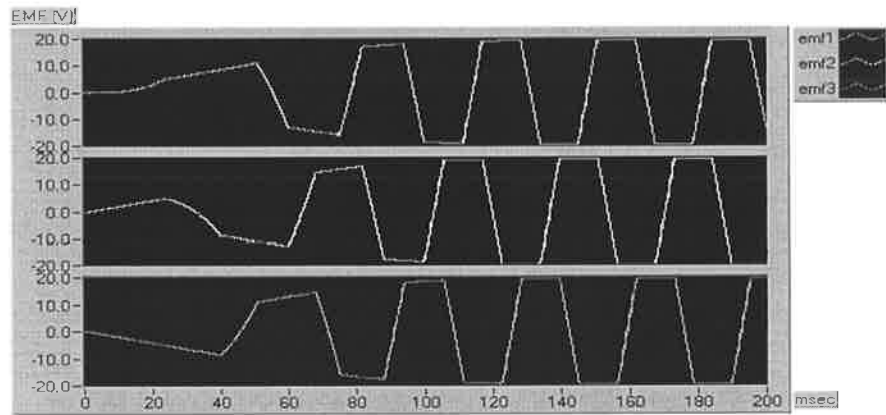
The principal objective of the tests in **Fig.4.24** and **Fig.4.25** is to demonstrate the operation of the drive under step load changing while it was accelerating from standstill.

In **Fig.4.24** and **Fig.4.25**, while the motor drive accelerated from standstill the load torque has been increased and reduced respectively. As it can be seen in the current and electromagnetic torque waveforms, the motor drive performs correctly and responds to the step load changes quickly.

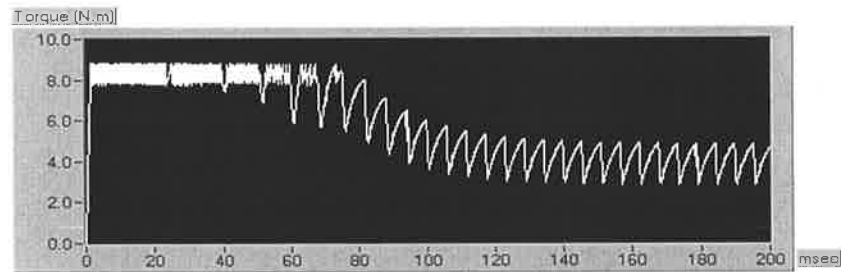
As demonstrated in the above simulation results, the motor drive program developed here can simulate the system correctly, and can work under many practical operating conditions. Hence, this simulation module can be utilised in the program of the current reconstruction system.



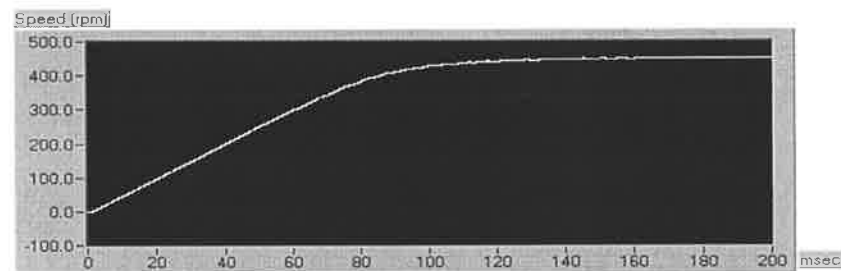
(a)



(b)

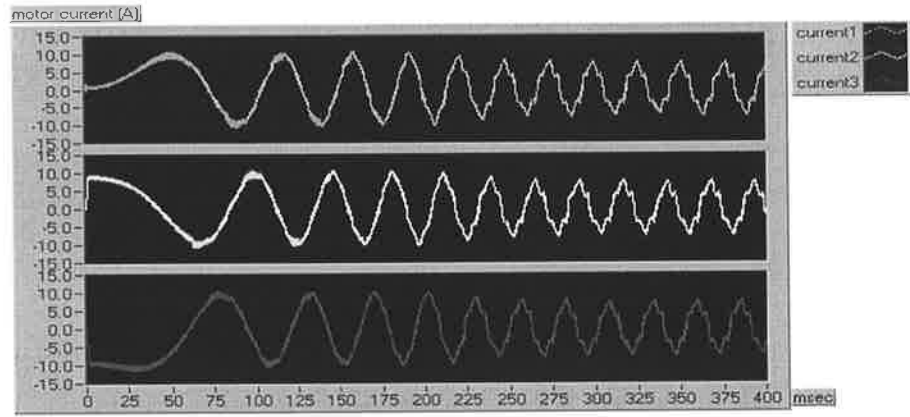


(c)

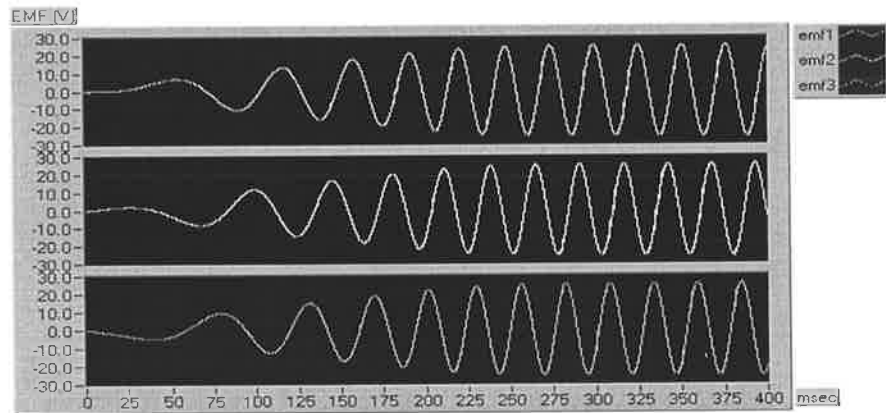


(d)

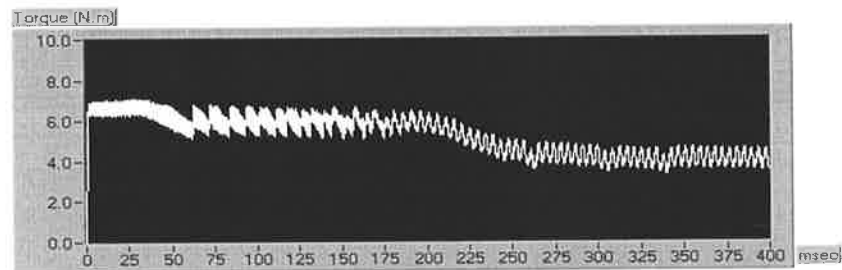
Figure 4.22 Simulation results of the motor drive with a rectangular current excitation, hysteresis current control and trapezoidal back emf waveforms: (a) Estimated three-phase currents, (b) Back emf waveforms, (c) Electromagnetic torque, (d) Rotor speed



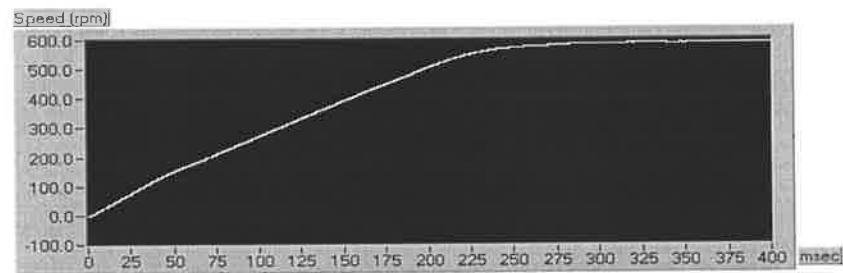
(a)



(b)

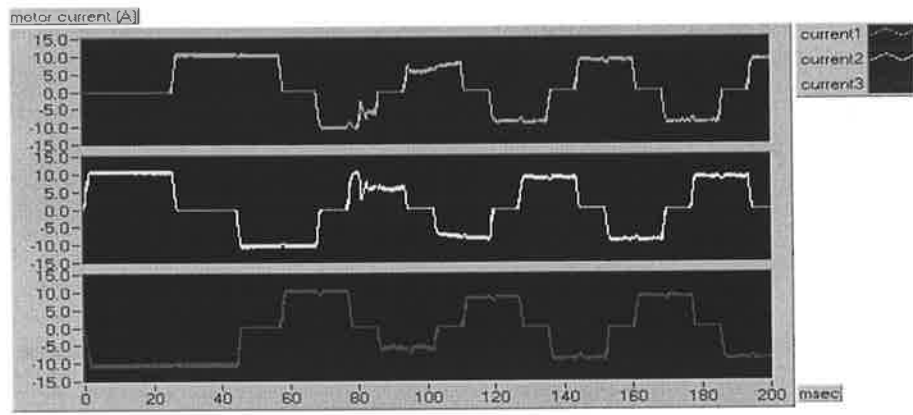


(c)

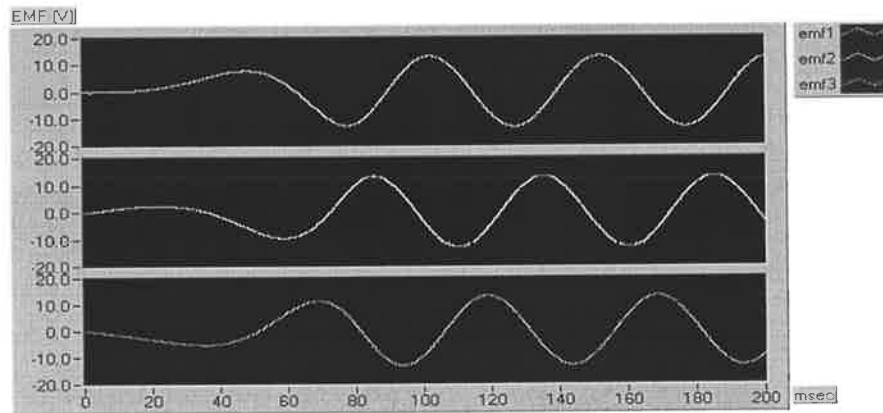


(d)

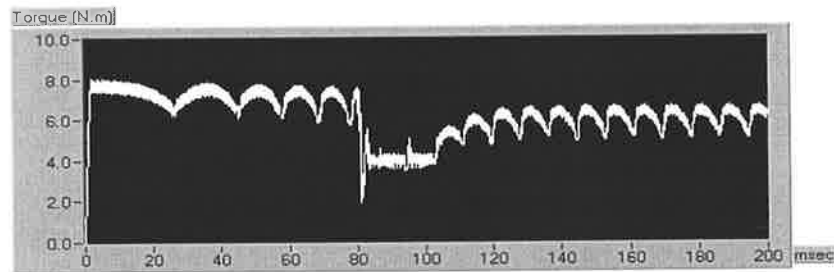
Figure 4.23 Simulation results of the motor drive under the transient operation, the sinusoidal current excitation with no current control, PWM current control and sinusoidal back emf waveforms: (a) Estimated three-phase currents, (b) Back emf waveforms, (c) Electromagnetic torque, (d) Rotor speed



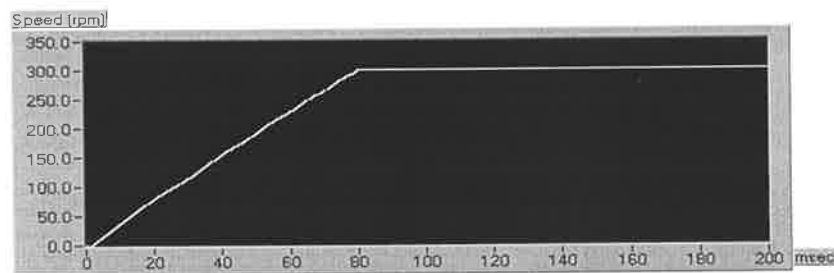
(a)



(b)

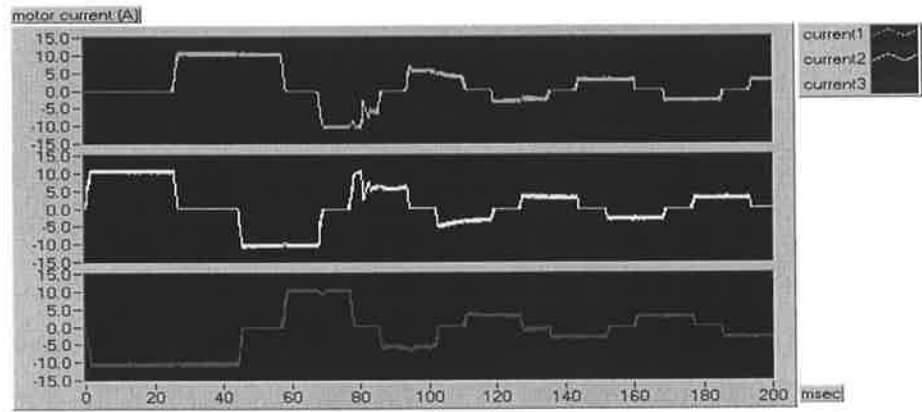


(c)

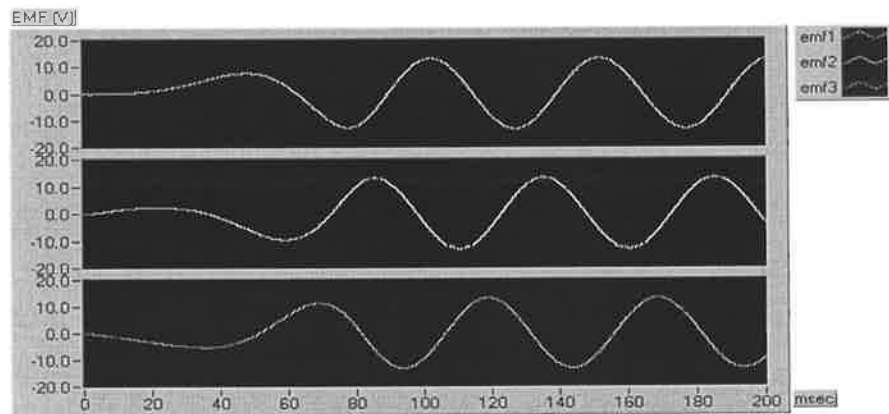


(d)

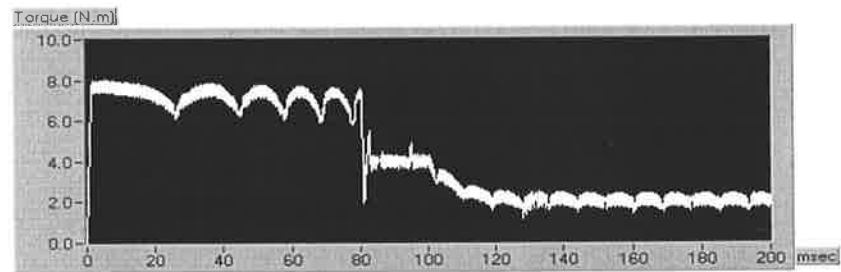
Figure 4.24 Simulation results of the motor drive under step loading (increasing load torque), the trapezoidal current excitation, PWM current control and sinusoidal back emf waveforms: (a) Estimated three-phase currents, (b) Back emf waveforms, (c) Electromagnetic torque, (d) Rotor speed



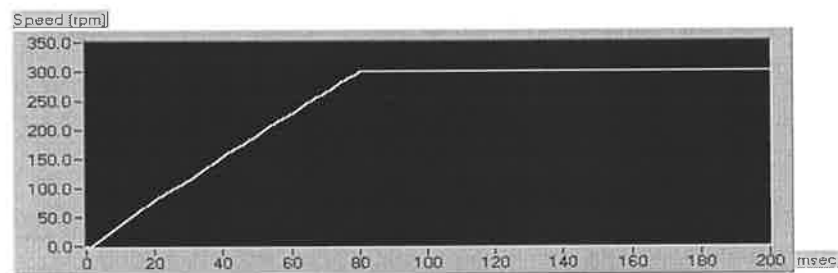
(a)



(b)



(c)



(d)

Figure 4.25 Simulation results of the motor drive under a step load change (reducing load torque), the trapezoidal current excitation, PWM current control and sinusoidal back emf waveforms: (a) Estimated three-phase currents, (b) Back emf waveforms, (c) Electromagnetic torque, (d) Rotor speed

4.5 Analysis of the Inverter Currents

As stated above, in the current reconstruction, the DC link current of Master Motor is a key to check and confirm that the values of the three-phase currents of Master Model are equal to those values of Master Motor. A method to do that is to compare the DC link current of Master Motor with the DC link current of Motor Model. Hence, the DC link currents of both motor drives are calculated. It is necessary to know the characteristic of the currents in the inverter accurately to calculate the DC link current and the currents in the inverters in a switching state.

The switching state was introduced in Section 3.5. However, this section explains the method to find the value of a DC link current and the phase number of a DC link phase from the information of a switching state. The DC link phase is the phase of which the absolute amplitude of the current is equal to the absolute amplitude of the DC link current. Switching states are classified into ten types, those are based on the conducting devices in the inverter. The switching states are briefly explained below, which can be used to identify the DC link phase.

1. State '3S'

In this state, there are three conducting power switches in the inverter, in which all three phases conduct currents. However, since two devices on the same leg cannot be turned on simultaneously, only two of the switches are linked to one of the DC rails. The other DC rail has a power switch linked. The absolute value of the current, which flows through this power switch, is equal to the absolute value of the DC link current. Thus, the phase of this switch is the DC link phase. In this conducting state, it can be said that the DC link current is positive since all phase currents flow through the power switches.

2. State '3D'

This is similar to the state explained above, except that the phase currents flow through the three freewheeling diodes in the inverter. The DC link current in this state is always negative because the conducting device in each phase is a diode. Although the power switches are turned on, the currents do not flow through them. Similarly,

two of the conducting diodes are linked to one of the DC rails. The DC link phase is described as the phase number that has only one device linked to the DC rail.

3. State '2S'

There are two power switches turned on and the two-phase currents flowing through those switches. There is no current in the other phase. In this state, the conducting switches are linked to the opposite rails. The phase current flows through the upper switch in one phase winding to the lower switch in another phase winding. The DC link current in this state is positive because the phase currents flow through only the power switches. The DC link phase is the phase number that is linked to the upper switch.

4. State '2D'

The currents flow through two-phase windings, and there is no phase current in the third phase. Moreover, the currents flow via only the diodes. Therefore, the DC link current in this state is always negative. The absolute value of the DC link current is equal to the absolute value of the phase current of which flow through the upper diode, the DC link phase.

5. State '2S1D+dc'

The state '2S1D' means that there are two switches and one diode conducting. Because this conducting characteristic has 2 states of a DC link current which is identified by with and without DC link current, the suffix '+dc' is put to indicate that there is a DC link current in this state. The two conducting power switches link both of the DC rails. The current flows from the positive DC rail to the negative DC rail, but some of the current circulates through the conducting diode within the inverter circuit. If the conducting diode links to the positive DC rail, DC link phase is the phase of which the power switch links to the negative DC rail and vice versa.

6. State '2S1D-dc'

This case is similar to the state '2S1D+dc'. However, there is no DC link current, '-dc', since the conducting switches are connected to the same DC rail, and there is only circulating current in this state.

7. State '1S2D+dc'

The state indicates that the current flows through one power switch and two diodes. The diodes are linked to the opposite DC rails. The DC link current flows through the sensor and the motor via one of the diodes, and then returns via the other diode. Therefore, the value of the DC link current is always negative. However, in addition to the DC link current, there is a circulating current as well. The circulating current flows through the switch. The DC link phase is the phase of which the conducting diode is connected to the opposite rail with the conducting switch.

8. State '1S2D-dc'

This state is similar to the above state, but there is no DC link current. All of the conducting devices are linked to the same rail, and so there is only circulating current.

9. State '1S1D'

The current flows through one power switch and one diode, which are connected to the same DC rail. There is only circulating current, no DC link current.

10. State 'No conduction'

In this state, there is no DC link current and circulating current in the inverter. All of the three-phase currents are equal to zero and the turned-on switches, link to the same DC rail.

4.6 Implementation of the DC Link Current

As explained in the previous section, the DC link current from Master Motor and the DC link current from Motor Model are compared with each other. If both of the DC link currents are equal, it can be assumed that the three-phase currents of Master Motor are equal to those of Motor Model. However, if the DC link currents are not equal, the three-phase currents of Motor Model are required corrections. In this section, the value adjustment of the three-phase currents of Motor Model is explained. It uses the DC link currents and DC link phase, which were described in the last section, to correct the values.

In the current compensation process, the DC link currents from the master motor (I_{motor}) and the model (I_{model}) are compared, and the current error (Δerror) is estimated.

$$\Delta\text{error} = I_{\text{motor}} - I_{\text{model}} \quad (4.4)$$

However, the value of the current in DC phase (I_{dcphase}) may not have the same sign as the value of the DC link current. Therefore, the signs of the DC link currents should be taken into account. If both of the DC link currents have the same sign, the current compensation is calculated by

$$I_{\text{compensate}} = I_{\text{dcphase}} + \Delta\text{error} \quad (4.5)$$

Here, I_{dcphase} is the value of the current in the DC phase estimated from the model motor. If the sign of the DC link current differs from the sign of the DC phase current,

$$I_{\text{compensate}} = I_{\text{dcphase}} - \Delta\text{error} \quad (4.6)$$

As explained above, there are a number of states, which accommodate DC link currents. Six of the states out of ten, have the DC link currents, which are 3S, 3D, 2S, 2D, 2S1D+dc, and 1S2D+dc. These states will again be considered below and the corresponding current compensation values will be analysed in detail.

1. State '3S'

Since all of the phase currents flow through the power switches, the DC link current is always positive. However, the current in the DC phase can be either positive or negative depending on the state of the conducting device of the DC phase current. If it is connected to the upper rail, the value of the current in the DC phase is positive. However, if the conducting device of the DC phase current is connected to the lower rail, the value of the current in the DC phase is negative.

Fig.4.26 illustrates a sample state, in which the value of the DC phase is positive. As shown, in the figure, T1, T6 and T2 are on in this state of operation. So the DC phase is Phase1, and from **Eq.4.5** the value of the compensating current can be given by

$$I_{\text{compensate1}} = I_{\text{model1}} + \Delta\text{error1} \quad (4.7)$$

Here, $I_{\text{compensate1}}$ is the current of Phase1, I_{model1} is the current of Phase1 from the model motor, and Δerror1 is the error of the current of Phase1.

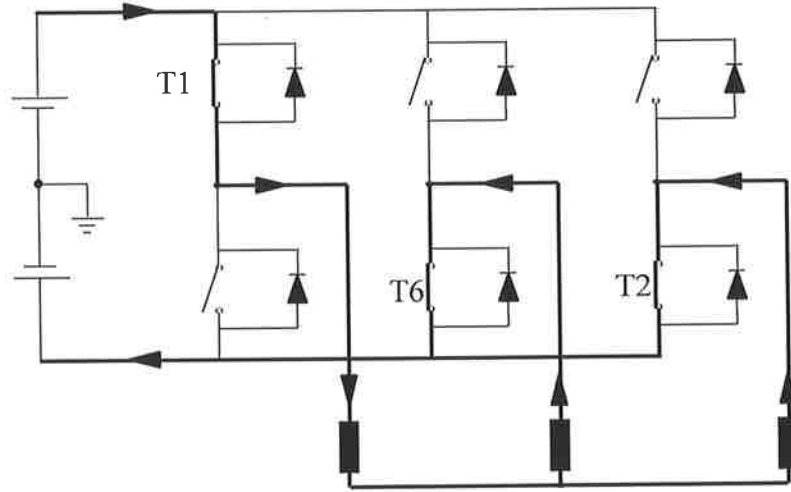


Figure 4.26 Bridge inverter diagram when T1, T6, T2 are conducting

Note that in this case, $\Delta error1$ is equal to the $\Delta error$, which is the different value between the DC link current from the real motor and the model, because the DC phase is Phase1. Similarly since the currents of Phase2 and Phase3 are negative, which flow through T6 and T2, the compensating current for these phase can be given as

$$I_{compensate2} = I_{model2} + \Delta error2 \quad (4.8)$$

$$I_{compensate3} = I_{model3} + \Delta error3$$

In the above equation, it is assumed that

$$\Delta error1 + \Delta error2 + \Delta error3 = 0 \quad (4.9)$$

Where, $\Delta error2$ is the error of the current of Phase2; $\Delta error3$ is the error current of Phase3; I_{model2} and I_{model3} are the model current of Phase2 and Phase3 respectively; and $I_{compensate2}$ and $I_{compensate3}$ are the compensated currents of Phase2 and Phase3 respectively.

Assuming that in the DC link current the error, $\Delta error$, is proportional to the current level in Phase3. In this example, the current error of Phase1, $\Delta error1$, is equal to $\Delta error$. Hence using this relationship, the current errors of Phase2 and Phase3 can be calculated as a function of $\Delta error$,

$$\Delta error1 = \Delta error$$

$$\Delta error2 = \Delta error \times \frac{I_{model2}}{I_{model1}} \quad (4.10)$$

$$\Delta error3 = \Delta error \times \frac{I_{model3}}{I_{model1}}$$

Hence, if the above equations are substituted in to **Eq.4.8** and rearranged,

$$\begin{aligned}
 I_{\text{compensate1}} &= I_{\text{model1}} + \Delta\text{error} \\
 I_{\text{compensate2}} &= I_{\text{model2}} + \Delta\text{error} \times \frac{I_{\text{model2}}}{I_{\text{model1}}} \\
 &= I_{\text{model2}} \times \left(1 + \frac{\Delta\text{error}}{I_{\text{model1}}} \right) \\
 I_{\text{compensate3}} &= I_{\text{model3}} + \Delta\text{error} \times \frac{I_{\text{model3}}}{I_{\text{model1}}} \\
 &= I_{\text{model3}} \times \left(1 + \frac{\Delta\text{error}}{I_{\text{model1}}} \right)
 \end{aligned}
 \tag{4.11}$$

Note that in the above equation

$$I_{\text{model1}} + I_{\text{model2}} + I_{\text{model3}} = 0 \tag{4.12}$$

In the other cases, the value of the current of the DC phase is negative. For example, the conducting devices are T3, T4 and T5 as shown in **Fig.4.27**. Therefore, the DC phase number is Phase1

$$\Delta\text{error} = -\Delta\text{error1} \tag{4.13}$$

As stated before, Δerror is proportional to the current level

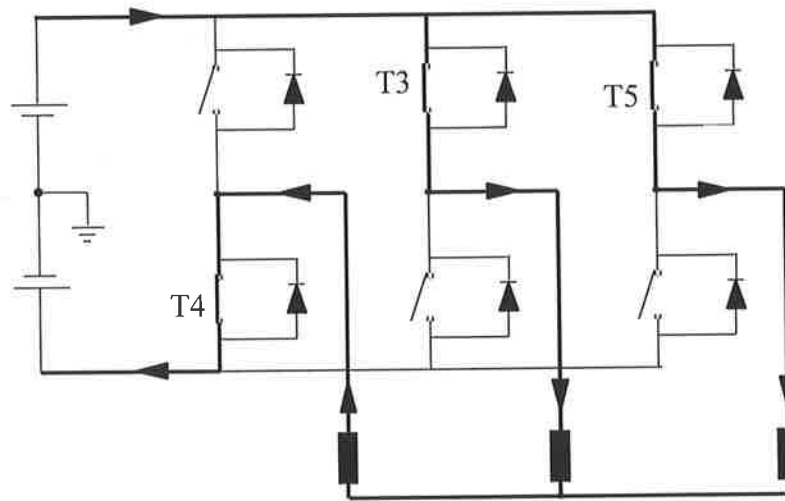


Figure 4.27 Bridge inverter diagram when T4, T3, T5 are conducting

Hence,

$$\begin{aligned}
 \Delta\text{error2} &= -\Delta\text{error} \times \frac{I_{\text{model2}}}{I_{\text{model1}}} \\
 \Delta\text{error3} &= -\Delta\text{error} \times \frac{I_{\text{model3}}}{I_{\text{model1}}}
 \end{aligned}
 \tag{4.14}$$

Hence, if the above equations are substituted into **Eq.4.7** and **Eq.4.8**,

$$\begin{aligned}
 I_{\text{compensate1}} &= I_{\text{model1}} - \Delta\text{error1} \\
 I_{\text{compensate2}} &= I_{\text{model2}} \times \left(1 - \frac{\Delta\text{error}}{(I_{\text{model2}} + I_{\text{model3}})} \right) \\
 I_{\text{compensate3}} &= I_{\text{model3}} \times \left(1 - \frac{\Delta\text{error}}{(I_{\text{model2}} + I_{\text{model3}})} \right)
 \end{aligned}
 \tag{4.15}$$

2. State '3D'

As mentioned previously, all of the phase currents in this state flow through the diodes. This state is similar to the state explained above. However, the DC link current is always negative. The current in the DC link phase can be either positive or negative. It is positive when the conducting device of the DC phase is linked to the negative DC rail, and it is negative when the conducting device of the DC phase is linked to the positive DC rail of the inverter.

A sample state is given in **Fig.4.28**, which shows that three diodes D3, D4 and D5 are conducting. The DC phase is Phase1 and the value of the current of Phase1 is positive, but the DC link negative. Therefore, **Eq.4.13**, **Eq.4.14** and **Eq.4.15** are also valid in this state.

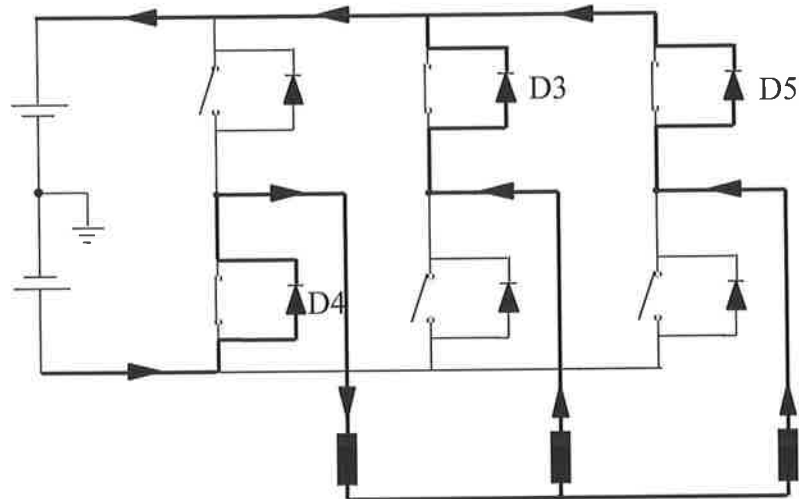


Figure 4.28 Bridge inverter diagram when D3, D4 and D5 are conducting.

However, if D1, D2 and D6 are the conducting devices, as shown in **Fig.4.29**, the DC phase is Phase1, the value of the current of the DC phase is negative and the DC link current is negative.

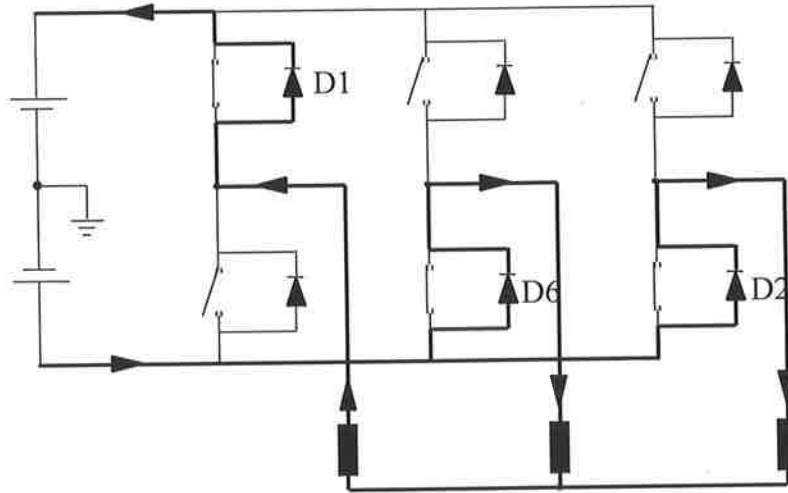


Figure 4.29 Bridge inverter diagram when D1, D2 and D6 are conducting

Hence, the current errors and the compensating currents of Phase1, Phase2 and Phase3 are given as in **Eq.4.10** and **Eq.4.11** respectively.

3. State '2S'

As the DC link current in this case is always positive and there are only two phase currents, only those two phase currents are compensated. Moreover, the absolute amplitude values of the two phase currents are equal, but one of those is positive and the other one is negative. In this case, the value of the DC phase current is always positive because the DC link current is always positive, which makes the current compensation easier.

For example, if the conducting devices are T1 and T6, as shown in **Fig. 4.30**, Phase1 is the DC phase. Therefore,

$$\Delta error1 = \Delta error \quad (4.16)$$

$$\Delta error2 = -\Delta error$$

$$\begin{aligned} I_{\text{compensate1}} &= I_{\text{model1}} + \Delta\text{error} \\ I_{\text{compensate2}} &= I_{\text{model2}} - \Delta\text{error} \\ I_{\text{compensate3}} &= I_{\text{model3}} = 0 \end{aligned} \quad (4.17)$$

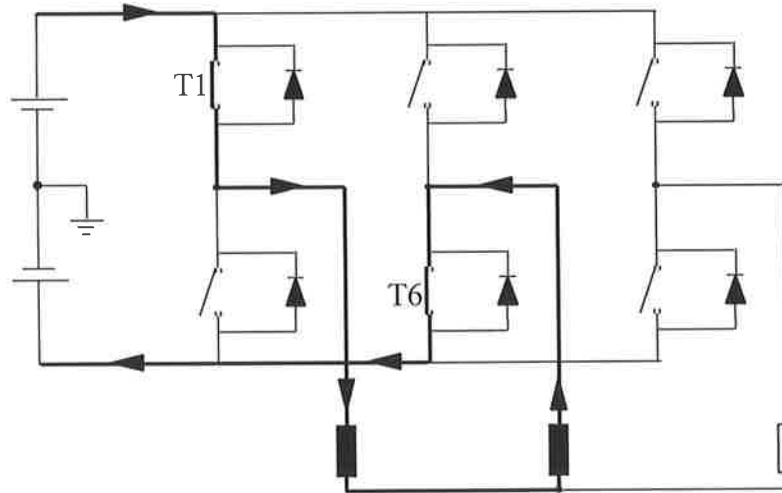


Figure 4.30 Bridge inverter diagram when T1 and T6 are conducting current.

4. State '2D'

The compensation in this case is similar to the compensation in the state '2S' because the characteristics of the currents are similar. However, the phase currents in this case flow through only two diodes. The DC link current is always negative. So the value of the current of the DC phase is always negative.

For instant, **Fig.4.31** is given. As seen, the current flowing through D1 is negative, so the DC phase is Phase1

$$\begin{aligned} \Delta\text{error1} &= \Delta\text{error} \\ \Delta\text{error2} &= -\Delta\text{error} \end{aligned} \quad (4.18)$$

$$\begin{aligned} I_{\text{compensate1}} &= I_{\text{model1}} + \Delta\text{error} \\ I_{\text{compensate2}} &= I_{\text{model2}} - \Delta\text{error} \\ I_{\text{compensate3}} &= I_{\text{model3}} = 0 \end{aligned} \quad (4.19)$$

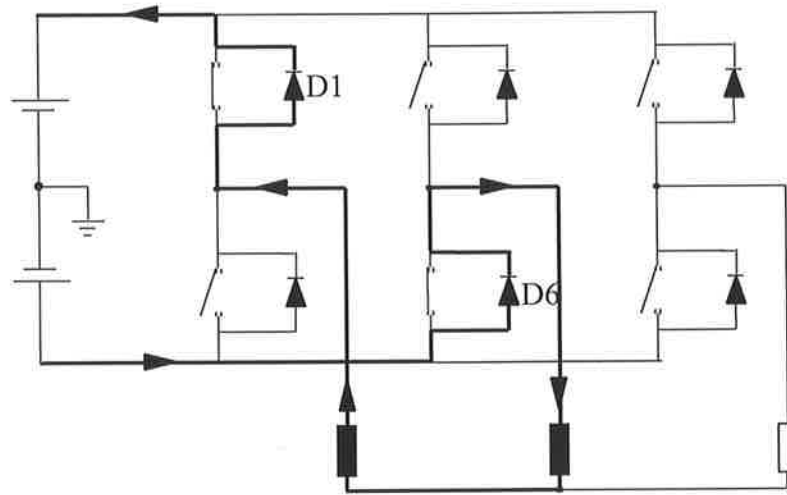


Figure 4.31 Bridge inverter diagram when D1 and D6 are conducting currents.

5. State '2S1D+dc'

In this state, there are both DC link current and circulating current in the inverter. DC link current flows through two power switches and circulating current flows through the diode. Therefore, only the currents that flow through diode is not compensated because the circulating current cannot be measured in this study. Since the value of the current of the DC phase in this case can be either positive or negative, during the compensation, the compensation of the currents of the DC phase depends upon the sign of the DC phase.

As an example, let us take the condition of the inverter as illustrated in Fig.4.32. In this state, the DC phase is Phase1 and the value of the current of Phase1 is positive. Hence,

$$\begin{aligned} \Delta error1 &= \Delta error \\ \Delta error2 &= -\Delta error \end{aligned} \tag{4.20}$$

and the compensating currents are

$$\begin{aligned} I_{compensate1} &= I_{model1} + \Delta error \\ I_{compensate2} &= I_{model2} - \Delta error \\ I_{compensate3} &= I_{model3} \end{aligned} \tag{4.21}$$

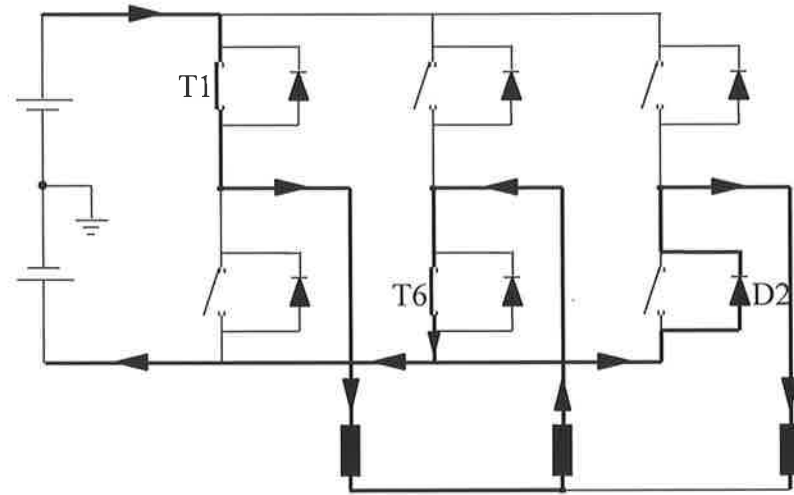


Figure 4.32 Bridge inverter diagram when T1, T6 and D2 are conducting.

When the sign of the current of the DC phase is negative, for example, the conducting devices are T4, T3 and D5, as shown in **Fig.4.33**.

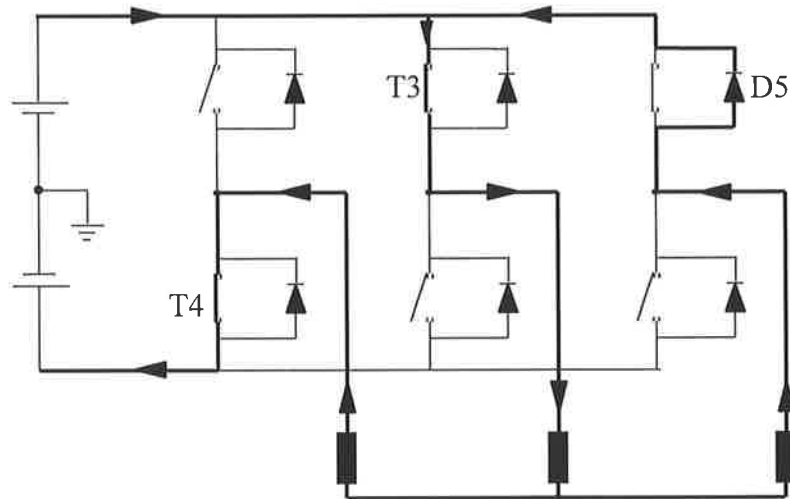


Figure 4.33 Bridge inverter diagram when T4, T3 and D5 are conducting currents.

Phase1 is the DC phase and the value of the current of Phase1 is negative. Therefore, the current errors are

$$\Delta error1 = -\Delta error \tag{4.22}$$

$$\Delta error2 = \Delta error$$

and the compensating currents become

$$\begin{aligned}
 I_{\text{compensate1}} &= I_{\text{model1}} - \Delta\text{error} \\
 I_{\text{compensate2}} &= I_{\text{model2}} + \Delta\text{error} \\
 I_{\text{compensate3}} &= I_{\text{model3}}
 \end{aligned}
 \tag{4.23}$$

6. State '1S2D+dc'

The characteristic of the current in this state is similar to the previous state, but the DC link current is negative in this state. However, the value of the current of the DC phase can be either positive or negative.

A sample state is shown in **Fig.4.34** where the value of the current of the DC phase is positive since D4, D3 and T5 are conducting devices. Phase1 is the DC phase and the current of Phase1 is positive. Phase3 is the circulating phase. Hence the current errors and the compensating current are similar to **Eq.4.22** and **Eq.4.23** respectively.

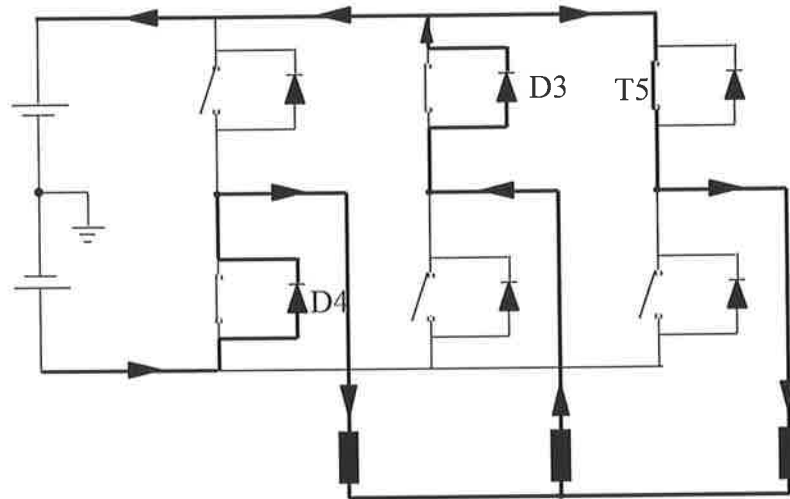


Figure 4.34 Bridge inverter diagram when D4, D3 and T5 are conducting currents.

When the value of the current of DC phase is negative, however, the conducting state is given in **Fig.4.35**, where D1, D6 and T2 are the conducting devices. Phase1 is the DC phase and the current of Phase1 is negative in this state, and Phase3 is the circulating phase. Hence, the current errors and the compensating current are similar to **Eq.4.20** and **Eq.4.21** respectively.

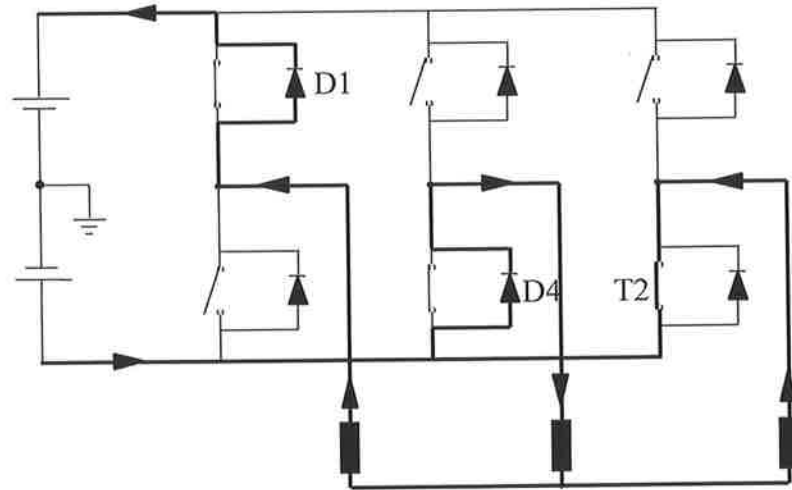


Figure 4.35 Bridge inverter diagram when D1, D4 and T2 are conducting current.

4.7 The Current Reconstruction Module

The layout of the current reconstruction system was described in Section 4.2, which has 2 motors: Master Motor, which reconstructs the three-phase currents, and Motor Model, which is a motor simulator of Master Motor. The DC link currents from both motors are compared to know if the three-phase currents of both motors are equal.

However, as known, measurement noise or other types of noises do exist in a practical motor drive. Therefore, the DC link currents from both motors can be made different to represent the real system. In the program of the current reconstruction module, since both of the DC link currents using the same parameters, they are equal. Some errors can be added to the DC link current of Master Motor in the program, as in **Fig.4.36**, which can represent a real motor. The figure shows the main loop program of the current reconstruction system, which has 4 parts as in **Fig.4.1**:

1. Master Motor, which consists of Drive1 SubVI and Motor1 SubVI
2. Motor Model, which consists of Drive2 SubVI and Motor2 SubVI
3. Current Compensation, named Comp SubVI in the figure
4. Motor Control, which consists of PID SubVI and Curr Contr SubVI

Furthermore, the program has 1 minor SubVIs named ω rpm SubVI. In **Fig.4.36**, the function and the inputs and outputs of Motor1 SubVI and Motor2 SubVI are similar to those of Motor SubVI, which was explained in Section 4.3. Moreover, the functions

and the inputs and outputs of PID SubVI, Curr Contr SubVI and ωrpm SubVI were described in Section 4.3.

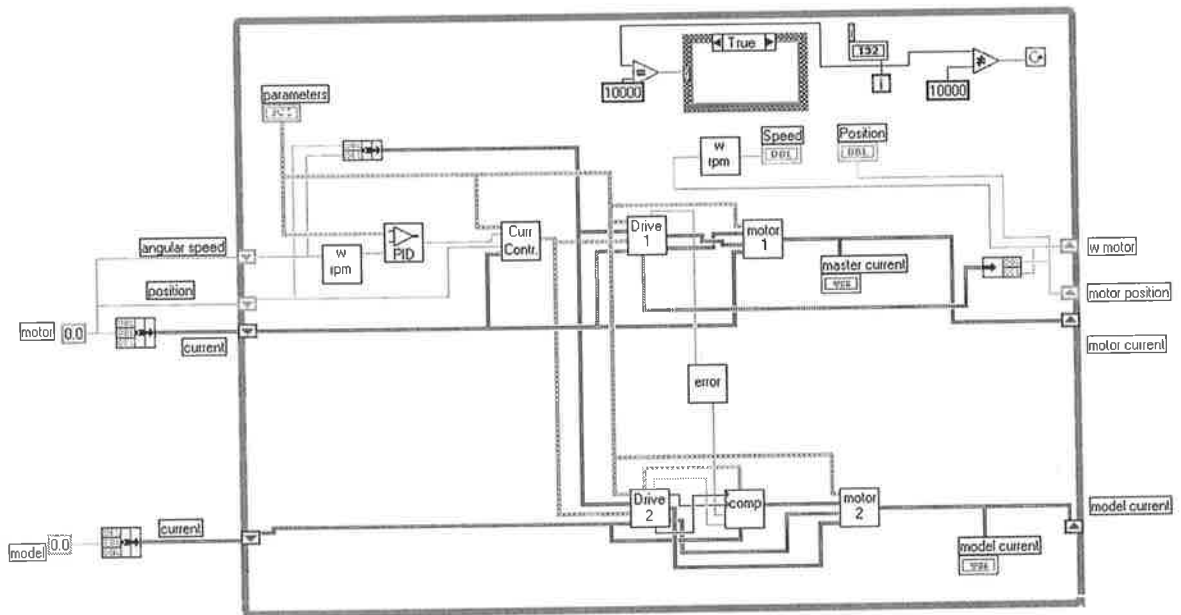


Figure 4.36 Main block diagram of the LabVIEW current reconstruction module

The inputs and outputs of Drive1 SubVI and Drive2 SubVI are similar to that of Drive SubVI in Section 4.3, except the torque value output because the program of the current reconstruction system does not show the torque. Therefore, it has no torque output. Moreover, the function of Drive SubVI in the program of the current reconstruction system is to input values not only to Motor SubVI but to Comp SubVI as well. Thus, the output terminal of Drive1 and Drive2 SubVI output the information for the current compensation progress. **Fig.4.37** shows the inputs and outputs terminal of Drive1 SubVI and Drive2 SubVI, but the block diagram of the Drive SubVIs is shown in **Fig.4.11**.

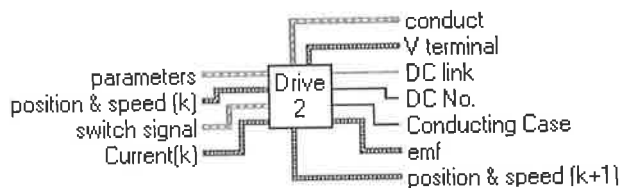


Figure 4.37 Drive1 or Drive2 SubVI

The function of Comp SubVI is to compensate and adjust the values of the three-phase currents of Motor Model. The principle of the current compensation is

described in the previous section. **Fig.4.38** shows the inputs and output of Comp SubVI. The function of Error SubVI is to add constant error and random error into the DC link current of Master Motor. The amplitude of the added error is proportional to the amplitude of the DC link current at that time step. **Fig.4.39** shows the input and output of Error SubVI.

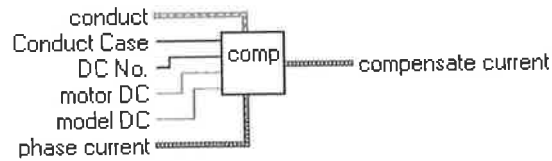


Figure 4.38 Comp SubVI (see Appendix A-2)



Figure 4.39 Error SubVI (see Appendix A-2)

In **Fig.4.36**, the operation principle of the current reconstruction module is similar to the motor simulator program. The motor control part (PID SubVI and Curr Contr SubVI) produces the switching signals for Drive SubVI (Drive1 SubVI and Drive2 SubVI). Next, Drive1 SubVI outputs the values for Motor1 SubVI and the DC link current. The DC link current from Drive1 SubVI is an input of Error SubVI to add some errors into the DC link current. After receiving the switching signals, Drive2 SubVI calculates the input values for Motor2 SubVI and the DC link current and the values, which are used to compensate the three-phase currents. Then, Comp SubVI has the DC link currents from Error SubVI and Drive2 SubVI, the three-phase currents of Motor Model from the previous time step loop, the DC link phase, the type of the switching states and the conducting devices from Drive2 SubVI to use in the compensation progress. Next, Comp SubVI outputs the compensated three-phase currents to Motor2 SubVI to calculate the three-phase currents of Motor Model of the next time step.

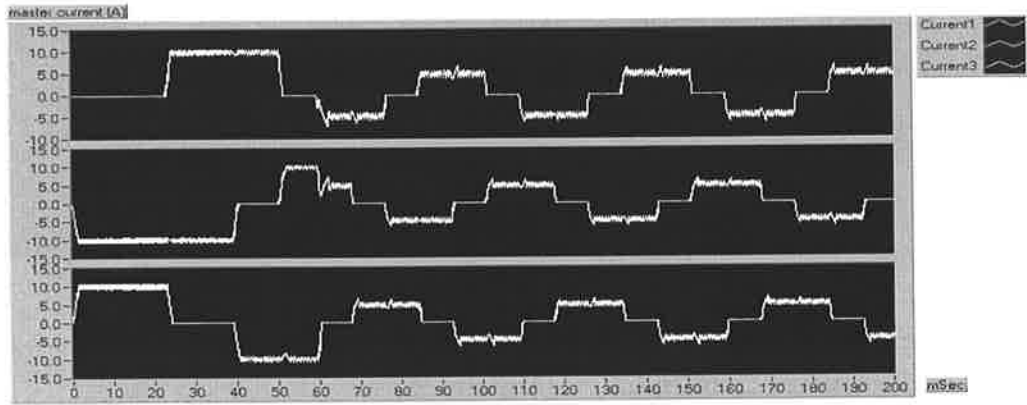
4.8 The Simulation Results of the Phase Current Reconstruction

This section shows some typical simulation results of the current reconstruction. The specification of the motor system in this system is shown in **Table 4.1**. To make the simulation study meaningful, some errors are introduced by using uniform and normal

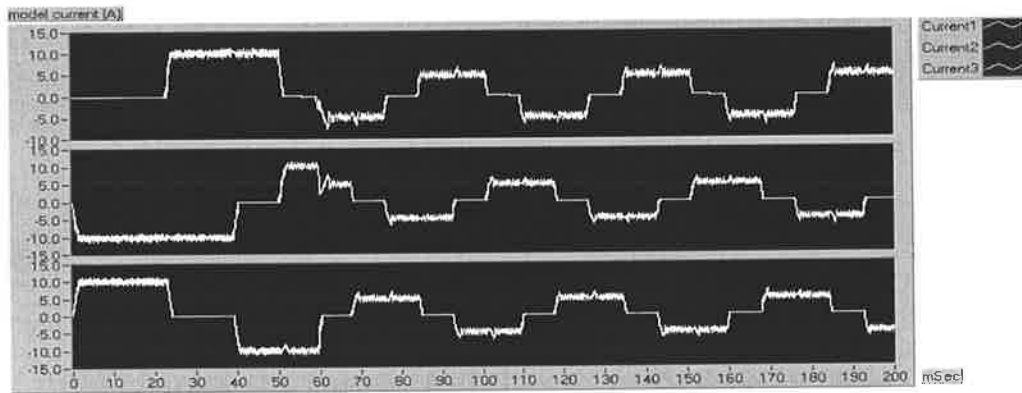
distribution and the current reconstruction is performed based on these synthetic errors.

The results are classified under six groups as explained below:

1. Hysteresis current control, rectangular current mode, trapezoidal back emf, a constant DC link current error of 2%, and a random DC link current error of 5%, as shown in **Fig.4.40**.
2. Hysteresis current control, rectangular current mode, trapezoidal back emf, a constant DC link current error of 5%, and a random DC link current error of 5%, as shown in **Fig.4.41**.
3. PWM current control, rectangular current mode, sinusoidal back emf, a constant DC link current error of 2%, and a random DC link current error of 5%, as shown in **Fig.4.42**.
4. PWM current control, rectangular current mode, sinusoidal back emf, a constant DC link current error of 5%, and a random DC link current error of 5%, as shown in **Fig.4.43**.
5. PWM current control, sinusoidal current mode, sinusoidal back emf, a constant DC link current error of 2%, and a random DC link current error of 5%, as shown in **Fig.4.44**.
6. PWM current control, sinusoidal current mode, sinusoidal back emf, a constant DC link current error of 5%, and a random DC link current error of 5%, as shown in **Fig.4.45**.



(a)

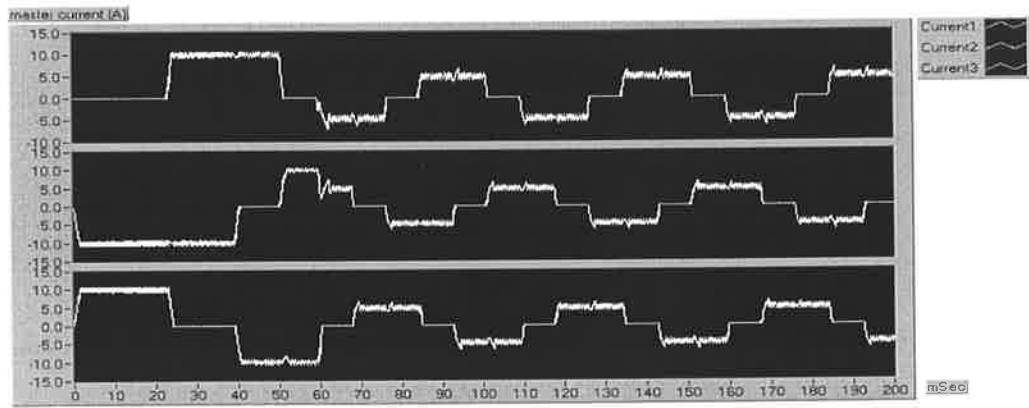


(b)

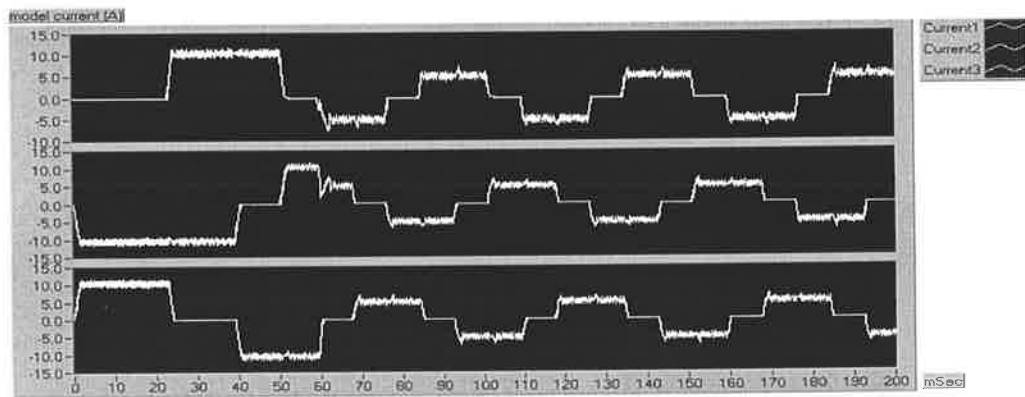
Figure 4.40 Simulation results under hysteresis current control, rectangular current excitation, trapezoidal back emf, 2% constant +5% random error on the DC link current

- a) Phase currents of the master motor, accelerating from standstill.
- b) Reconstructed phase currents when the DC link current errors are considered.

Fig.4.40 shows the rectangular simulated three-phase currents of the master motor and the motor model operating with a rectangular reference current. The currents from the motor model are reconstructed by using the information from the DC link current, which had a 2% constant and 5% random noise. As seen in **Fig.4.40(b)**, the current reconstruction algorithm functioned correctly and generated the three-phase currents accurately. Although some increase of the ripple current was observed, this was expected due to the artificially introduced noise on the DC link current of the motor drive.



(a)

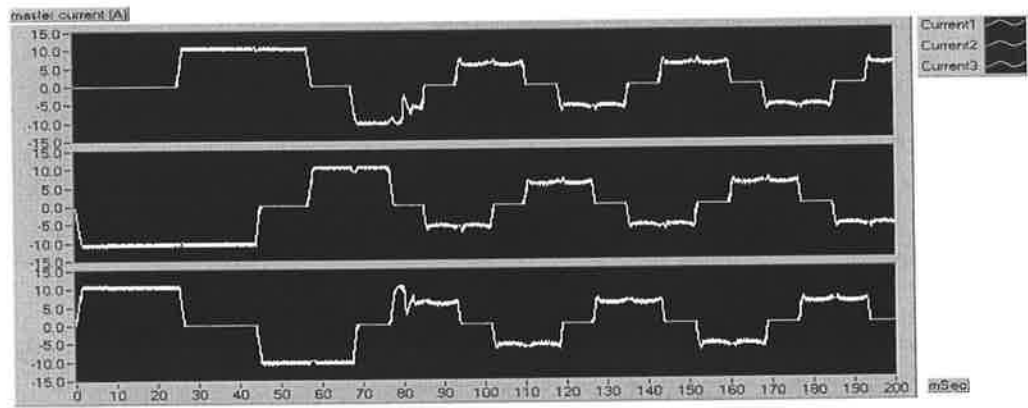


(b)

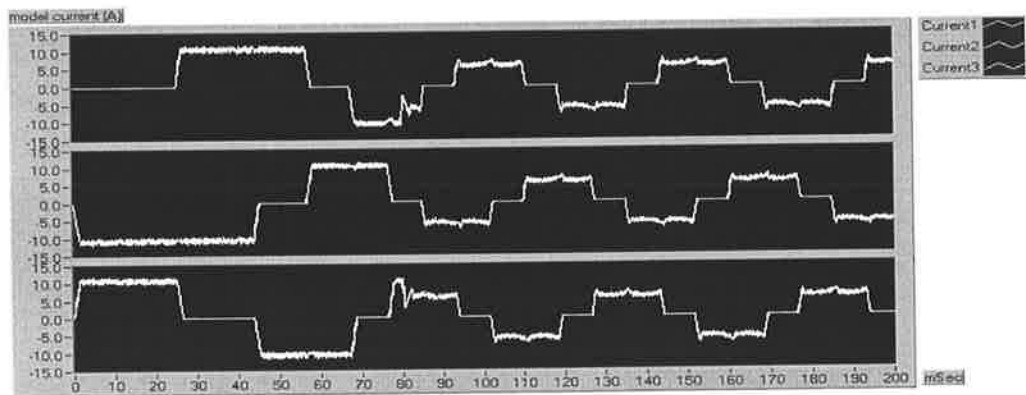
Figure 4.41 Simulation results under hysteresis current control, rectangular current excitation, trapezoidal back emf, 5% constant +5% random error on the DC link current

- a) Phase currents of the master motor, accelerating from standstill.
- b) Reconstructed phase currents when the DC link current errors are considered.

Fig.4.41 shows the simulation studies of the motor drive under identical operating conditions as in **Fig.4.40**. However, the level of constant noise introduced onto the DC link current as increased to 5%. The results of the reconstructed currents indicated a satisfactory outcome (**Fig.4.41(b)**).



(a)

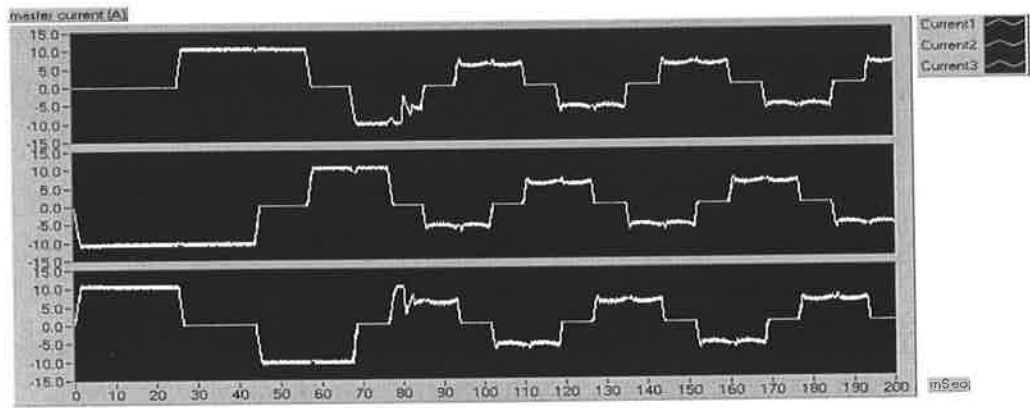


(b)

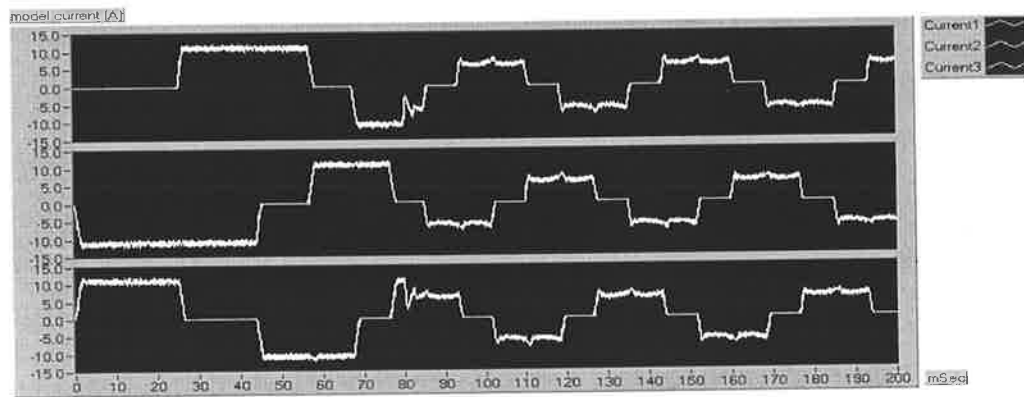
Figure 4.42 Simulation results under PWM current control, rectangular excitation current, sinusoidal back emf, 2% constant +5% random error on the DC link current

- a) Phase currents of the master motor, accelerating from standstill.
- b) Reconstructed phase currents when the DC link current errors are considered.

At this stage, the operating condition of the simulated motor drive was slightly altered and the results were provided in **Fig.4.42**. The back emf shape of the motor drive was set to "sinusoidal waveform" in this operation. However, it was found that the algorithm could still follow the real phase currents closely, as given in **Fig.4.42(b)**.



(a)

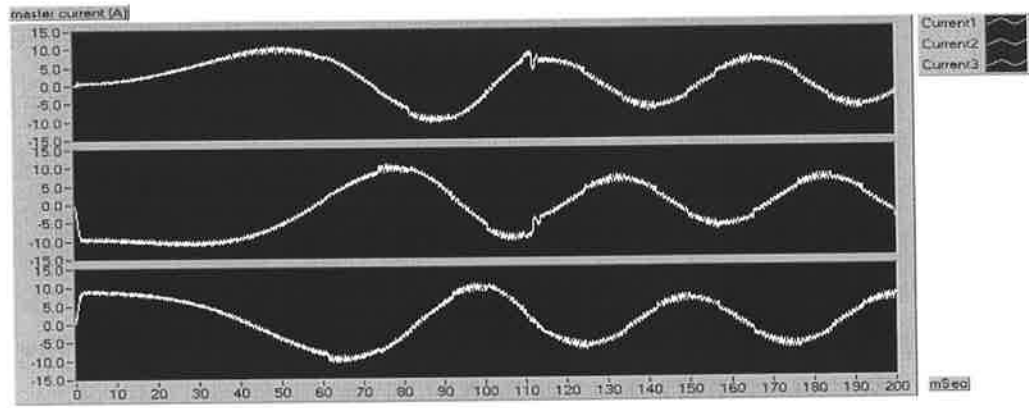


(b)

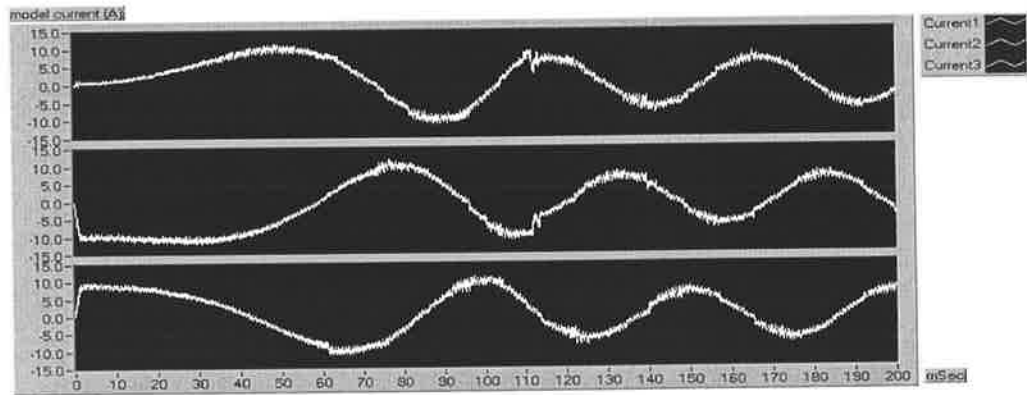
Figure 4.43 Simulation results under PWM current control, rectangular excitation current, sinusoidal back emf, 5% constant +5% random error on the DC link current

- a) Phase currents of the master motor, accelerating from standstill.
- b) Reconstructed phase currents when the DC link current errors are considered.

Similarly, increasing the DC current error by 3% constant, error did not influence the reconstruction of the currents significantly, which is presented in **Fig.4.43(b)**.



(a)



(b)

Figure 4.44 Simulation results under PWM current control, sinusoidal excitation current, sinusoidal back emf, 2% constant +5% random error on the DC link current

- a) Phase currents of the master motor, accelerating from standstill.
- b) Reconstructed phase currents when the DC link current errors are considered.

Fig.4.44(a) shows the simulated three-phase currents with the sinusoidal current excitation current and sinusoidal back emf. **Fig.4.44(b)** illustrates the reconstructed three-phase currents under the influence of errors on the DC link current. As shown in the figure, the current reconstruction algorithm operated accurately. Although the error in the reconstructed current was noticeable this was mainly due to the synthetic error introduced.

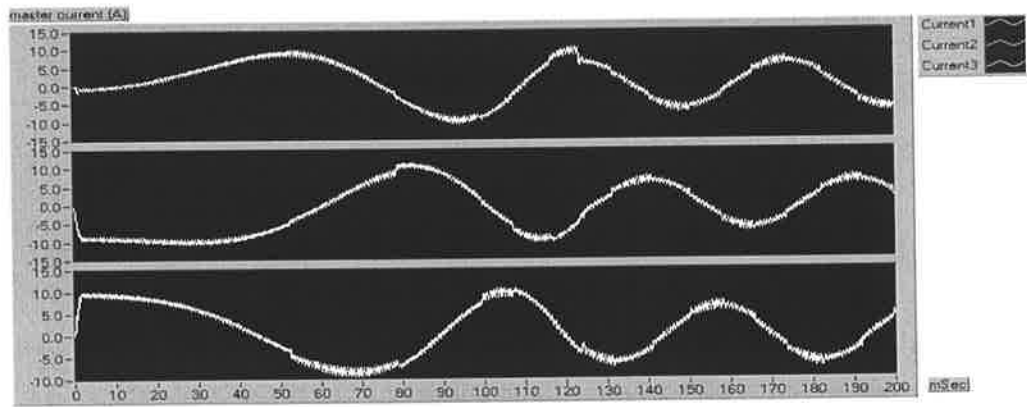


Fig.4.45 (a)

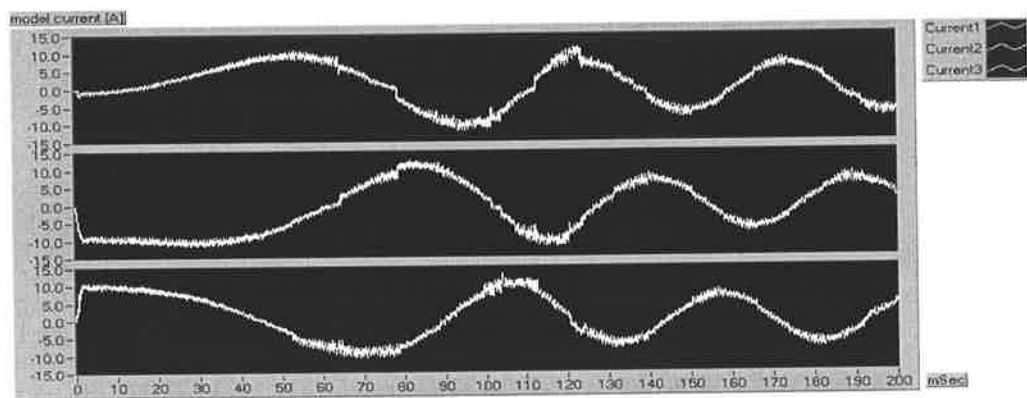


Fig4.45 (b)

Figure 4.45 Simulation results under PWM current control, sinusoidal excitation current, sinusoidal back emf, 5% constant +5% random error on the DC link current

- a) Phase currents of the master motor, accelerating from standstill.
- b) Reconstructed phase currents when the DC link current errors are considered.

Finally, **Fig.4.45** demonstrates that even under more synthetic errors, the algorithm developed in this project could achieve the reconstruction of the currents.

4.9 Conclusion

The layout of the current reconstruction concept has been explained. The real motor, which the three-phase currents would be reconstructed, and the motor simulator operated synchronously. The motor simulator simulated the three-phase currents of the real motor. However, the values of the simulated three-phase currents were just

near but not exactly the values of the three-phase currents of the real motor drive. Therefore, the DC link current from the real motor drive was used to make the simulated three-phase currents near to the three-phase currents of the real motor drive. The simulated three-phase currents were adjusted when the DC link currents of the real motor were generated.

As demonstrated the absolute value of the DC link current was equal to the absolute value of the current in the DC link phase. The current in the DC link phase was adjusted by using the DC link current of the real motor. Moreover, the currents of the other two phases in the motor simulator were altered in order to keep the current summation zero.

To demonstrate the reconstruction method, a complete and flexible motor simulator of the BLPM motor drive and the simulation modules of the current reconstruction system have been implemented by using the LabVIEW program and some artificial noises were added onto the DC link current of the real motor. The details of the program of the motor simulator and the current reconstruction module have been given. A number of the simulation results were provided to demonstrate both the operations of the motor drive and the current reconstruction. The motor drive could operate under various operating conditions and could predict the drive's operation accurately, and it was possible to reconstruct the phase currents by using the compensation method.

Chapter V

Experimental Results

5.1 Introduction

In Chapter 4, the three-phase currents from the motor simulator and the reconstructed three-phase currents from the simulator of the current reconstruction system were given. As seen, the values of the reconstructed three-phase currents were close to the values of the original three-phase currents from the master motor. To validate the simulation developed in this thesis, the experiment with the real motor was set up and a number of data set from the real motor drive were obtained to reconstruct the phase currents. This chapter will explain how data were acquired, provide the details of the experimental setup, and demonstrate the set of reconstructed currents from the data of the real motor drive.

As demonstrated earlier, the motor simulation was designed to be similar to the real motor drive. To achieve this, the motor parameters were measured accurately and used in the simulation. Moreover, the switching signals that occurred in the real motor drive were also used to execute the motor simulation. Hence, it was expected that the simulation results will be similar to the experimental results. However, as stated earlier, the real system contains various types of noises and component inaccuracies. Hence, the modelling of such errors become very difficult in the motor simulation. Hence, the motor phase currents in the simulation are only as accurate as the model equation.

The function of the DC link current was to confirm how high the amplitude of the three-phase currents in the experimental motor was. Since the absolute value of the DC link current was equal to the absolute value of one of the phase current, this confirmation was possible. After processing the DC real link current, the three-phase currents of the simulated motor were altered to make the three-phase currents as near as possible to the real motor currents.

As shown in Chapter 4, the real motor and the motor simulator operated synchronously. The DC link current of the real motor and the simulator were compared with reconstruct the three-phase currents. To validate the simulation developed in this thesis, a number of data sets from the real motor drive were used. The measured data was then processed to reconstruct the three-phase currents.

Ideally, the switching signals, three-phase currents and the DC link current should be measured to validate the simulation program. However, because of the hardware limitations, only the analog signals were measured, and the digital signals (the switching signals) were generated from these quantities. To generate the switching signals, the phase voltages of the motor were utilised. This process is illustrated in **Fig.5.1**. Eight-channel data were captured and stored first, as shown in **Fig.5.1 (a)**. Then these data sets were used to generate the switching signals.

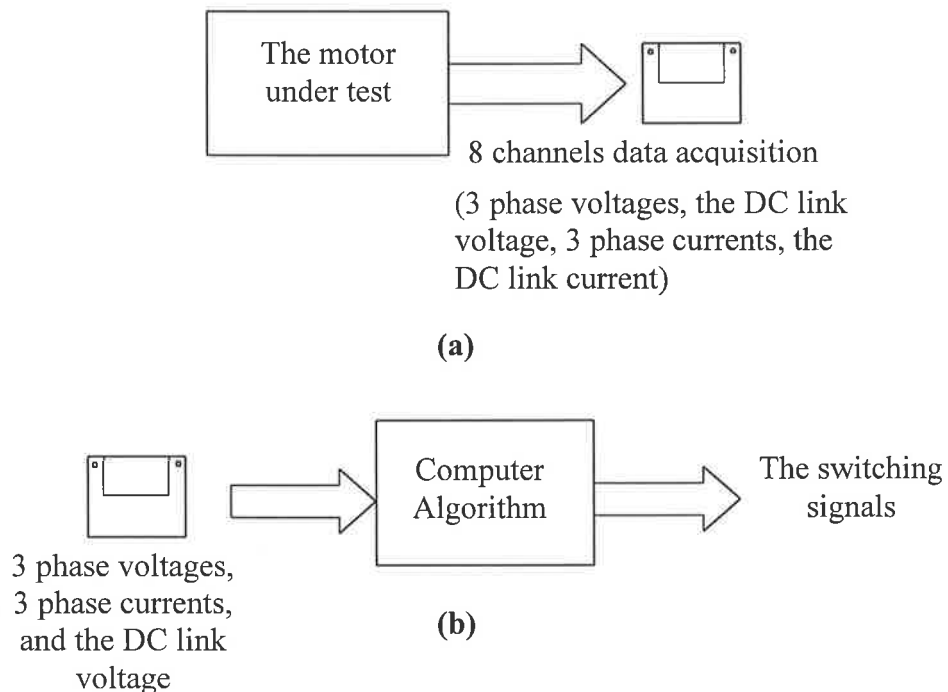


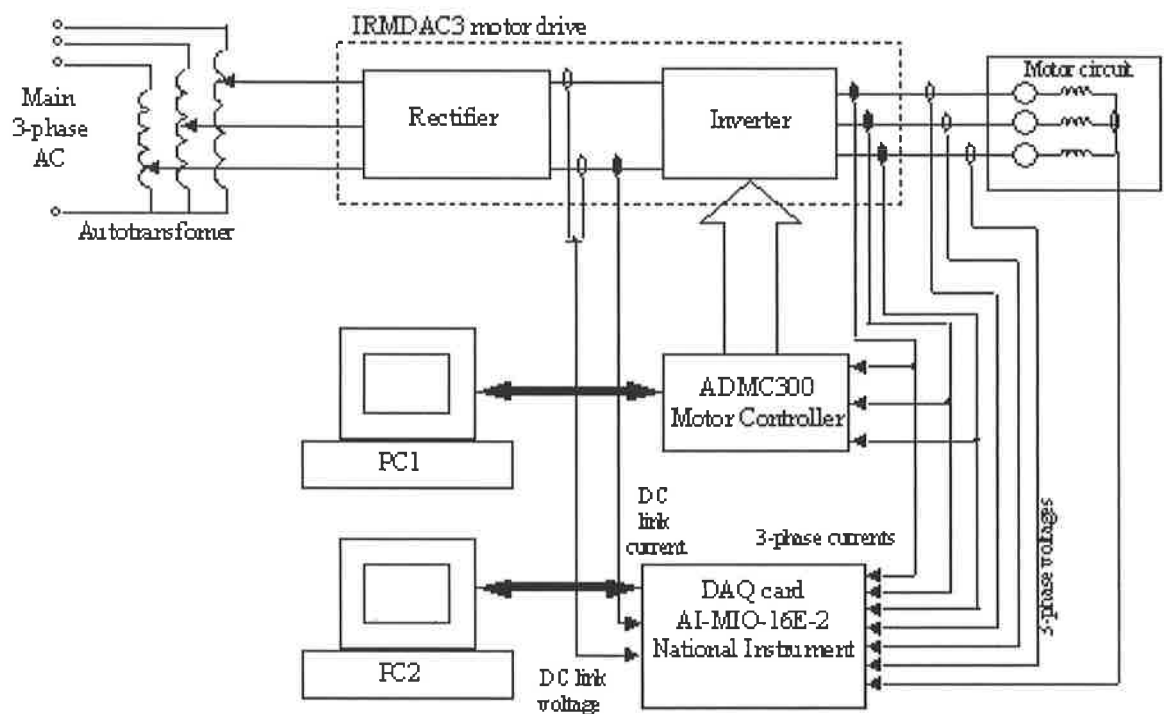
Figure 5.1 Steps followed to obtain the switching signals

5.2 Hardware of the experimental setup

Fig.5.2 shows the hardware of the motor drive, which was used to collect the three-phase currents, the three-phase voltages, the DC link current and the DC link voltage from the real BLPM motor. The specifications of the motor are given in **Table 5.1**.

Table 5.1 Specifications of the motor in the experimental setup

| Parameters | Size | Unit |
|---|-------|---------------|
| The number of pole pair | 28 | Pole pairs |
| Resistance of each phase winding | 6.4 | Ohm, Ω |
| Equivalent inductance of each phase winding | 32.8 | mH |
| The constant of back emf voltage | 3.785 | V·sec/rad |

**Figure 5.2** Schematic diagram of the hardware used in the tests

As shown in **Fig.5.2**, the main supply (240V, 50Hz) was fed to the rectifier via an autotransformer. The output of the rectifier was connected to the three-phase bridge inverter that is controlled by ADMC300 motor control DSP. There were two PCs used in this experimental setup. PC1 was used to program the DSP, and PC2 was used to control the data acquisition card and to store the captured data.

International Rectifier's IRMDAC3 converter card was utilised as a power circuit, which accommodated both the rectifier and the inverter circuits. The specification of this card is shown in **Table 5.2** [17] below,

Table 5.2 Specifications of the IRMDAC3

- Monolithic HVIC Integrates control and drive yields compact, robust, economical designs
- Compatible with short circuit, ground fault and over-temperature protection schemes
- 460V three phase AC, 50/60 Hz
- Inrush current limit and surge suppression
- Integral +15V and +5 bias supplies
- DC bus voltage and current feedback
- 150% overload capability (1 minute)

As mentioned above, the power switches in the inverter circuit of the IRMDAC3 card are controlled by the motor control DSP, ADMC300 from Analog Devices. The specifications of this DSP are shown in **Table 5.3** [18].

Table 5.3 Specifications of ADMC300

- 25 MIPS Fixed-Point DSP Core
- 4K x 24-Bit Program Memory RAM
- 2K x 24-Bit Program Memory ROM
- 1K x 16-Bit Data Memory RAM
- High-Resolution Multichannel ADC System
- Five Independent 16-Bit Sigma-Delta ADCs
- Arranged in Two Independently Clocked Banks
- Differential or Single-Ended Inputs
- Programmable Sample Frequency to 32.5 kHz
- Three-Phase PWM Generation Subsystem
- 16-Bit Dedicated PWM Generator

The three-phase currents were measured by the LEM current transducers, which are connected to the DSP to generate the switching signals. The currents were sampled by the DAQ cards, which were controlled by the LabVIEW program. Two PCI6110

DAQ cards (National Instruments) are used to acquire the data. Although the maximum scan rate of the DAQ card is 5 Ms/sec, a scan rate of 100 Ks/sec was found sufficient in the tests. The specifications of the DAQ card are given in **Table 5.4** [19].

Table 5.4 Specifications of PCI6110 DAQ card

| |
|---|
| <ul style="list-style-type: none"> ▪ Simultaneous-sampling ▪ Analog Inputs <ul style="list-style-type: none"> • 4 pseudodifferential inputs • 5 MS/s simultaneous-sampling rate • 12-bit resolution ▪ Analog Output <ul style="list-style-type: none"> • 2 channels, 16-bit resolution ▪ Digital I/O <ul style="list-style-type: none"> • 8 lines ▪ Counter/Timers <ul style="list-style-type: none"> • 24-bit resolution, 20 MHz counter/timers |
|---|

5.3 Current Reconstruction Algorithm used in the real tests

The motor drive setting and other parameters used in the calculation are given in **Table 5.5**. It should be noted here that the load torque was not employed in the calculations, and only the steady state DC-link current data was used to reconstruct the three-phase currents. Moreover, various other limitations were made to process the off-line data. The initial speed was assumed to be equal to the average speed (at the steady state) and the initial current was determined by plotting the measured phase currents and by determining the current value at the starting position.

As mentioned previously, 8 channels of the DAQ system were used to acquire a number of real time data set available in the motor drive. However, only the switching signals, the DC link current and the DC link voltage were utilised in the current reconstruction algorithm. The block diagram of the algorithm is given in **Fig.5.3**.

Table 5.5 Motor parameters and initial values used in the algorithm

| Parameters | Abbreviation | Unit | Remark |
|---|-----------------|-------------------|---|
| Time interval or scan rate | Δt | second | Defines the time step in the algorithm |
| The mode of back emf waveform: trapezoidal or sinusoidal | | | Used to determine the value of the back emf voltage that represents the real motor. |
| The back emf voltage constant | k_e | V·sec/rad | Used to determine the value of the back emf voltage |
| The resistance of the each phase | R | ohm | Used to model the motor phases |
| The equivalent inductance of the winding | L | H | Used to model the motor phase |
| Load torque | T_L | N·m | Used in the dynamic motor equation to find the speed and the position |
| Pole pairs | N_p | | Used to find the motor's speed and the position. |
| Inertia | J | | Used in the dynamic equation of the motor |
| Initial currents of the phases | i_1, i_2, i_3 | A | Used to set the initial values |
| Initial position of each phase | θ | Rad | Used to set the initial value |
| Initial speed | n | rad/sec, ω | Used to set the initial value |

In **Fig.5.3**, there are 2 sets of data from the motor simulator. The first set, which is composed of "Drive1", "Comp1" and "Motor1" SubVI, is to reconstruct three-phase currents without the information from the DC link current of the real motor. The second set, which is composed of "Drive2", "Comp2" and "Motor2" SubVI, is to reconstruct the three-phase currents with the information from the DC link current from the experimental data. The program details of the "Drive1" and "Drive2" SubVI

are similar. They are shown in **Fig.4.11** and **Fig.4.37**. The program detail of "Motor1" and "Motor2" SubVI are also similar. They are shown in **Fig.4.7** and **Fig.4.10**. The program details of "Comp1" and "Comp2" SubVI are also similar to that of Comp SubVI in the program of the current reconstruction system. They are shown in **Fig.4.38** and **Appendix A-2**.

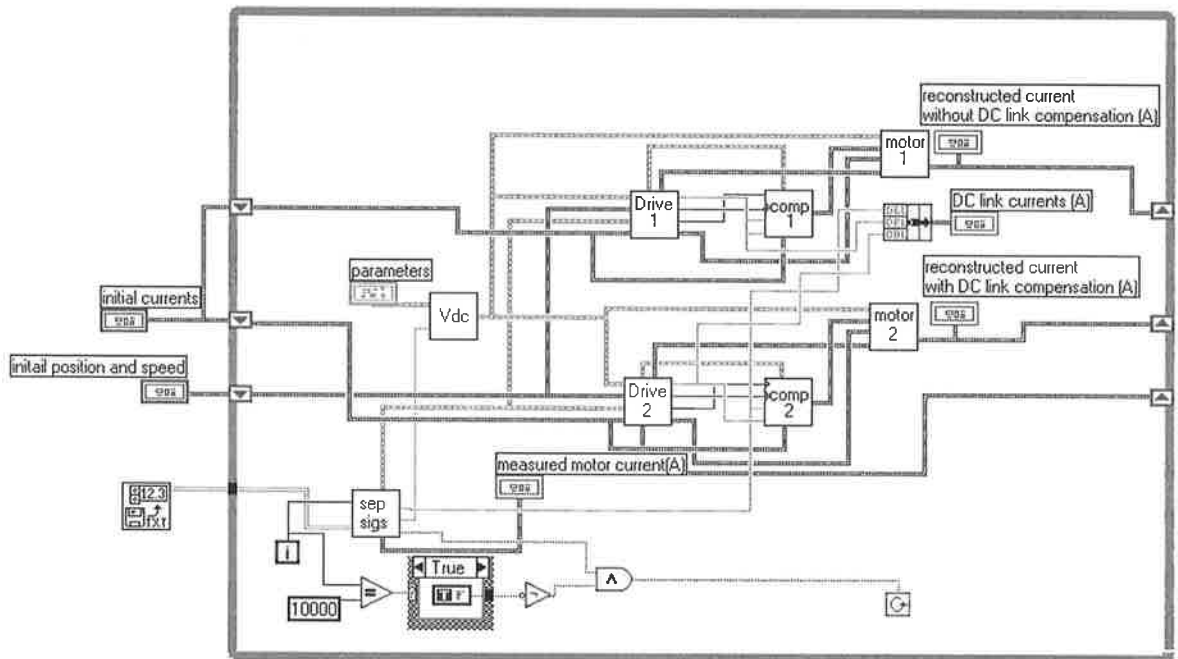


Figure 5.3 Diagram of the program to reconstruct the phase current using the experimental data

The inputs of the "Comp2" SubVI are the 2 DC link currents from the motor simulator and from the separate signal SubVI ("Sep Sigs"), and the three-phase currents of the simulator. The DC link current of the real motor from the "Sep Sigs" SubVI is compared with the DC link current from the "Drive2" SubVI, and then the output values of the compensated three-phase currents are linked to the "Motor2" SubVI, which calculates the three-phase currents for the next time step.

As stated in Chapter 4, the function of "Motor1" and "Motor2" is to calculate the values of the phase currents for the next time step. "Drive1" and "Drive2" SubVIs supply the inputs for "Motor1" and "Motor2" SubVI respectively. The function of "Comp1" and "Comp2" is to compensate the simulated three-phase current by using

the information from the DC link current. In the case of the set of the first motor SubVIs, the simulated three-phase currents are not compensated. The both DC link current inputs of "Comp1" SubVI are the simulated DC link current value from "Drive1" SubVI. In the case of the second motor SubVIs, the simulated three-phase currents are compensated by using the DC link current value from the experimental data. Therefore, one from two DC link inputs of "Comp2" SubVI is the value of DC link current from the experimental data and the other DC link input is the value of the DC link current from "Drive2" SubVI.

As illustrated in **Fig.5.3**, the program starts by reading the status of the switching signals, the DC link current and the DC link voltages from a file that store the data in the spreadsheet file format. Then these data are used to separate the parameters in the SubVI named "Sep Sigs". The detail of "Sep Sigs" SubVI is shown in **Appendix A-3**. The outputs of this SubVI are linked to three main SubVIs, "Vdc", "Drive1" and "Drive2". "Vdc" SubVI is used to condition the DC link voltage to be used in the algorithm. The detail of "Vdc" SubVI is shown in **Appendix A-3**. The DC link voltage from this VI, the DC link voltage, and the switching signals from "Sep Sigs" SubVI are linked to "Drive1" and "Drive2" SubVI. Then, "Drive1" and "Drive2" calculate the DC link current and outputs the data for supplying the current compensation SubVI, "Comp1" and "Comp2" consequently. The output terminal voltages and the DC link voltage from "Drive1" and "Drive2" are provided to the SubVI named "Motor1" and "Motor2" respectively.

5.4 Experimental Results

Two sets of experimental results were obtained and presented in this section: trapezoidal current excitation (**Fig.5.4** and **Fig.5.5**) and sinusoidal current excitation (**Fig.5.6** and **Fig.5.7**). In each set, the motor drive is operated at two different speeds, 50 Hz and 25 Hz, and the current reconstruction algorithm was executed off-line.

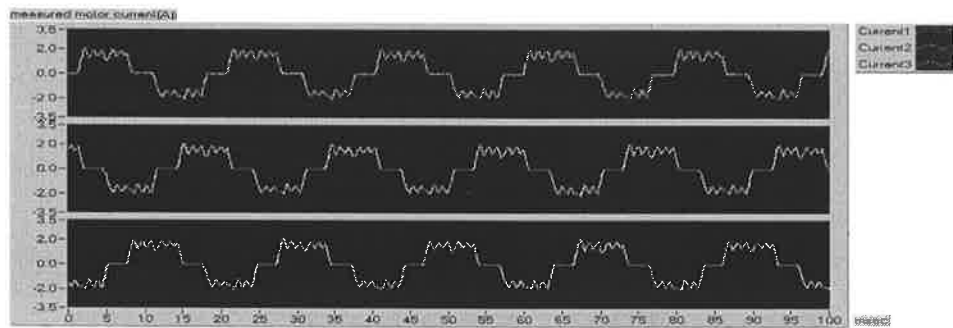
Fig.5.4 (a) shows the three-phase motor current while operating at 50 Hz. The current control mode in this test was hysteresis current control and rectangular current excitation. **Fig.5.4 (b)** illustrates the reconstructed current waveforms without compensation, which means that the currents were reconstructed by using the

switching signals only. The reconstructed currents after the current compensation were given in **Fig.5.4 (c)** and were obtained by using the switching signals and the DC link current. As seen in **Fig.5.4(b)**, the reconstructed currents without compensation had no transient at zero current levels. However, it was observed that the magnitude of the currents increases over the time when compared with **Fig5.4(c)**.

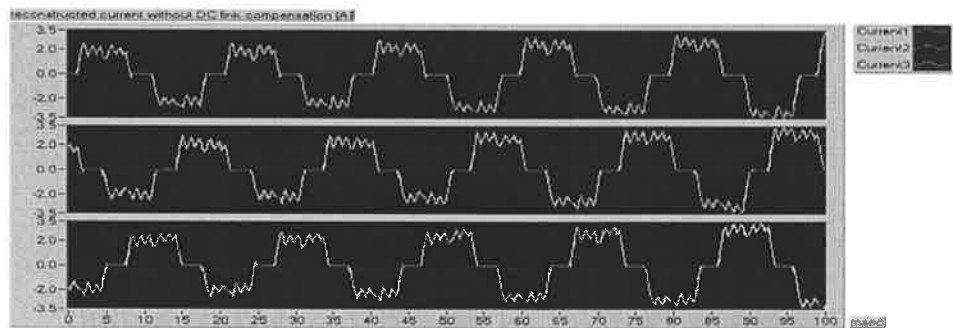
The corresponding DC link current waveforms without and with current compensation were given in **Fig.5.4 (d)**. It was observed in these figures that the measured DC link current waveforms (above trace) had noises. In addition, the magnitude change of the current without the current compensation was also observed on the estimated DC link current (middle trace in **Fig.5.4(d)**).

The test results of the trapezoidal current excited motor drive at low speed (25Hz) were given in **Fig.5.5**. The results in this test were presented in the same order as **Fig.5.4**.

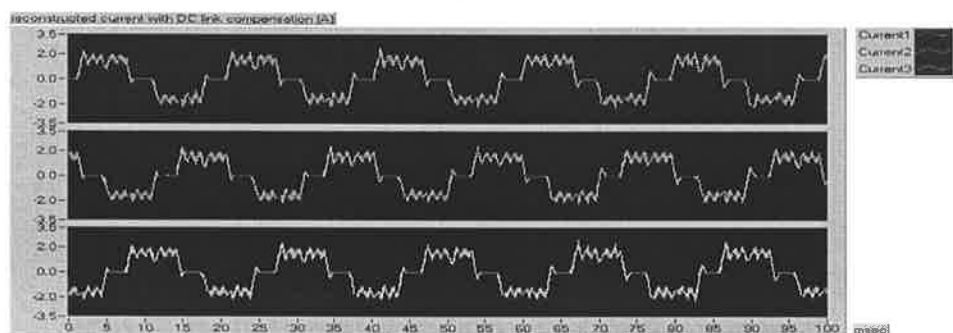
It should be noted here that, in this mode of operation, the current was limited by the back emf waveform and hence did not reach the level set by the current controller. The zero current level transients are also observed on the DC link currents that was compensated as shown in **Fig.5.5(c)**. Similarly, the DC link currents without and with the current compensation are given in **Fig.5.5 (d)**.



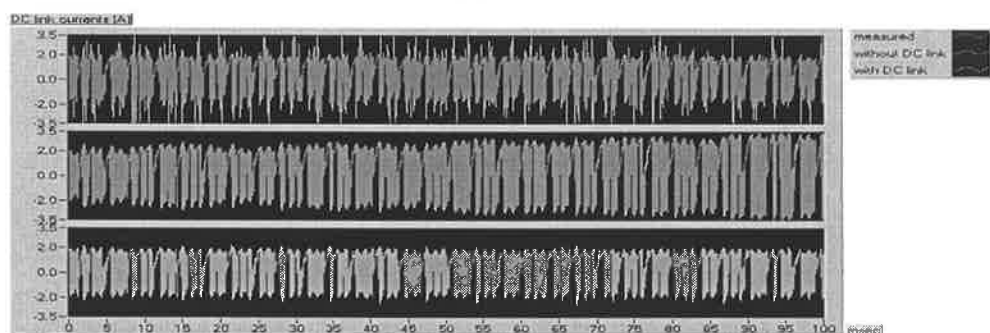
(a)



(b)

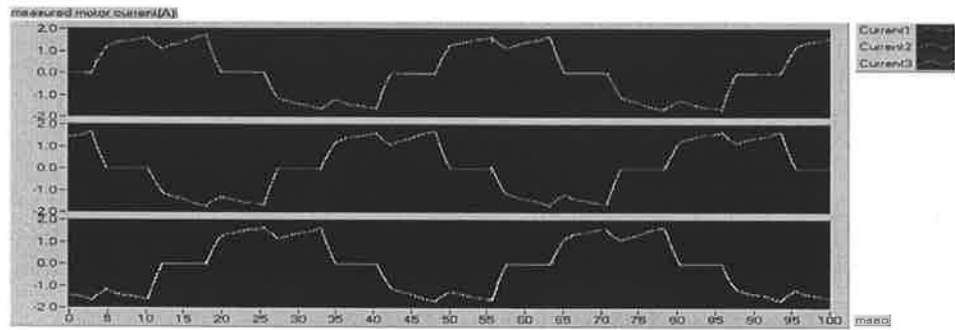


(c)

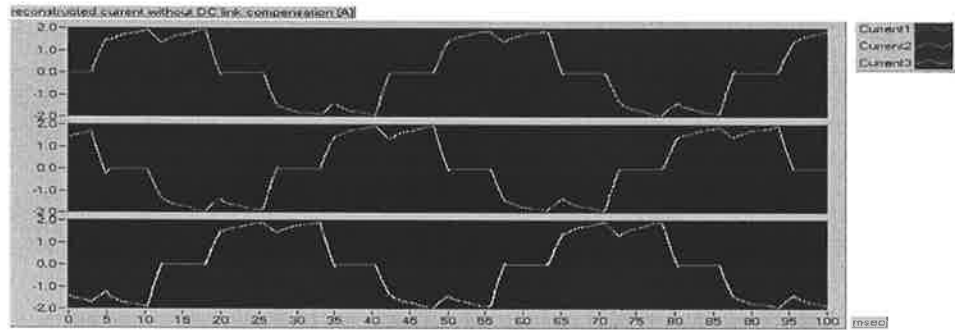


(d)

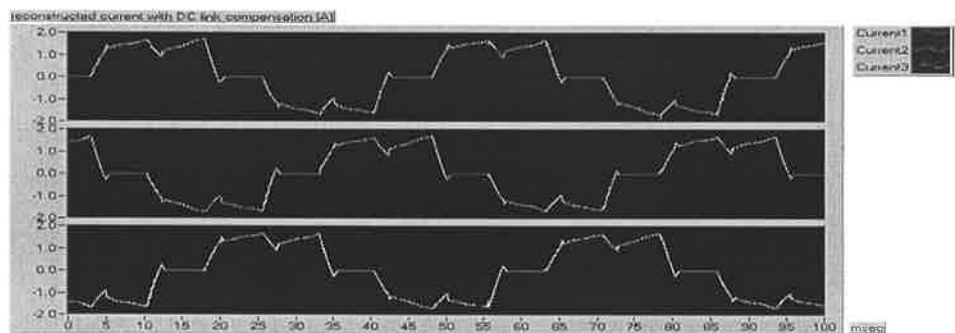
Figure 5.4 Test results at a speed of 50 Hz with the rectangular current excitation of the motor drive: (a) Measured three-phase currents, (b) Reconstructed three-phase currents without the DC link current compensation, (c) Reconstructed three-phase currents with the DC link current compensation, (d) Measured DC link current, the reconstructed DC link current without and with the DC link current compensation



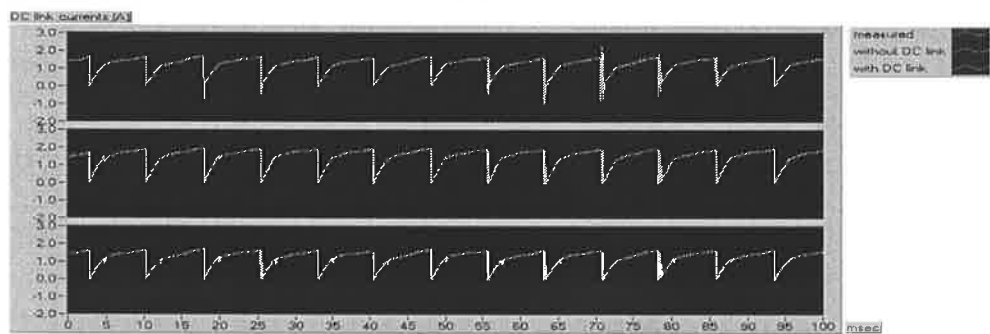
(a)



(b)



(c)



(d)

Figure 5.5 Test results at a speed of 25 Hz with the rectangular current excitation of the motor drive: (a) Measured three-phase currents, (b) Reconstructed three-phase currents without the DC link current compensation, (c) Reconstructed three-phase currents with the DC link current compensation, (d) Measured DC link current, the reconstructed DC link current without and with the DC link current compensation

As indicated above, the second set of the test results was obtained by using the sinusoidal current excitation in the motor drive. The current reconstruction algorithm was performed, which was based on the measured data and the identical set of results to the earlier test were illustrated in **Fig.5.6**. **Fig.5.6(a)** shows the three-phase measured currents of the BLPM motor operating a speed at 50 Hz, sinusoidal excitation. **Fig.5.6(b)** and **Fig.5.6(c)** illustrate the reconstructed three-phase currents without and with the DC link current compensation respectively. As seen in **Fig.5.6 (b)**, the magnitude of the current increases over time if the current compensation was not performed. However, some switching transients were observed after the compensation was introduced. (**Fig.5.6(c)**).

It should be emphasised here that the measured DC link current waveforms could not have such fast current transients and negative currents (**Fig.5.6(d)** above trace). These were due to the proximity effect of the switches onto the current transducers used to measure the real currents in the experimental setup.

The results given in **Fig.5.7** were similar to the operating settings explained in **Fig.5.6**. However, the speed of the motor drive was set to 25 Hz, in this case, the current control was not achieved but the current was limited by the back emf voltage.

Two important conclusions in these tests were that the magnitudes of the reconstructed currents were significantly less than the real current. In addition, significant phase delay was observed on the reconstructed current values. As reported in Section 5.1, it is believed that these discrepancies might be due to the inaccurate values of the motor parameters and the impacts of the measurement errors in the setup.

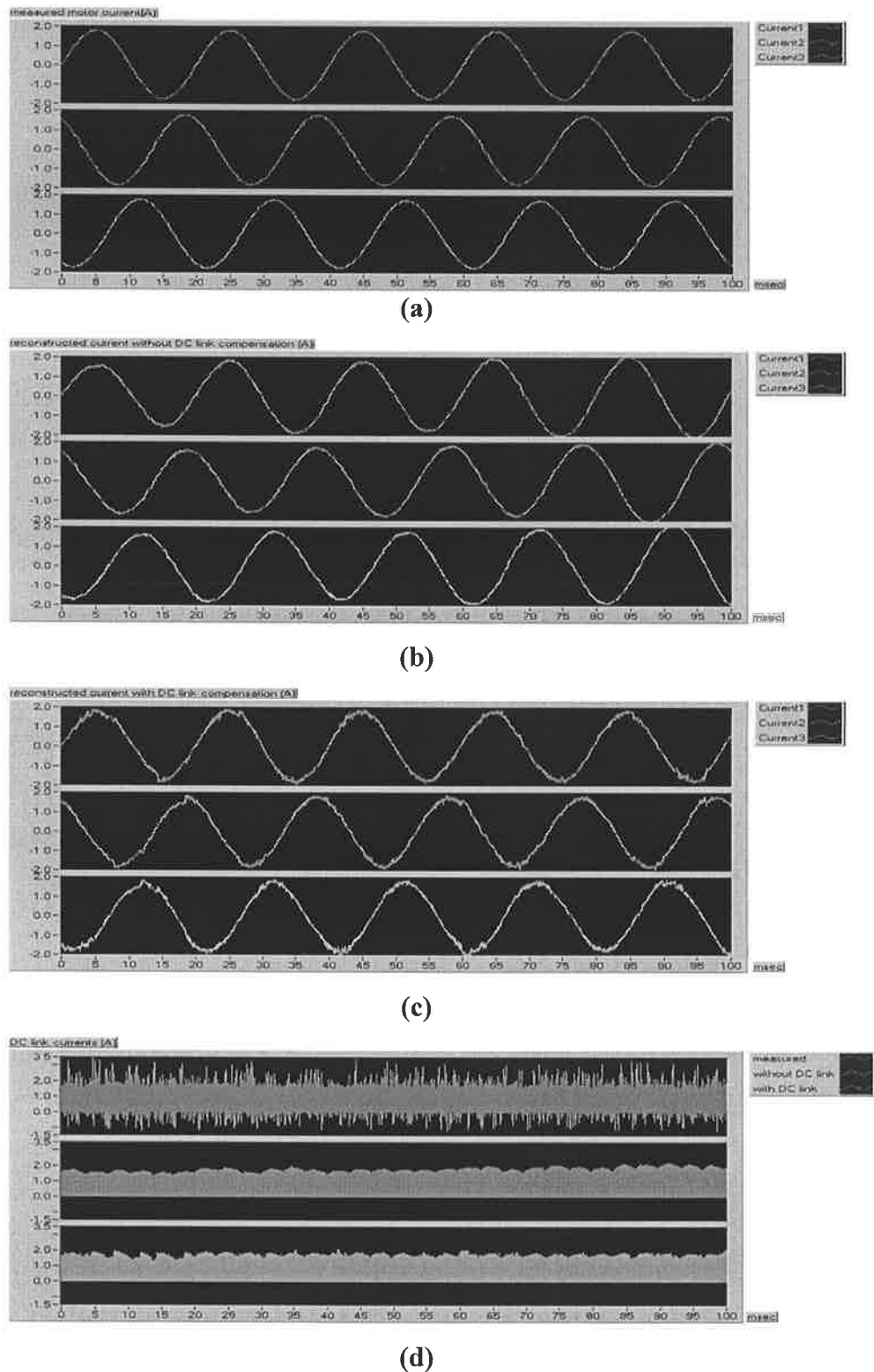
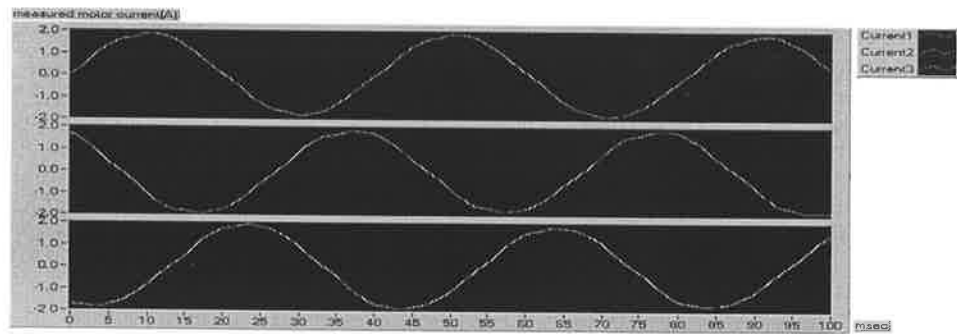
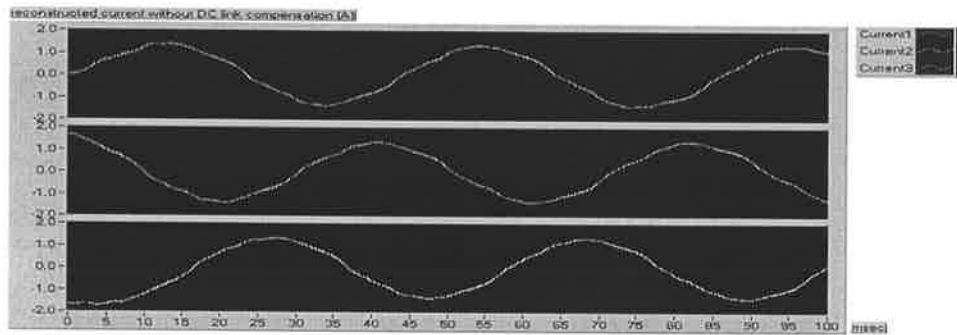


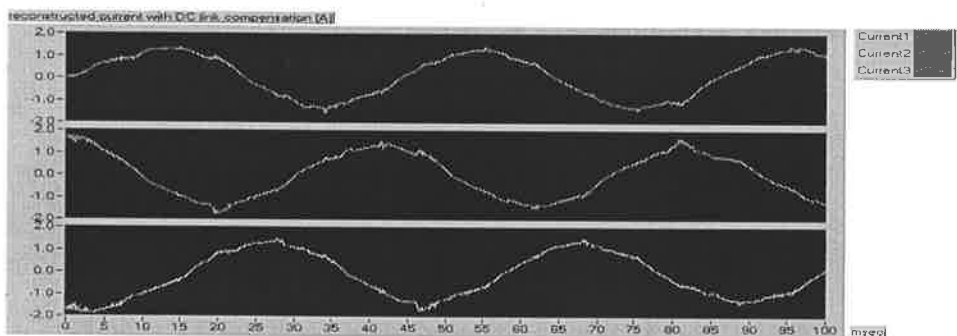
Figure 5.6 Test results at a speed of 50 Hz with the sinusoidal current excitation of the motor drive: (a) Measured three-phase currents, (b) Reconstructed three-phase currents without the DC link current compensation, (c) Reconstructed three-phase currents with the DC link current compensation, (d) Measured DC link current, the reconstructed DC link current without and with the DC link current compensation



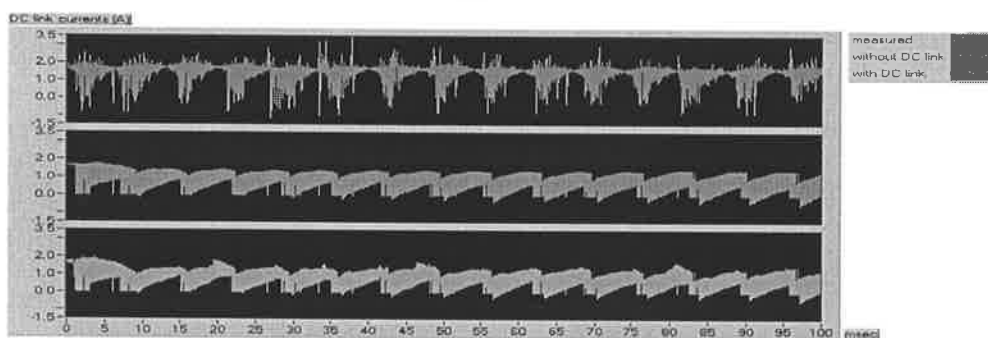
(a)



(b)



(c)



(d)

Figure 5.7 Test results at a speed of 25 Hz with the sinusoidal current excitation of the motor drive: (a) Measured three-phase currents, (b) Reconstructed three-phase currents without the DC link current compensation, (c) Reconstructed three-phase currents with the DC link current compensation, (d) Measured DC link current, the reconstructed DC link current without and with the DC link current compensation

5.5 Conclusion

The chapter has presented the experimental diagram, hardware connection, and the real data measured from the real motor drive that can implement various control schemes, including the rectangular current and sinusoidal current excitation, which effectively cover all brushless PM motor types. In this experiment, the off-line data was used to perform the confirmation of the current reconstruction algorithm. The data was acquired by a fast DAQ system.

The test results provided here illustrate that the reconstruction of the phase currents could be achieved under some excitations and operating conditions of the motor drive. However, this is very much depended upon the accuracy of the used motor model. Moreover, at low speed operation under sinusoidal excitation, the results of the current reconstruction might not be acceptable in close-loop real drive because the magnitude and phase of the reconstructed currents were error. Therefore, the algorithm of the current compensation might be improved in the future.

Chapter VI

Conclusions and Suggestions

6.1 Conclusions

The Brushless Permanent Magnet (BLPM) motor is a popular motor configuration because of its benefits, which are lightweight, small size, high efficiency and low maintenance. Since the shape and the magnitude of the phase currents are the key to control the motor torque, the motor drive requires the values of the three-phase currents to feedback to the controller. Normally, two types of current sensors are used to measure the values of the currents: low-value resistor and Hall-Effect device. Due to the power loss in the resistor method, it is not preferred. In addition this method does not provide electrical isolation. Hall-Effect device, however, is expensive. Moreover, at least 2 current sensors are required in a star connected motor to measure the three-phase currents. This research investigated an alternative current detection technique and recommended a method to use a single current sensor. In the method, the DC link current of the inverter was measured and the three-phase currents were reconstructed by using the switching signals of the inverter.

A number of literatures were surveyed and it was identified that there are 2 main methods to analyse the relationship between the DC link current and the three-phase currents: Voltage Space Vector method and Switching State Analysis method. It was found that the Voltage Space Vector method could be used effectively only in the PWM current control method. Therefore, to cover the various control techniques, Switching State Analysis was used in this research. Switching State Analysis method revealed that there were possible 351 switching states in a practical three-phase inverter, which were obtained by multiplying 27 switching patterns with 13 current direction patterns.

The motor simulator was investigated, which was used to generate the values of the simulated three-phase currents. It was believed that the motor simulator could yield the values of the three-phase currents near the values of the three-phase currents of the real motor. However, it was recognised that the values of the three-phase currents

from the motor simulator cannot be exactly equal to the real motor due to the inaccuracies in modelling.

The simulation algorithm was written in LabVIEW, and identical motor drive parameters were used in the calculations, which were measured from the actual motor drive. However, when the DC link current from the motor is not equal to the measured DC link current from the real motor, it was assumed that the three-phase currents of the motor simulator were not equal to the three-phase currents of the real motor. Therefore, the three-phase currents in the motor simulator were compensated.

In addition, artificial noise was introduced and the original DC link current estimated by the simulator was altered. Although the simulation results were satisfactory, it was found that the sinusoidal current operation could not tolerate a high level of noise that is about 15% of the amplitude of the DC link current.

Following the simulation study, the real DC link current from the experimental setup was used in the current reconstruction algorithm. It was observed in this study that the results of the current reconstruction using the real data were not as accurate as the computer simulation. It was believed that this was mainly due to measurement errors, high level of noise in the practical system, modelling inaccuracies and in accurate current compensation. In addition, as stated above, the noise in the real DC link current data might be higher than 15% of the amplitude of the DC link current. Therefore, this could cause the reconstructed three-phase currents to be distorted significantly. Furthermore, the concept of the compensation reinforced the noise adding to the reconstructed three-phase currents, which effectively made the amplitude of the noise double.

Chapter 2 described the general information about the BLPM motor. Though the BLPM motor was expensive when compared with the other types of motors, it was required in high efficient and maintenance free work. The mathematical model, voltage equation, back emf voltage equation and torque equation, which were provided, were used to explain to concept of torque generation and also used in the computer simulation. The equations showed the torque of the BLPM motor depended on three-phase currents. Therefore, to control the motor is to control the phase

currents. This chapter also investigated the inverter circuit and the current conduction status: commutation and conduction, which were used in the simulator. The chapter included some explanations about the current control techniques: Hysteresis and PWM. The switching patterns generated in these methods were also studied.

The purpose of **Chapter 3** was to analyse the current measurement methods and the switching states of the inverter. Firstly, types, benefits and drawbacks of the practical current sensors were described, and the single current sensor that could be used in practical motor systems are identified.

Chapter 3 also contained a comprehensive literature survey that was focused on the minimum number of current sensors and current reconstruction techniques. The chapter highlighted two current reconstruction techniques that were based on the DC link current measurement: Voltage Space Vector and Switching State Analysis. It was observed that the Voltage Space Vector method was obtained by the analysis of only the PWM current control. The method was limited to 8 switching patterns in PWM current control, and it cannot be applied to the Hysteresis current control. However, Switching State Analysis method can be utilised to identify the status of the inverter circuit directly. The investigation of this method revealed that both PWM and Hysteresis current control can be used. However, not all of the switching states were covered in this method. In this chapter, the analysis of the switching state was done to cover all possible switching states in a three-phase inverter, and then the Switching State Analysis method was chosen in this study to reconstruct the phase currents from the DC link current.

The complete motor drive simulation was explained and some selected results were presented in **Chapter 4**. The layout of the Motor simulator consisted of two major block of the motor program: Master Motor and Motor Model. The parameters in both systems were identical and identical set of the switching signals were used. This arrangement allowed us to perform very flexible simulation study. The details of the program of the both motor systems and the functions of the SubVIs in the main program were also described in the chapter. A number of simulation results from Master Motor showed that the Master Motor program could be used to accurately generate the waveforms of the phase currents, the back emf voltage, the torque, and

the speed of the BLPM motor. After that the relationship of the inverter currents and the DC link current was described that the absolute value of the DC link current was equal to the absolute value of one of the three-phase currents. Moreover, the number of the phase current and the direction of the DC link current could be calculated. Then, the compensation method of the current reconstruction was explained. The DC link values from Master Motor and Motor Model were compared. If the both of the DC link current were not equal, the phase currents of Motor Model were adjusted by using the value of the DC link current from Master Motor. A number of the simulation results of the adjusted phase currents from Motor Model were also given. It demonstrated the effectiveness of the proposed method under the influence of noise.

To validate the simulation results, the data from the real motor drive were obtained and presented in **Chapter 5**. The experimental setup used in this section was explained. As explained in the chapter, due to the limitation of the hardware, the switching signals were not measured, which were obtained by using the measured currents and voltages in the inverter. The real data of the DC link current and the switching signals were saved into a data file, and the reconstruction of the phase currents was performed by using this off-line data. The results indicated that the method described and implemented in this study provided the prediction of the phase current satisfactorily. However, due to the high level of noise and inaccurate measurements, some operating conditions did not provide satisfactory results as mentioned in the chapter.

6.2 Suggestions

As demonstrated in the thesis, the reconstruction of the phase currents can be achieved by using the switching signals and only one current sensor on the DC link. However, some additional measures are required to use the method in the real motor drive. Firstly, to reduce the distortion on the reconstructed currents, it is suggested that the measurement system should be carefully designed to minimise the noise, and the current compensation method should be improved for more accurate compensation. It is also suggested that the impact of inverter switching noise can be eliminated by using Fuzzy Logic that can separate the real signals from the noise

component. Although filtering may reduce such noise, the degradation of the real signal and phase shift introduced by filter are not desirable in current measurement.

Secondly, the current compensation section of the algorithm requires modification and further study. The impact of the noise is very significant specially when the DC link current has high noise. Therefore, the compensation module should be altered to compensate the DC link current and the correct phase, not the other two phases. However, a method should be developed to balance the three-phase currents.

Finally, a more accurate motor model is required for the accurate reconstruction of the currents. An accurate motor model may include the influence of the winding currents onto the resistance, the inductance and the back emf constant of the phase winding. In addition, the speed of the motor can be included to improve the operation of the method at a low speed of the motor drive.

Reference:

- [1] S.A. Nasar, I. Boldea and L.E. Unnewehr, *Permanent Magnet Reluctance and Self-Synchronous Motors*, CRC Press, Inc., USA, 1993.
- [2] P.C. Sen, *Principles of Electric Machine and Power Electronics*, 2nd Edition, John Wiley&Sons, 1997.
- [3] T.J.E Miller, *Brushless Permanent-Magnet and Reluctance Motor Drives*, Clarendon Press, Oxford, 1993.
- [4] N. Ertugrul, "Position Estimation and Performance Prediction for Permanent-Magnet Motor Drives," Thesis submitted to the Faculty of Engineering for the degree of doctor of Philosophy, University of Newcastle upon Tyne, 1993.
- [5] P.D. Evans and R.J. Hill-Cottingham, "DC Link Current in PWM Inverters," Proc.IEE, vol.133, Pt.B, no.4, 1986.
- [6] International Rectifier, "Solving IGBT Protection in AC or BLDC Motor Drive," Technical Paper, Retrieved September 1999 from <http://www.irf.com/technical-info/papers.html>
- [7] P.P. Acarnley, "Observability Criteria for Winding Currents in Three-Phase Brushless DC Drives," IEEE Trans. Power Electron., vol.8, pp.264-270,1993.
- [8] US Patent No. 5,214,575. Dec.16, 1991, E. Sugishima, T. Ando, "Ground Fault Detector for an Inverter and a Method therefore," 1993.
- [9] F. Blaabjerg and J.K. Pedersen, "A new low-cost fully fault protected PWM-VSI inverter with true phase-current information," in Proc. IPEC'95, 1995, vol.2, pp.984-991.
- [10] F. Blaabjerg and J.K. Pedersen, "Single Current Sensor Technique in the DC Link of Three-Phase PWM-VS Inverters : A Review and a novel Solution," IEEE Trans. Ind. App., vol.33, pp.1241-1253, 1997.
- [11] T.M. Jahns, R.C. Becerra and M. Ehsani, "Integrated Current Regulation for a Brushless ECM Drive," IEEE Trans. Power Electron., vol.6, no.1, pp.118-126, Jan. 1991.
- [12] J.T. Boys, "Novel current sensor for PWM AC drives," Proc. IEE, vol.135, no.1, pp. 27-32, 1988.

- [13] R.C. Kavanagh, J.M.D. Murphy and M.G. Egan, "*Innovation Current Sensing for Brushless DC Drives*," Proc.IEE Conference on Power Electronics and Variable-Speed Drives, pp.354-357, 1988.
- [14] T.C. Green and B.W. Williams, "*Derivation of motor line-current waveforms from the DC-link current of an inverter*," Proc.IEE, vol.136, pp.196-204, July 1989.
- [15] J.F. Moynihan, S. Bolognani, R.C. Kavanagh, M.G. Egan and J.M.D. Murphy, "*Single Sensor Current Control of AC Servodrives Using Digital Signal Processors*," Proc. of the 1993 European Power Electronics Conference, pp.415-421.
- [16] R.C. Becerra, M. Ehsani and T. Jahns, "*Four Quadrant Brushless ECM Drive with Integrated Current Regulation*," Proc. of the 1989 IEEE Industry Application Society Annual Meeting (IAS'89), pp.819-828.
- [17] International Rectifier, "*IR2233 Reference Design Kit: 3-phase 460VAC 3HP Motor Drive*," Technical Paper, Retrieved January 2001 from World Wide Web:
http://www.irf.com/technical_info/papers.html
- [18] Analog Device, "*High Performance DSP-Based Motor Controller*," Retrieved January 2001, from World Wide Web:
<http://www.analog.com/products/info.asp?product=ADMC300>
- [19] National Instruments, "*Simultaneous-Sampling Multifunction DAQ 5MS/s, 12-Bit, 2 or 4 Analog Inputs*," Retrieved January 2001, from World Wide Web:
<http://www.sine.ni.com/apps/we/nioc.vp?lang=US&PC=mn&cid=1039>

Appendices

A-1 The detailed analysis of the switching state

Table A-1 shows the switching pattern, the current direction, the conducting devices, the phase number, of which the current amplitude is equal to the amplitude of the DC link current, and the phase number, of which the current amplitude is equal to the amplitude of the circulating current.

Definition of the abbreviation

In the first three columns, Sp1, Sp2 and Sp3 are the switching pattern. Sp1 indicates which the power switch of phase1 is turned on. U in Sp1 column means T1 is turned on and L in Sp1 column means T4 is turned on. Sp2 indicates which the power switch of phase2 is turned on. U in Sp2 column means T3 is turned on and L in Sp2 column means T6 is turned on. Sp3 indicates which the power switch of phase3 is turned on. U in Sp3 column means T5 is turned on and L in Sp3 column means T2 is turned on.

In the next three columns, i1, i2 and i3 are the current directions. i1 indicates the direction of the phase1 current; i2 indicates the direction of phase2 current; i3 indicates the direction of phase3 current. + in each column means the phase current flows from the inverter circuit to the motor and – means the phase current flows from the motor to the inverter circuit.

Cp1, Cp2 and Cp3 indicate the conducting devices in phase1, phase2 and phase3 respectively. SU means the upper power switch of that phase is conducting. SL means the lower switch of that phase is conducting. DU means the upper diode of that phase is conducting. DL means the lower diode of that phase is conducting.

In DC link column, the number indicates the number of phase of which the absolute amplitude current is equal to the absolute amplitude current of the DC link current. In case “0” means there is no DC link current.

In circulate column, the number indicates the number of phase which the absolute amplitude current is equal to the absolute amplitude current of circulating current in the inverter circuit. "0" means there is no circulating current in that switching state.

Table A-1 Switching state, conducting device, DC link number and circulate number

| Sp1 | Sp2 | Sp3 | i1 | i2 | i3 | Cp1 | Cp2 | Cp3 | DC link | circulate |
|-----|-----|-----|----|----|----|----------------|----------------|----------------|---------|-----------|
| 0 | 0 | 0 | + | + | - | D _L | D _L | D _U | 3 | 0 |
| | | | + | 0 | - | D _L | - | D _U | 3 | 0 |
| | | | + | - | + | D _L | D _U | D _L | 2 | 0 |
| | | | + | - | 0 | D _L | D _U | - | 2 | 0 |
| | | | + | - | - | D _L | D _U | D _U | 1 | 0 |
| | | | 0 | + | - | - | D _L | D _U | 3 | 0 |
| | | | 0 | 0 | 0 | - | - | - | 0 | 0 |
| | | | 0 | - | + | - | D _U | D _L | 2 | 0 |
| | | | - | + | + | D _U | D _L | D _L | 1 | 0 |
| | | | - | + | 0 | D _U | D _L | - | 1 | 0 |
| | | | - | + | - | D _U | D _L | D _U | 2 | 0 |
| | | | - | - | + | D _U | D _U | D _L | 3 | 0 |
| | | | - | 0 | + | D _U | - | D _L | 1 | 0 |
| U | U | U | + | + | - | S _U | S _U | D _U | 0 | 3 |
| | | | + | 0 | - | S _U | S _U | D _U | 0 | 3 |
| | | | + | - | + | S _U | D _U | S _U | 0 | 2 |
| | | | + | - | 0 | S _U | D _U | S _U | 0 | 2 |
| | | | + | - | - | S _U | D _U | D _U | 0 | 1 |
| | | | 0 | + | - | S _U | S _U | D _U | 0 | 3 |
| | | | 0 | 0 | 0 | S _U | S _U | S _U | 0 | 0 |
| | | | 0 | - | + | S _U | D _U | S _U | 0 | 2 |
| | | | - | + | + | D _U | S _U | S _U | 0 | 1 |
| | | | - | + | 0 | D _U | S _U | S _U | 0 | 1 |
| | | | - | + | - | D _U | S _U | D _U | 0 | 2 |
| | | | - | - | + | D _U | D _U | S _U | 0 | 3 |
| | | | - | 0 | + | D _U | S _U | S _U | 0 | 1 |
| L | L | L | + | + | - | D _L | D _L | S _L | 0 | 3 |
| | | | + | 0 | - | D _L | S _L | S _L | 0 | 1 |
| | | | + | - | + | D _L | S _L | D _L | 0 | 2 |
| | | | + | - | 0 | D _L | S _L | S _L | 0 | 1 |
| | | | + | - | - | D _L | S _L | S _L | 0 | 1 |
| | | | 0 | + | - | S _L | D _L | S _L | 0 | 2 |
| | | | 0 | 0 | 0 | S _L | S _L | S _L | 0 | 0 |
| | | | 0 | - | + | S _L | S _L | D _L | 0 | 3 |
| | | | - | + | + | S _L | D _L | D _L | 0 | 1 |
| | | | - | + | 0 | S _L | D _L | S _L | 0 | 2 |
| | | | - | + | - | S _L | D _L | S _L | 0 | 2 |
| | | | - | - | + | S _L | S _L | D _L | 0 | 3 |
| | | | - | 0 | + | S _L | S _L | D _L | 0 | 3 |

Table A-1 Switching state, conducting device, DC link number and circulate number
(continued)

| Sp1 | Sp2 | Sp3 | i1 | i2 | i3 | Cp1 | Cp2 | Cp3 | DC link | circulate |
|-----|-----|-----|----|----|----|----------------|----------------|----------------|---------|-----------|
| U | O | O | + | + | - | S _U | D _L | D _U | 2 | 1 |
| | | | + | 0 | - | S _U | - | D _U | 0 | 1 |
| | | | + | - | + | S _U | D _U | D _L | 3 | 1 |
| | | | + | - | 0 | S _U | D _U | - | 0 | 1 |
| | | | + | - | - | S _U | D _U | D _U | 0 | 1 |
| | | | 0 | + | - | S _U | D _L | D _U | 2 | 1 |
| | | | 0 | 0 | 0 | S _U | - | - | 0 | 0 |
| | | | 0 | - | + | S _U | D _U | D _L | 3 | 1 |
| | | | - | + | + | D _U | D _L | D _L | 1 | 0 |
| | | | - | + | 0 | D _U | D _L | - | 1 | 0 |
| | | | - | + | - | D _U | D _L | D _U | 2 | 0 |
| | | | - | - | + | D _U | D _U | D _L | 3 | 0 |
| | | | - | 0 | + | D _U | - | D _L | 1 | 0 |
| O | U | O | + | + | - | D _L | S _U | D _U | 1 | 2 |
| | | | + | 0 | - | D _L | S _U | D _U | 1 | 2 |
| | | | + | - | + | D _L | D _U | D _L | 2 | 0 |
| | | | + | - | 0 | D _L | D _U | - | 2 | 0 |
| | | | + | - | - | D _L | D _U | D _U | 1 | 0 |
| | | | 0 | + | - | - | S _U | D _U | 0 | 2 |
| | | | 0 | 0 | 0 | - | S _U | - | 0 | 0 |
| | | | 0 | - | + | - | D _U | - | 2 | 0 |
| | | | - | + | + | D _U | S _U | D _L | 3 | 2 |
| | | | - | + | 0 | D _U | S _U | D _L | 0 | 2 |
| | | | - | + | - | D _U | S _U | - | 0 | 2 |
| | | | - | - | + | D _U | D _U | D _L | 3 | 0 |
| | | | - | 0 | + | D _U | S _U | D _L | 3 | 2 |
| O | O | U | + | + | - | D _L | D _L | D _U | 3 | 0 |
| | | | + | 0 | - | D _L | - | D _U | 3 | 0 |
| | | | + | - | + | D _L | D _U | S _U | 1 | 3 |
| | | | + | - | 0 | D _L | D _U | S _U | 1 | 3 |
| | | | + | - | - | D _L | D _U | D _U | 1 | 0 |
| | | | 0 | + | - | - | D _L | D _U | 3 | 0 |
| | | | 0 | 0 | 0 | - | - | S _U | 0 | 0 |
| | | | 0 | - | + | - | D _U | S _U | 0 | 3 |
| | | | - | + | + | D _U | D _L | S _U | 2 | 3 |
| | | | - | + | 0 | D _U | D _L | S _U | 2 | 3 |
| | | | - | + | - | D _U | D _L | D _U | 2 | 0 |
| | | | - | - | + | D _U | D _U | S _U | 0 | 3 |
| | | | - | 0 | + | D _U | - | S _U | 0 | 3 |

Table A-1 Switching state, conducting device, DC link number and circulate number
(continued)

| Sp1 | Sp2 | Sp3 | i1 | i2 | i3 | Cp1 | Cp2 | Cp3 | DC link | circulate |
|-----|-----|-----|----|----|----|----------------|----------------|----------------|---------|-----------|
| L | O | O | + | + | - | D _L | D _L | D _U | 3 | 0 |
| | | | + | 0 | - | D _L | - | D _U | 3 | 0 |
| | | | + | - | + | D _L | D _U | D _L | 2 | 0 |
| | | | + | - | 0 | D _L | D _U | - | 2 | 0 |
| | | | + | - | - | D _L | D _U | D _U | 1 | 0 |
| | | | 0 | + | - | S _U | D _L | D _U | 3 | 1 |
| | | | 0 | 0 | 0 | S _U | - | - | 0 | 0 |
| | | | 0 | - | + | S _U | D _U | D _L | 2 | 1 |
| | | | - | + | + | S _U | D _L | D _L | 0 | 1 |
| | | | - | + | 0 | S _U | D _L | - | 0 | 1 |
| | | | - | + | - | S _U | D _L | D _U | 3 | 1 |
| | | | - | - | + | S _U | D _U | D _L | 2 | 1 |
| | | | - | 0 | + | S _U | - | D _L | 0 | 1 |
| O | L | O | + | + | - | D _L | D _L | D _U | 3 | 0 |
| | | | + | 0 | - | D _L | S _L | D _U | 3 | 2 |
| | | | + | - | + | D _L | S _L | D _L | 0 | 2 |
| | | | + | - | 0 | D _L | S _L | - | 0 | 2 |
| | | | + | - | - | D _L | S _L | D _U | 3 | 2 |
| | | | 0 | + | - | - | D _L | D _U | 3 | 0 |
| | | | 0 | 0 | 0 | - | S _L | - | 0 | 0 |
| | | | 0 | - | + | - | S _L | D _L | 0 | 2 |
| | | | - | + | + | D _U | D _L | D _L | 1 | 0 |
| | | | - | + | 0 | D _U | D _L | - | 1 | 0 |
| | | | - | + | - | D _U | D _L | D _U | 2 | 0 |
| | | | - | - | + | D _U | S _L | D _L | 1 | 2 |
| | | | - | 0 | + | D _U | S _L | D _L | 1 | 2 |
| O | O | L | + | + | - | D _L | D _L | S _L | 0 | 3 |
| | | | + | 0 | - | D _L | - | S _L | 0 | 3 |
| | | | + | - | + | D _L | D _U | D _L | 2 | 0 |
| | | | + | - | 0 | D _L | D _U | S _L | 2 | 3 |
| | | | + | - | - | D _L | D _U | S _L | 2 | 3 |
| | | | 0 | + | - | - | - | S _L | 0 | 3 |
| | | | 0 | 0 | 0 | - | - | S _L | 0 | 0 |
| | | | 0 | - | + | - | D _U | D _L | 2 | 0 |
| | | | - | + | + | D _U | D _L | D _L | 1 | 0 |
| | | | - | + | 0 | D _U | D _L | S _L | 1 | 3 |
| | | | - | + | - | D _U | D _L | S _L | 1 | 3 |
| | | | - | - | + | D _U | D _U | D _L | 3 | 0 |
| | | | - | 0 | + | D _U | - | D _L | 1 | 0 |

Table A-1 Switching state, conducting device, DC link number and circulate number
(continued)

| Sp1 | Sp2 | Sp3 | i1 | i2 | i3 | Cp1 | Cp2 | Cp3 | DC link | circulate |
|-----|-----|-----|----|----|----|----------------|----------------|----------------|---------|-----------|
| U | U | O | + | + | - | S _U | S _U | D _U | 0 | 3 |
| | | | + | 0 | - | S _U | S _U | D _U | 0 | 3 |
| | | | + | - | + | S _U | D _U | D _L | 3 | 1 |
| | | | + | - | 0 | S _U | D _U | - | 0 | 1 |
| | | | + | - | - | S _U | D _U | D _U | 0 | 1 |
| | | | 0 | + | - | S _U | S _U | D _U | 0 | 3 |
| | | | 0 | 0 | 0 | S _U | S _U | - | 0 | 0 |
| | | | 0 | - | + | S _U | D _U | D _L | 3 | 1 |
| | | | - | + | + | D _U | S _U | D _L | 3 | 2 |
| | | | - | + | 0 | D _U | S _U | - | 0 | 2 |
| | | | - | + | - | D _U | S _U | D _U | 0 | 2 |
| | | | - | - | + | D _U | D _U | D _L | 3 | 0 |
| | | | - | 0 | + | D _U | S _U | D _L | 3 | 2 |
| U | O | U | + | + | - | S _U | D _L | D _U | 2 | 1 |
| | | | + | 0 | - | S _U | - | D _U | 0 | 1 |
| | | | + | - | + | S _U | D _U | S _U | 0 | 2 |
| | | | + | - | 0 | S _U | D _U | S _U | 0 | 2 |
| | | | + | - | - | S _U | D _U | D _U | 0 | 1 |
| | | | 0 | + | - | S _U | D _L | D _U | 2 | 1 |
| | | | 0 | 0 | 0 | S _U | - | S _U | 0 | 0 |
| | | | 0 | - | + | S _U | D _U | S _U | 0 | 2 |
| | | | - | + | + | D _U | D _L | S _U | 2 | 3 |
| | | | - | + | 0 | D _U | D _L | S _U | 2 | 3 |
| | | | - | + | - | D _U | D _L | D _U | 2 | 0 |
| | | | - | - | + | D _U | D _U | S _U | 0 | 3 |
| | | | - | 0 | + | D _U | - | S _U | 0 | 3 |
| O | U | U | + | + | - | D _L | S _U | D _U | 1 | 2 |
| | | | + | 0 | - | D _L | S _U | D _U | 1 | 2 |
| | | | + | - | + | D _L | D _U | S _U | 1 | 3 |
| | | | + | - | 0 | D _L | D _U | S _U | 1 | 3 |
| | | | + | - | - | D _L | D _U | D _U | 1 | 0 |
| | | | 0 | + | - | - | S _U | D _U | 0 | 2 |
| | | | 0 | 0 | 0 | - | S _U | S _U | 0 | 0 |
| | | | 0 | - | + | - | D _U | S _U | 0 | 3 |
| | | | - | + | + | D _U | S _U | S _U | 0 | 1 |
| | | | - | + | 0 | D _U | S _U | S _U | 0 | 1 |
| | | | - | + | - | D _U | S _U | D _U | 0 | 2 |
| | | | - | - | + | D _U | D _U | S _U | 0 | 3 |
| | | | - | 0 | + | D _U | S _U | S _U | 0 | 1 |

Table A-1 Switching state, conducting device, DC link number and circulate number
(continued)

| Sp1 | Sp2 | Sp3 | i1 | i2 | i3 | Cp1 | Cp2 | Cp3 | DC link | circulate |
|-----|-----|-----|----|----|----|----------------|----------------|----------------|---------|-----------|
| L | L | O | + | + | - | D _L | D _L | D _U | 3 | 0 |
| | | | + | 0 | - | D _L | S _L | D _U | 3 | 2 |
| | | | + | - | + | D _L | S _L | D _L | 0 | 2 |
| | | | + | - | 0 | D _L | S _L | - | 0 | 2 |
| | | | + | - | - | D _L | S _L | D _U | 3 | 2 |
| | | | 0 | + | - | S _L | D _L | D _U | 3 | 1 |
| | | | 0 | 0 | 0 | S _L | S _L | - | 0 | 0 |
| | | | 0 | - | + | S _L | S _L | D _L | 0 | 3 |
| | | | - | + | + | S _L | D _L | D _L | 0 | 1 |
| | | | - | + | 0 | S _L | D _L | - | 0 | 1 |
| | | | - | + | - | S _L | D _L | D _U | 3 | 1 |
| | | | - | - | + | S _L | S _L | D _L | 0 | 3 |
| | | | - | 0 | + | S _L | S _L | D _L | 0 | 3 |
| L | O | L | + | + | - | D _L | D _L | S _L | 0 | 3 |
| | | | + | 0 | - | D _L | - | S _L | 0 | 3 |
| | | | + | - | + | D _L | D _U | D _L | 2 | 0 |
| | | | + | - | 0 | D _L | D _U | S _L | 2 | 3 |
| | | | + | - | - | D _L | D _U | S _L | 2 | 3 |
| | | | 0 | + | - | S _L | D _L | S _L | 0 | 2 |
| | | | 0 | 0 | 0 | S _L | - | S _L | 0 | 0 |
| | | | 0 | - | + | S _L | D _U | D _L | 2 | 1 |
| | | | - | + | + | S _L | D _L | D _L | 0 | 1 |
| | | | - | + | 0 | S _L | D _L | S _L | 0 | 2 |
| | | | - | + | - | S _L | D _L | S _L | 0 | 2 |
| | | | - | - | + | S _L | D _U | D _L | 2 | 1 |
| | | | - | 0 | + | S _L | - | D _L | 0 | 1 |
| O | L | L | + | + | - | D _L | D _L | S _L | 0 | 3 |
| | | | + | 0 | - | D _L | S _L | S _L | 0 | 1 |
| | | | + | - | + | D _L | S _L | D _L | 0 | 2 |
| | | | + | - | 0 | D _L | S _L | S _L | 0 | 1 |
| | | | + | - | - | D _L | S _L | S _L | 0 | 1 |
| | | | 0 | + | - | - | D _L | S _L | 0 | 3 |
| | | | 0 | 0 | 0 | - | S _L | S _L | 0 | 0 |
| | | | 0 | - | + | - | S _L | D _L | 0 | 2 |
| | | | - | + | + | D _U | D _L | D _L | 1 | 0 |
| | | | - | + | 0 | D _U | D _L | S _L | 1 | 3 |
| | | | - | + | - | D _U | D _L | S _L | 1 | 3 |
| | | | - | - | + | D _U | S _L | D _L | 1 | 2 |
| | | | - | 0 | + | D _U | S _L | D _L | 1 | 2 |

Table A-1 Switching state, conducting device, DC link number and circulate number
(continued)

| Sp1 | Sp2 | Sp3 | i1 | i2 | i3 | Cp1 | Cp2 | Cp3 | DC link | circulate |
|-----|-----|-----|----|----|----|----------------|----------------|----------------|---------|-----------|
| U | L | O | + | + | - | S _U | D _L | D _U | 2 | 1 |
| | | | + | 0 | - | S _U | S _L | D _U | 2 | 1 |
| | | | + | - | + | S _U | S _L | D _L | 1 | 3 |
| | | | + | - | 0 | S _U | S _L | - | 1 | 0 |
| | | | + | - | - | S _U | S _L | D _U | 2 | 3 |
| | | | 0 | + | - | S _U | D _L | D _U | 2 | 1 |
| | | | 0 | 0 | 0 | S _U | S _L | - | 1 | 0 |
| | | | 0 | - | + | S _U | S _L | D _L | 1 | 2 |
| | | | - | + | + | D _U | D _L | D _L | 1 | 0 |
| | | | - | + | 0 | D _U | D _L | - | 1 | 0 |
| | | | - | + | - | D _U | D _L | D _U | 2 | 0 |
| | | | - | - | + | D _U | S _L | D _L | 1 | 2 |
| | | | - | 0 | + | D _U | S _L | D _L | 1 | 2 |
| L | U | O | + | + | - | D _L | S _U | D _U | 1 | 2 |
| | | | + | 0 | - | D _L | S _U | D _U | 1 | 2 |
| | | | + | - | + | D _L | D _U | D _L | 2 | 0 |
| | | | + | - | 0 | D _L | D _U | - | 2 | 0 |
| | | | + | - | - | D _L | D _U | D _U | 1 | 0 |
| | | | 0 | + | - | S _L | S _U | D _U | 1 | 3 |
| | | | 0 | 0 | 0 | S _L | S _U | - | 2 | 0 |
| | | | 0 | - | + | S _L | D _U | D _L | 2 | 1 |
| | | | - | + | + | S _L | S _U | D _L | 2 | 3 |
| | | | - | + | 0 | S _L | S _U | - | 2 | 0 |
| | | | - | + | - | S _L | S _U | D _U | 1 | 3 |
| | | | - | - | + | S _L | D _U | D _L | 2 | 1 |
| | | | - | 0 | + | S _L | S _U | D _L | 2 | 3 |
| L | O | U | + | + | - | D _L | D _L | D _U | 3 | 0 |
| | | | + | 0 | - | D _L | - | D _U | 3 | 0 |
| | | | + | - | + | D _L | D _U | S _U | 1 | 3 |
| | | | + | - | 0 | D _L | D _U | S _U | 1 | 3 |
| | | | + | - | - | D _L | D _U | D _U | 1 | 0 |
| | | | 0 | + | - | S _L | D _L | D _U | 3 | 1 |
| | | | 0 | 0 | 0 | S _L | - | S _U | 3 | 0 |
| | | | 0 | - | + | S _L | D _U | S _U | 1 | 2 |
| | | | - | + | + | S _L | D _L | S _U | 3 | 2 |
| | | | - | + | 0 | S _L | D _L | S _U | 3 | 2 |
| | | | - | + | - | S _L | D _L | D _U | 3 | 1 |
| | | | - | - | + | S _L | D _U | S _U | 1 | 2 |
| | | | - | 0 | + | S _L | - | S _U | 3 | 0 |

Table A-1 Switching state, conducting device, DC link number and circulate number
(continued)

| Sp1 | Sp2 | Sp3 | i1 | i2 | i3 | Cp1 | Cp2 | Cp3 | DC link | circulate |
|-----|-----|-----|----|----|----|----------------|----------------|----------------|---------|-----------|
| U | O | L | + | + | - | S _U | D _L | S _L | 1 | 2 |
| | | | + | 0 | - | S _U | - | S _L | 1 | 0 |
| | | | + | - | + | S _U | D _U | D _L | 3 | 1 |
| | | | + | - | 0 | S _U | D _U | S _L | 3 | 2 |
| | | | + | - | - | S _U | D _U | S _L | 3 | 2 |
| | | | 0 | + | - | S _U | D _L | S _L | 1 | 2 |
| | | | 0 | 0 | 0 | S _U | - | S _L | 1 | 0 |
| | | | 0 | - | + | S _U | D _U | D _L | 3 | 1 |
| | | | - | + | + | D _U | D _L | D _L | 1 | 0 |
| | | | - | + | 0 | D _U | D _L | S _L | 1 | 3 |
| | | | - | + | - | D _U | D _L | S _L | 1 | 3 |
| | | | - | - | + | D _U | D _U | D _L | 3 | 0 |
| | | | - | 0 | + | D _U | - | D _L | 1 | 0 |
| O | U | L | + | + | - | D _L | S _U | S _L | 2 | 1 |
| | | | + | 0 | - | D _L | S _U | S _L | 2 | 1 |
| | | | + | - | + | D _L | D _U | D _L | 2 | 0 |
| | | | + | - | 0 | D _L | D _U | S _L | 2 | 3 |
| | | | + | - | - | D _L | D _U | S _L | 2 | 3 |
| | | | 0 | + | - | - | S _U | S _L | 2 | 0 |
| | | | 0 | 0 | 0 | - | S _U | S _L | 2 | 0 |
| | | | 0 | - | + | - | D _U | D _L | 2 | 0 |
| | | | - | + | + | D _U | S _U | D _L | 3 | 2 |
| | | | - | + | 0 | D _U | S _U | S _L | 3 | 1 |
| | | | - | + | - | D _U | S _U | S _L | 3 | 1 |
| | | | - | - | + | D _U | D _U | D _L | 3 | 0 |
| | | | - | 0 | + | D _U | S _U | D _L | 3 | 2 |
| O | L | U | + | + | - | D _L | D _L | D _U | 3 | 0 |
| | | | + | 0 | - | D _L | S _L | D _U | 3 | 2 |
| | | | + | - | + | D _L | S _L | S _U | 3 | 1 |
| | | | + | - | 0 | D _L | S _L | S _U | 3 | 1 |
| | | | + | - | - | D _L | S _L | D _U | 3 | 2 |
| | | | 0 | + | - | - | D _L | D _U | 3 | 0 |
| | | | 0 | 0 | 0 | - | S _L | S _U | 3 | 0 |
| | | | 0 | - | + | - | S _L | S _U | 3 | 0 |
| | | | - | + | + | D _U | D _L | S _U | 2 | 3 |
| | | | - | + | 0 | D _U | D _L | S _U | 2 | 3 |
| | | | - | + | - | D _U | D _L | D _U | 2 | 0 |
| | | | - | - | + | D _U | S _L | S _U | 2 | 1 |
| | | | - | 0 | + | D _U | S _L | S _U | 2 | 1 |

Table A-1 Switching state, conducting device, DC link number and circulate number
(continued)

| Sp1 | Sp2 | Sp3 | i1 | i2 | i3 | Cp1 | Cp2 | Cp3 | DC link | circulate |
|-----|-----|-----|----|----|----|----------------|----------------|----------------|---------|-----------|
| U | L | L | + | + | - | S _U | D _L | S _L | 1 | 2 |
| | | | + | 0 | - | S _U | S _L | S _L | 1 | 0 |
| | | | + | - | + | S _U | S _L | D _L | 1 | 3 |
| | | | + | - | 0 | S _U | S _L | S _L | 1 | 0 |
| | | | + | - | - | S _U | S _L | S _L | 1 | 0 |
| | | | 0 | + | - | S _U | D _L | S _L | 1 | 2 |
| | | | 0 | 0 | 0 | S _U | S _L | S _L | 1 | 0 |
| | | | 0 | - | + | S _U | S _L | D _L | 1 | 3 |
| | | | - | + | + | D _U | D _L | D _L | 1 | 0 |
| | | | - | + | 0 | D _U | D _L | S _L | 1 | 3 |
| | | | - | + | - | D _U | D _L | S _L | 1 | 3 |
| | | | - | - | + | D _U | S _L | D _L | 1 | 2 |
| | | | - | 0 | + | D _U | S _L | D _L | 1 | 2 |
| L | U | L | + | + | - | D _L | S _U | S _L | 2 | 1 |
| | | | + | 0 | - | D _L | S _U | S _L | 2 | 1 |
| | | | + | - | + | D _L | D _U | D _L | 2 | 0 |
| | | | + | - | 0 | D _L | D _U | S _L | 2 | 3 |
| | | | + | - | - | D _L | D _U | S _L | 2 | 3 |
| | | | 0 | + | - | S _L | S _U | S _L | 2 | 0 |
| | | | 0 | 0 | 0 | S _L | S _U | S _L | 2 | 0 |
| | | | 0 | - | + | S _L | D _U | D _L | 2 | 1 |
| | | | - | + | + | S _L | S _U | D _L | 2 | 3 |
| | | | - | + | 0 | S _L | S _U | S _L | 2 | 0 |
| | | | - | + | - | S _L | S _U | S _L | 2 | 0 |
| | | | - | - | + | S _L | D _U | D _L | 2 | 1 |
| | | | - | 0 | + | S _L | S _U | D _L | 2 | 3 |
| L | L | U | + | + | - | D _L | D _L | D _U | 3 | 0 |
| | | | + | 0 | - | D _L | S _L | D _U | 3 | 2 |
| | | | + | - | + | D _L | S _L | S _U | 3 | 2 |
| | | | + | - | 0 | D _L | S _L | S _U | 3 | 2 |
| | | | + | - | - | D _L | S _L | D _U | 3 | 2 |
| | | | 0 | + | - | S _L | D _L | D _U | 3 | 1 |
| | | | 0 | 0 | 0 | S _L | S _L | S _U | 3 | 0 |
| | | | 0 | - | + | S _L | S _L | S _U | 3 | 0 |
| | | | - | + | + | S _L | D _L | S _U | 3 | 2 |
| | | | - | + | 0 | S _L | D _L | S _U | 3 | 2 |
| | | | - | + | - | S _L | D _L | D _U | 3 | 1 |
| | | | - | - | + | S _L | S _L | S _U | 3 | 0 |
| | | | - | 0 | + | S _L | S _L | S _U | 3 | 0 |

Table A-1 Switching state, conducting device, DC link number and circulate number

| Sp1 | Sp2 | Sp3 | i1 | i2 | i3 | Cp1 | Cp2 | Cp3 | DC link | circulate |
|-----|-----|-----|----|----|----|----------------|----------------|----------------|---------|-----------|
| L | U | U | + | + | - | D _L | S _U | D _U | 1 | 2 |
| | | | + | 0 | - | D _L | S _U | D _U | 1 | 2 |
| | | | + | - | + | D _L | D _U | S _U | 1 | 3 |
| | | | + | - | 0 | D _L | D _U | S _U | 1 | 3 |
| | | | + | - | - | D _L | D _U | D _U | 1 | 0 |
| | | | 0 | + | - | S _L | S _U | D _U | 1 | 3 |
| | | | 0 | 0 | 0 | S _L | S _U | S _U | 1 | 0 |
| | | | 0 | - | + | S _L | D _U | S _U | 1 | 2 |
| | | | - | + | + | S _L | S _U | S _U | 1 | 0 |
| | | | - | + | 0 | S _L | S _U | S _U | 1 | 0 |
| | | | - | + | - | S _L | S _U | D _U | 1 | 3 |
| | | | - | - | + | S _L | D _U | S _U | 1 | 2 |
| | | | - | 0 | + | S _L | S _U | S _U | 1 | 0 |
| U | L | U | + | + | - | S _U | D _L | D _U | 2 | 1 |
| | | | + | 0 | - | S _U | S _L | D _U | 2 | 3 |
| | | | + | - | + | S _U | S _L | S _U | 2 | 0 |
| | | | + | - | 0 | S _U | S _L | S _U | 2 | 0 |
| | | | + | - | - | S _U | S _L | D _U | 2 | 3 |
| | | | 0 | + | - | S _U | D _L | D _U | 2 | 1 |
| | | | 0 | 0 | 0 | S _U | S _L | S _U | 2 | 0 |
| | | | 0 | - | + | S _U | S _L | S _U | 2 | 0 |
| | | | - | + | + | D _U | D _L | S _U | 2 | 3 |
| | | | - | + | 0 | D _U | D _L | S _U | 2 | 3 |
| | | | - | + | - | D _U | D _L | D _U | 2 | 0 |
| | | | - | - | + | D _U | S _L | S _U | 2 | 1 |
| | | | - | 0 | + | D _U | S _L | S _U | 2 | 1 |
| U | U | L | + | + | - | S _U | S _U | S _L | 3 | 0 |
| | | | + | 0 | - | S _U | S _U | S _L | 3 | 0 |
| | | | + | - | + | S _U | D _U | D _L | 3 | 1 |
| | | | + | - | 0 | S _U | D _U | S _L | 3 | 2 |
| | | | + | - | - | S _U | D _U | S _L | 3 | 2 |
| | | | 0 | + | - | S _U | S _U | S _L | 3 | 0 |
| | | | 0 | 0 | 0 | S _U | S _U | S _L | 3 | 0 |
| | | | 0 | - | + | S _U | D _U | D _L | 3 | 1 |
| | | | - | + | + | D _U | S _U | D _L | 3 | 2 |
| | | | - | + | 0 | D _U | S _U | S _L | 3 | 1 |
| | | | - | + | - | D _U | S _U | S _L | 3 | 1 |
| | | | - | - | + | D _U | D _U | D _L | 3 | 0 |
| | | | - | 0 | + | D _U | S _U | D _L | 3 | 2 |

A-2 The details in the block diagram of the motor simulation program

In this research, the motor simulated program from LabVIEW program is used. Some of the programs were explained in Chapter 4. The detail of the block diagram of each SubVI is shown in this appendix.

PID SubVI

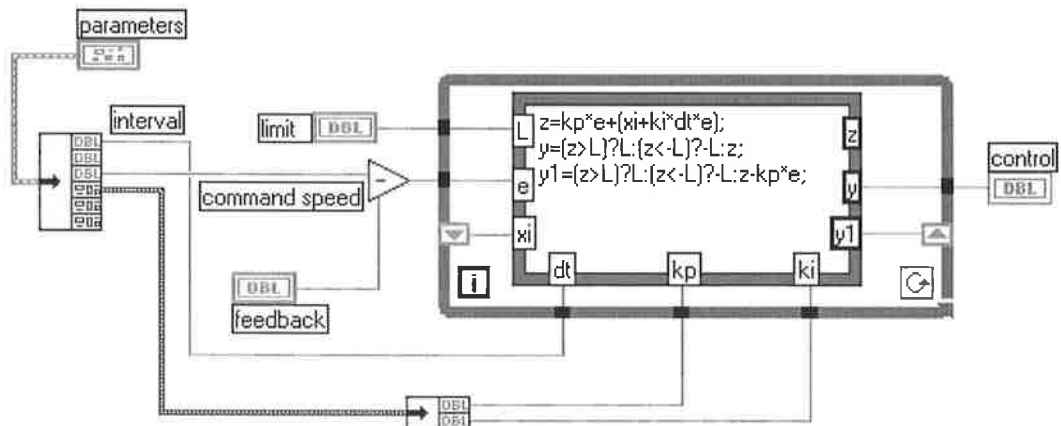


Figure A.1 Block diagram of PID SubVI

Chg point SubVI

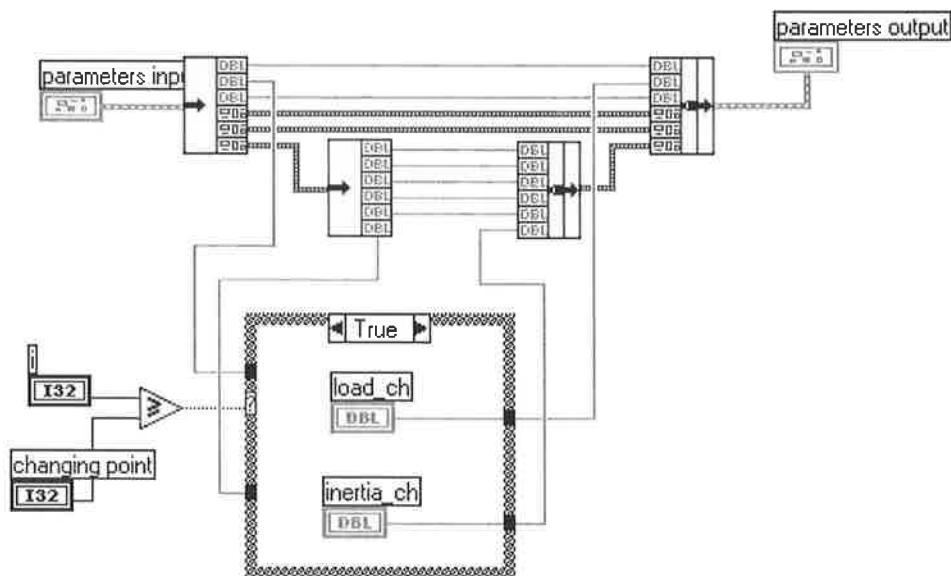


Figure A.2 Block diagram of Chg point SubVI

Current Control SubVI

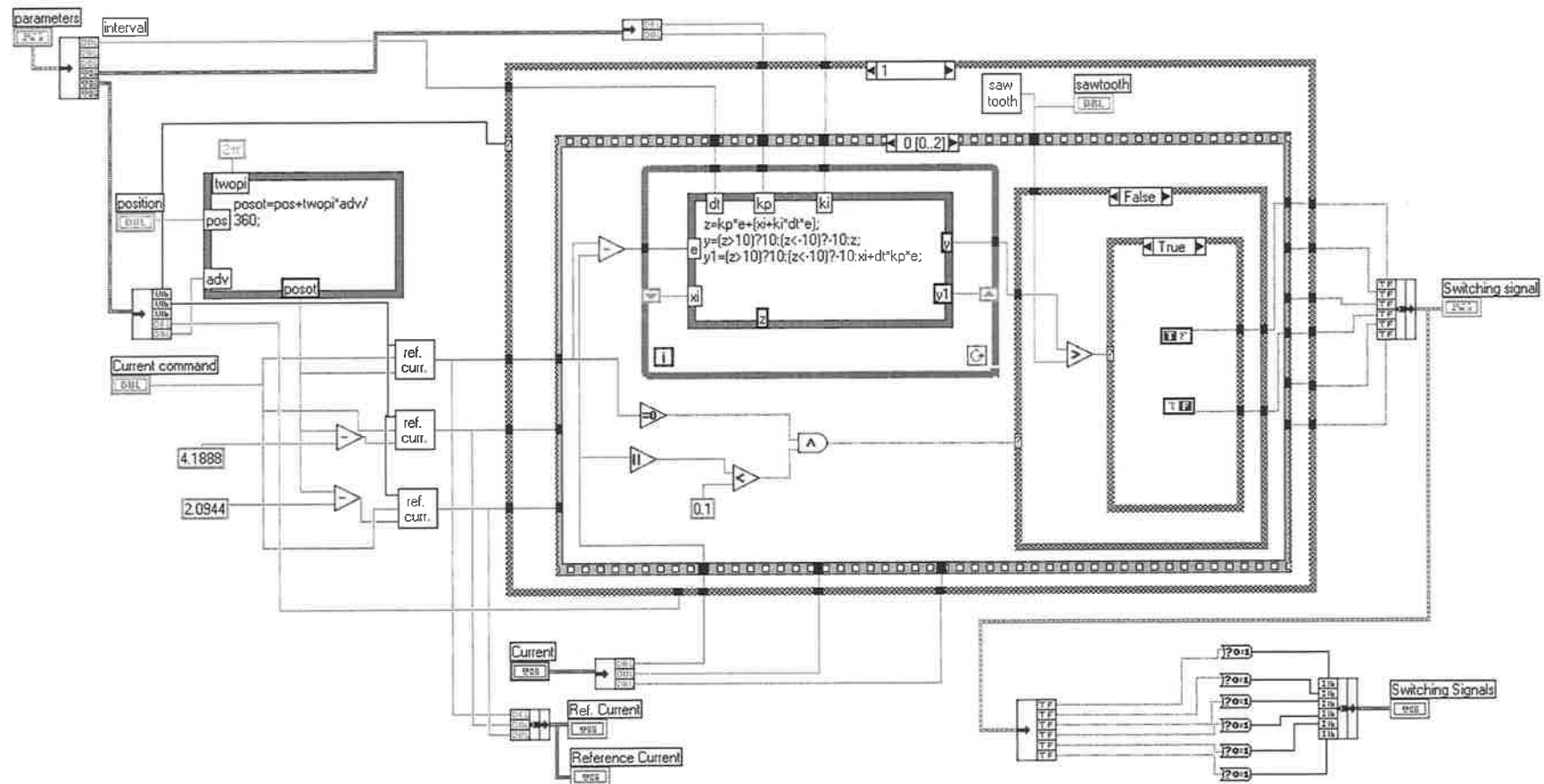


Figure A.3 Block diagram of Current Control SubVI

ω and rpm SubVI

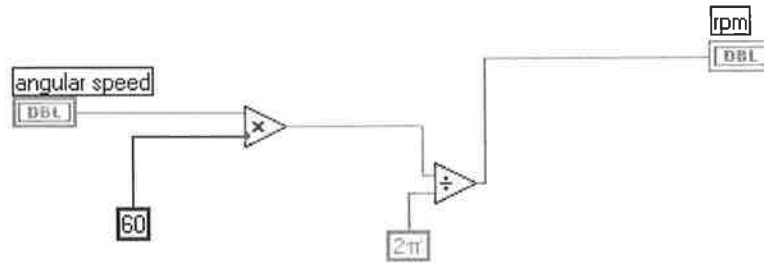


Figure A.4 Block diagram of ω and rpm SubVI

TPS SubVI

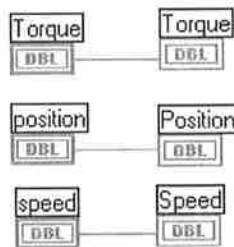


Figure A.5 Block diagram of TPS SubVI

Emf SubVI

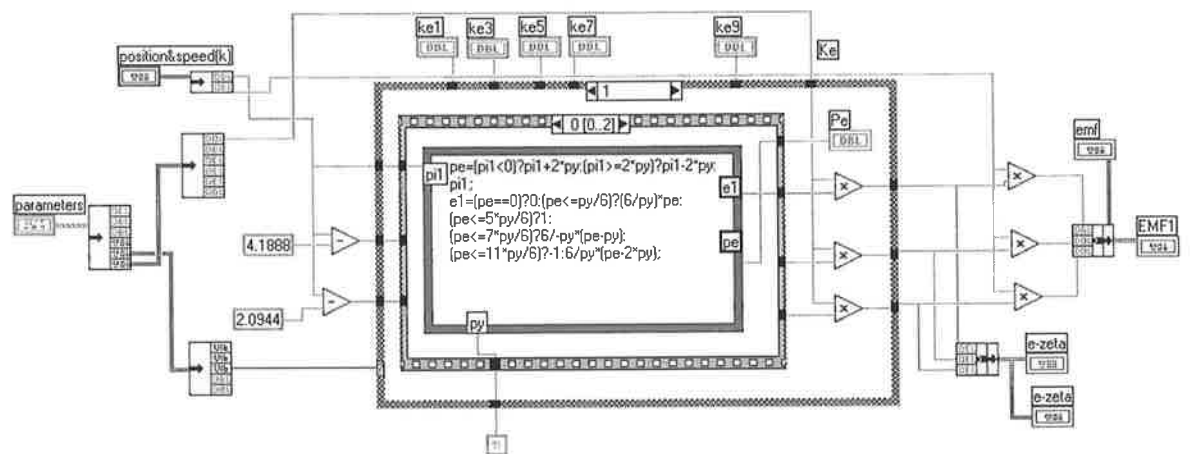


Figure A.6 Block diagram of Emf SubVI

Torque SubVI

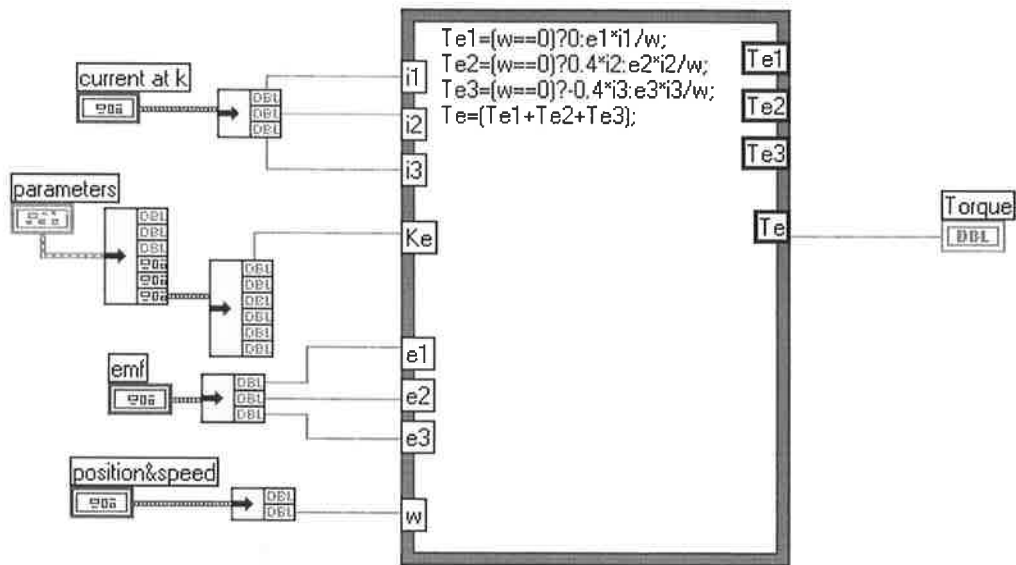


Figure A.7 Block diagram of Torque SubVI

Speed SubVI

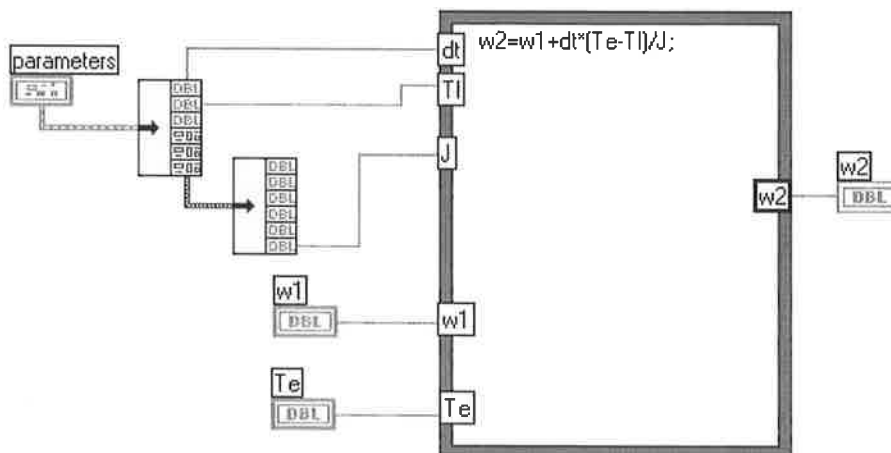


Figure A.8 Block diagram of Speed SubVI

Position SubVI

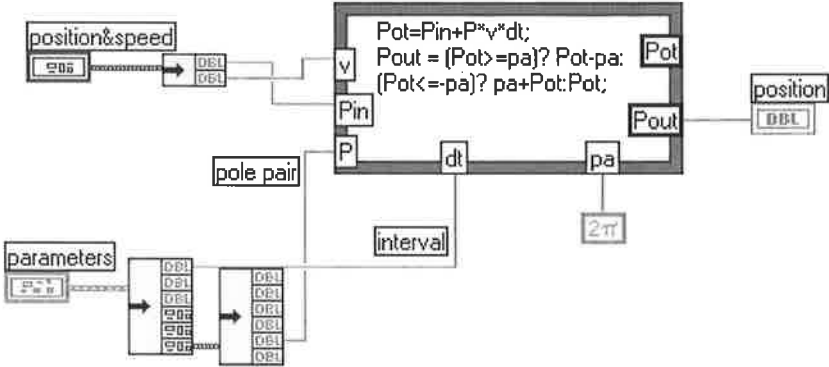


Figure A.9 Block diagram of Position SubVI

Terminal Voltage SubVI

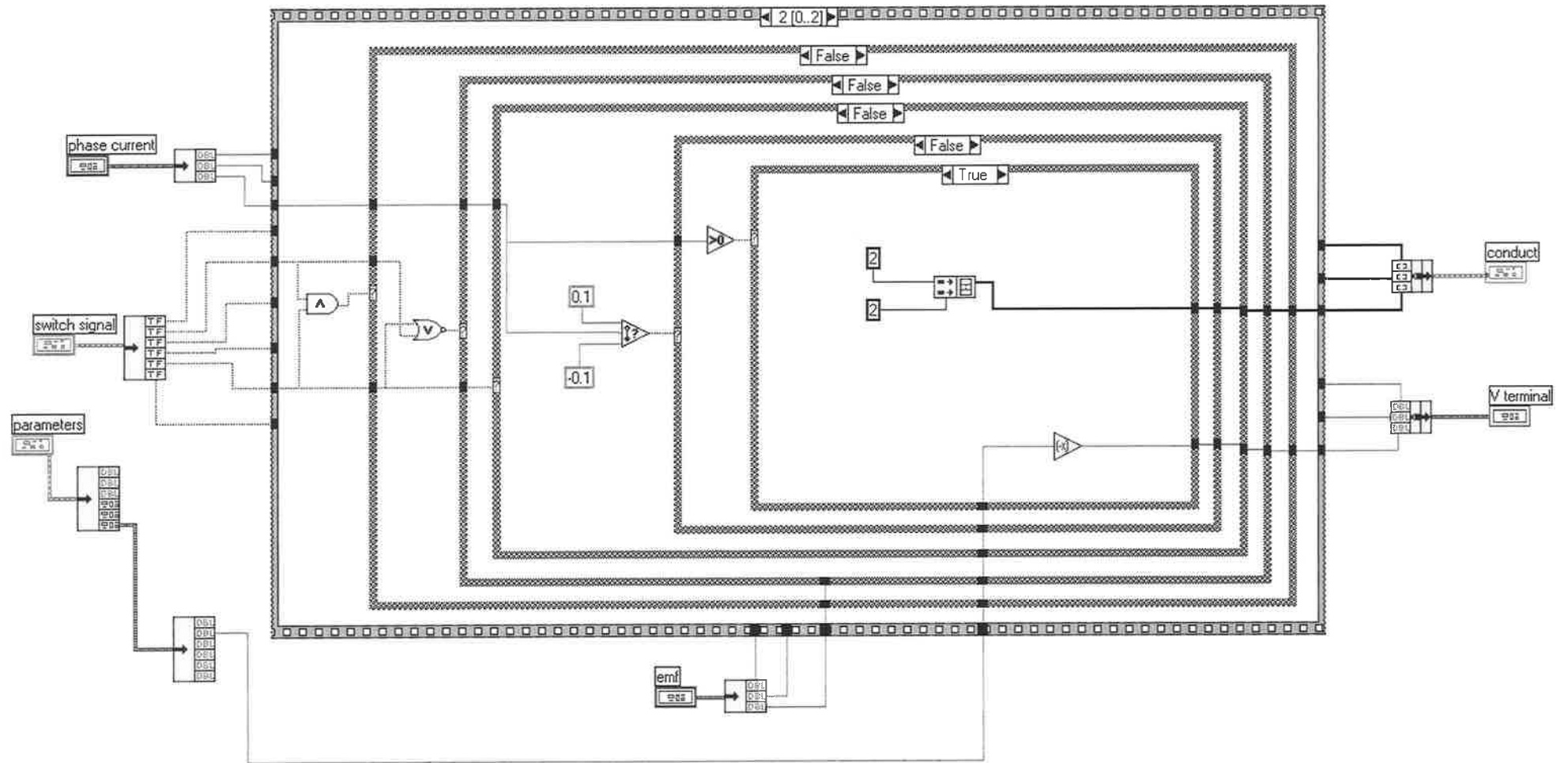


Figure A.10 Block diagram of Terminal Voltage SubVI

DC link SubVI

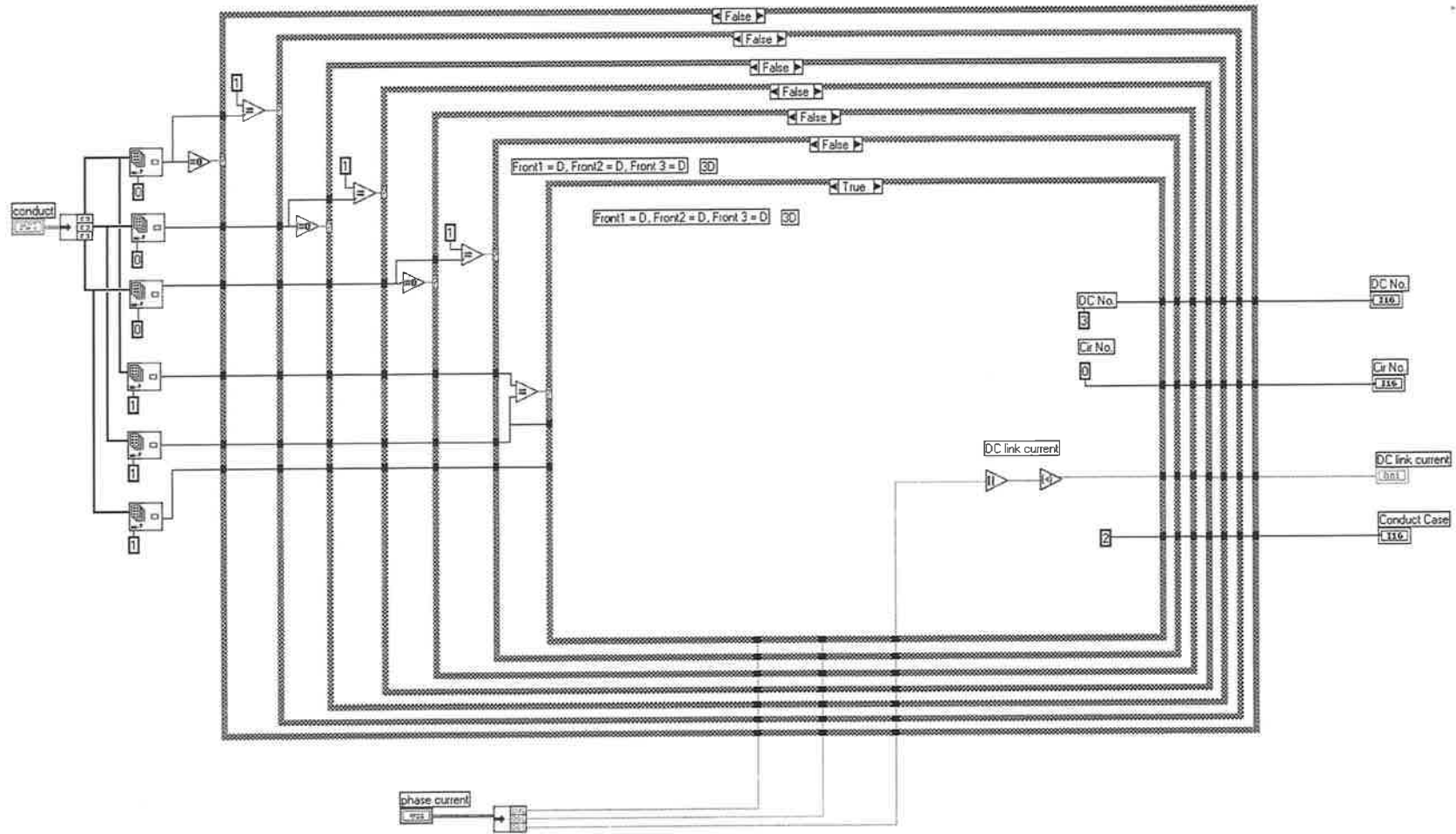


Figure A.11 Block diagram of DC link SubVI

Comp SubVI

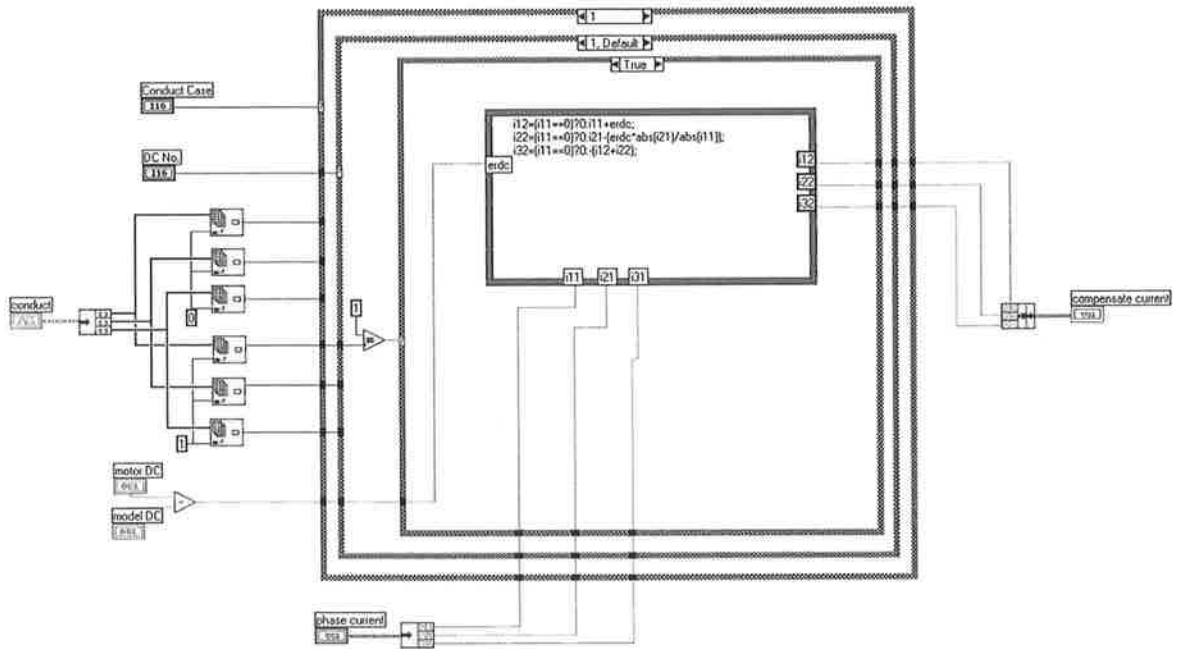


Figure A.12 Detail in the block diagram of Comp SubVI

Error SubVI

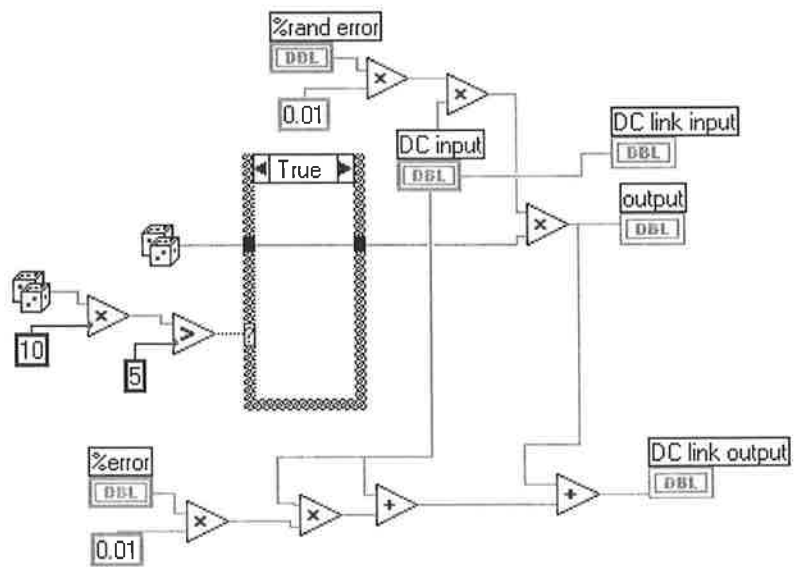


Figure A.13 Detail in the block diagram of Error SubV

A-3 The details in the main block diagram of the program to reconstruct the phase current using the experimental data

Some of the details of the main block diagram of the program reconstruct the phase currents are shown here. The details of "Sep Sigs" SubVI, "Vdc" SubVI, and "Comp1" or "Comp2" SubVI

Sep Sigs SubVI

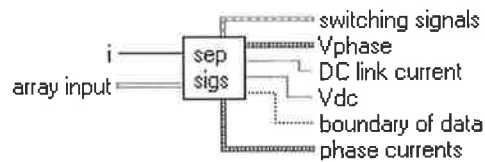


Figure A.14 Input and output parameter of Sep Sigs SubVI

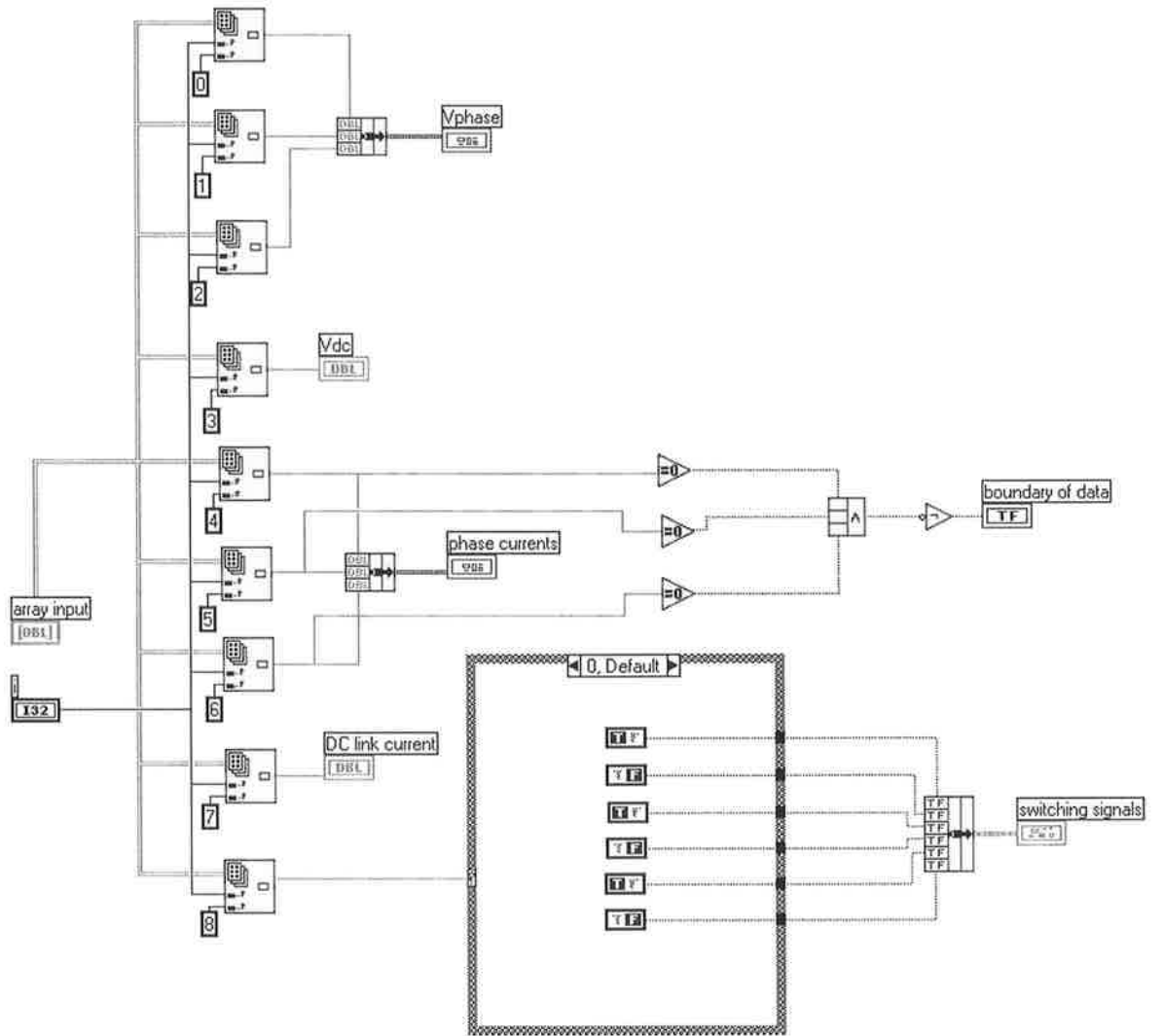


Figure A.15 Detail in the block diagram of Sep Sigs SubVI

Vdc SubVI

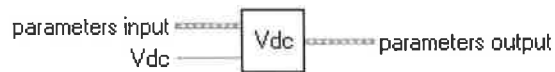


Figure A.16 Input and output of Vdc SubVI

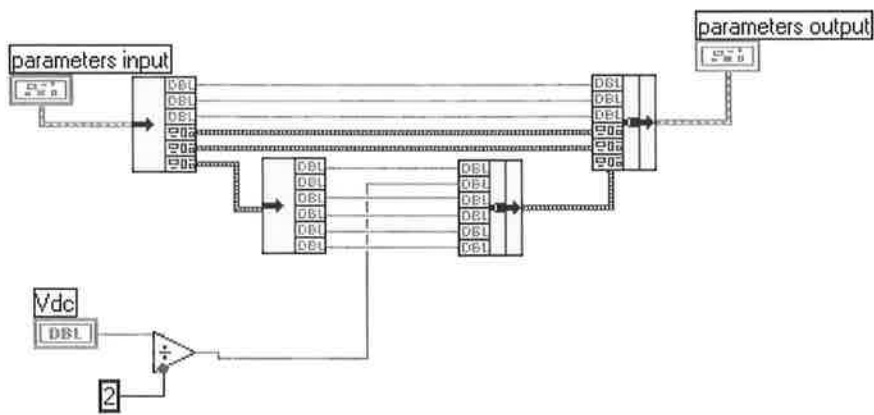


Figure A.17 Detail in the block diagram of Vdc SubVI